SUPPORTING INFORMATION

Two step activation of Ru-PN^{3}P pincer catalysts for CO_2 hydrogenation

Alex S. Tossaint,[a,†] Christophe Rebreyend,[a,†] Vivek Sinha,[a] Manuela Weber,[b] Stefano Canossa[c] and Evgeny A. Pidko,[a,*] Georgy A. Filonenko[a,*]

a) Inorganic Systems Engineering Group, Department of Chemical Engineering, Faculty of Applied Sciences, Delft University of Technology, Van der Maasweg 9, 2629 HZ, Delft, The Netherlands

b) Freie Universität Berlin, Instiut für Chemie und Biochemie, Anorganische Chemie, Fabreckstrasse 34/36, D-14195 Berlin-Dahlem, Germany

c) Max Planck Institute for Solid State Research, Heisenbergstr. 1, 70569 Stuttgart, Germany

† A.S.T. and C.R. contributed equally to this manuscript

Corresponding authors: Georgy A. Filonenko (g.a.filonenko@tudelft.nl), Evgeny A. Pidko (e.a.pidko@tudelft.nl)

DATA AVAILABILITY NOTE:

Reference raw spectral data for new complexes and machine-readable DFT data are deposited under DOI: 10.4121/19190237 and are available from 4TU.ResearchData centre free of charge

Contents

S0. General considerations

All manipulations unless stated otherwise were performed using Schlenk or glovebox techniques under dry argon atmosphere. Anhydrous solvents were dispensed from a solvent purification system manufactured by INERT (USA) and degassed prior to use. Anhydrous deuterated solvents were purchased from Eurisotop, degassed and stored over 4Å molecular sieves. All other chemicals unless noted otherwise were purchased from major commercial suppliers (TCI Europe and Merck) and used without purification.

Ruthenium precursor ligand **L1**[1] and reference Ru-PNP pincer catalyst[2] were prepared according to literature procedures.

Instrumentation and methods:

NMR spectra were measured on Agilent 400-MR DD2 spectrometer. LCMS measurements were performed using LTQ XL spectrometer equipped with Shimadzu HPLC setup operating at 0.2 mL/min flow rate with water/MeCN mobile phase containing 0.1%$_{vol}$ formic acid and Discovery C18 column.

IR spectroscopy was performed using Bruker Alpha II spectrometer operating in either transmission or attenuated total reflectance (ATR) modes. Solid samples of 1 were analysed as prepared and THF soluble derivatives of **1** we cast as thin films on the ATR crystal.

S1. Synthesis characterization and reactivity of RuPN^{3}P pincers

RuPN^{3}P pincer 1:

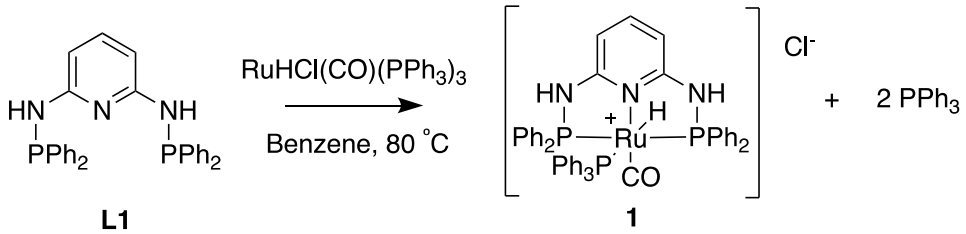

477.5 mg of ligand **L1** (1 mmol, 1 eq.) were combined with equivalent amount of $RuHCl(CO)(PPh_3)_3$ (952 mg, 1 mmol, 1eq.) in a Schlenk flask in 20 mL benzene. The suspension was stirred for 20 minutes at room temperature and the solids dissolved to form a clear pale green solution with a small amount of fine suspended solid. The solution was then heated under argon at 80°C for 4 hours and solution color turned pale yellow and waxy green solids deposited on the flask wall. The solution was then separated by hot filtration and dried. Resulting oily residue was washed several times with ether to remove PPh_3 and with small amounts of dichloromethane (3x2 mL) to remove unreacted Ru precursor. After drying under vacuum, 651 mg of white solid (ca. 72%) was obtained. Analytically pure samples were obtained by recrystallization from DMF-diethyl ether mixtures using slow vapour diffusion technique.

NOTE: Spectroscopic characterization was initially preformed in DMSO-d_6. We noted a lack of long term stability of **1** in this solvent due to PPh_3 ligand substitution by DMSO occurring within several hours that impacts the quality of ^{13}C spectra obtained. Full spectroscopic characterization was repeated in DCM-d_2-MeOD (10/1) solvent to avoid ligand exchange and obtain accurate ^{13}C spectra.

Assignments are made using ^{31}P decoupled ^1H spectrum:

^{1}H {31P} NMR (400 MHz, DCM-d_2 + MeOD) δ 7.99 (d, J = 7.4 Hz, 4H, -PPh_2 C**H**-*o*), 7.39 (m, overlap of , -PPh_2 C**H**-*m*, 4H, -PPh_2 C**H**-*p* 2H, total 6H), 7.20 (d, J = 7.2 Hz, 4H, -PPh_2 C**H**-*o*), 7.11 (t, J = 7.3 Hz, -PPh_2 C**H**-*p* 2H), 7.02 (m, overlap of PPh_3-C**H** 6H+3H, -PPh_2 C**H**-*m* 4H, total 13 H), 6.89 (m, overlap of 1H py-C**H**-p and PPh_3-C**H** 6H, total 7H), 6.30 (d, J = 8.0 Hz, py-C**H**-*m* 2H), -7.15 (s, Ru-H).

^{13}C NMR (101 MHz, DCM-d_2 + MeOD) δ 163.21 (co-crystallized DMF impurity), 158.71 (t, J = 7.9 Hz, py-***C*$_q$**), 143.84 (apparent td, -PPh_2-***C*$_q$**), 139.86 (s, py-***C***H-para), 135.55 (apparent dt, -PPh_2-***C*$_q$**), 134.07 (d, J = 19.5 Hz, PPh_3, ***C*$_q$**), 132.51 (d, J = 11.8 Hz PPh_3, C***H***), 132.42 (t, J=8Hz, -PPh_2-***C***H ortho), 130.99 (s, -PPh_2-***C***H para), 130.64 (t, J = 6.6 Hz, -PPh_2-***C***H ortho), 130.55 (s, -PPh_2-***C***H para), 129.44 (d, J = 1.5 Hz, PPh_3-***C***H para), 128.83 (t, J = 5.1 Hz, -PPh_2-***C***H meta), 128.63 (t, J = 5.6 Hz, -PPh_2-***C***H meta), 128.45 (d, J = 9.2 Hz, PPh_3-***C***H), 100.92 (t, J=4Hz, py-***C***H meta).

^{31}P {^{1}H}NMR (162 MHz, DCM-d_2 + MeOD) δ 94.09 (d, J = 18.8 Hz), 30.82 (t, J = 18.9 Hz).

Additional characterization performed in DMSO:

^{1}H NMR (400 MHz, DMSO): δ9.91 (s, 2H, N*H*), δ7.94 (d, $^3J_{HH}$ = 6.2 Hz), 4H, Ph-o-Ph_2P), δ7.54 – 7.44 (*3*t, 7H, 4H of Ph-p-Ph_2P and 3H of Ph-p-Ph_3P), δ7.34 (t, 1H, Py-p-C*H*), δ7.15 – 7.10 (m, 12H, 4H of o-Ph_2P and 8H of m-Ph_2P), δ7.00 – 6.91 (m, 12H, 6H of m-Ph_3P and 6 of Ph-o-Ph^{3}P), δ6.42 (d, 2H, $^3J_{HH}$ = 8.0 Hz Py-m-C*H*), δ-7.41 (dt, $^2J_{PH}$ = 88.9, $^2J_{PH}$ = 23.5, 1H, RuH). Unassigned peaks are solvent impurities, or neutral complex (RuHCl(CO)PN_3P) impurities.

^{31}P {^{1}H} NMR (162 MHz, DMSO): δ92.76 (d, $^2J_{PP}$ = 19.72, 2P, NH-*P*Ph_2), δ30.04 (t, $^2J_{PP}$ = 19.72, 1P, *P*Ph_3).

EA: C:H:N for $C_{48}H_{41}N_3Cl_1P_3O_1Ru_1$ - Found (Calc.): 63.43 (63.68), 4.60 (4.57), 4.61 (4.64)

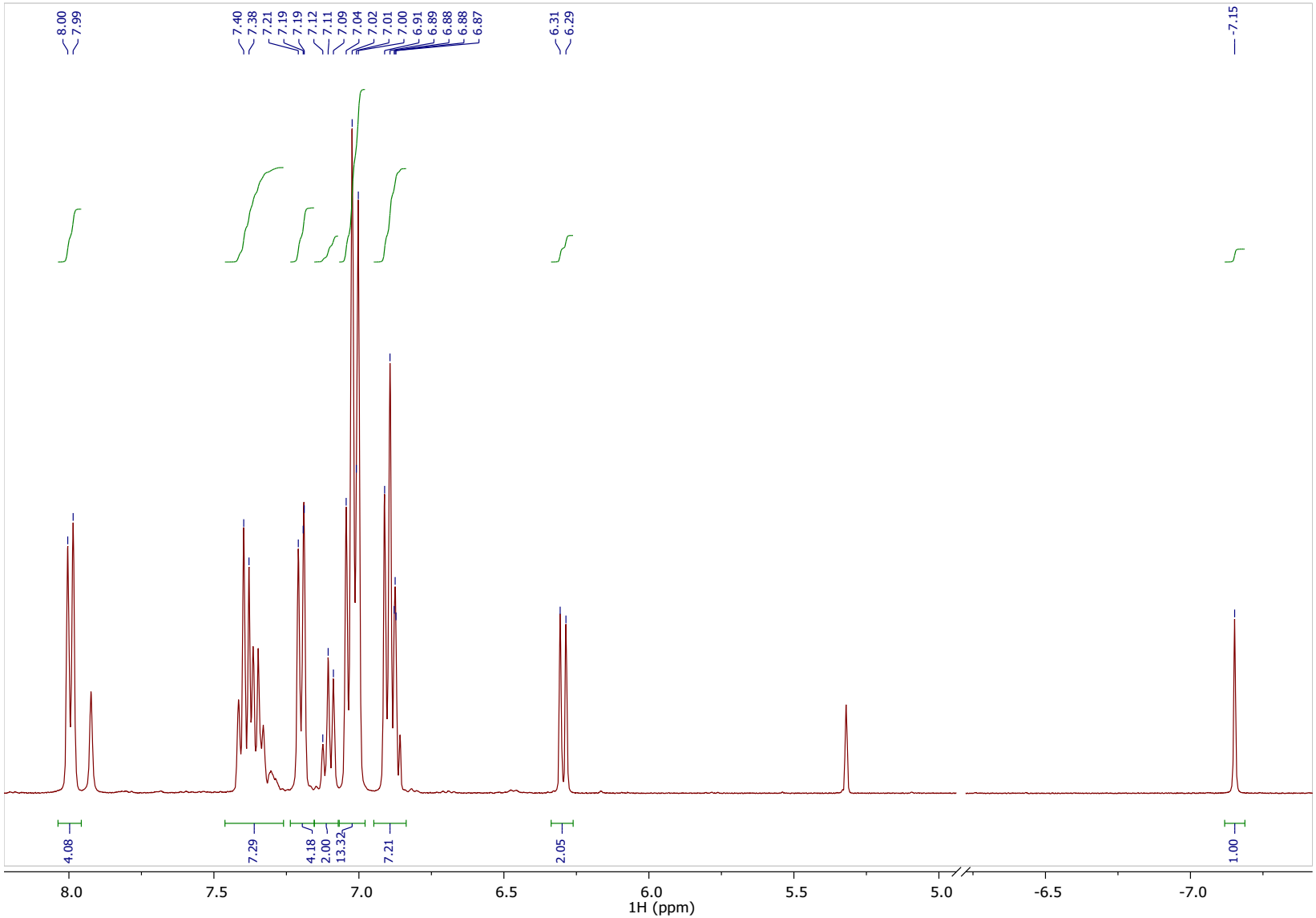

Figure S1. $^{1}H\{^{31}P\}$-NMR spectrum of complex **1** in DCM-d_2 – MeOD

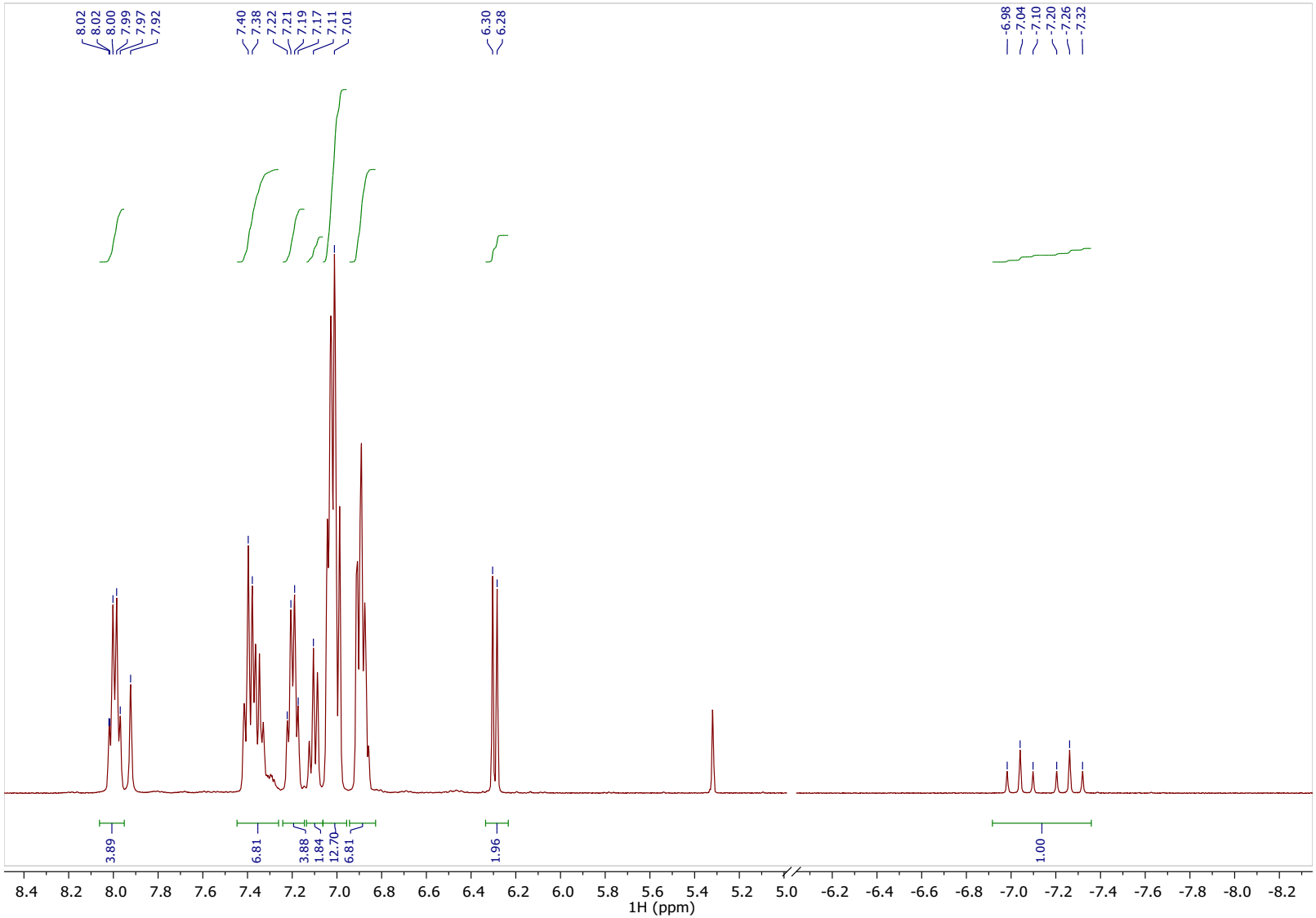

Figure S2. ^{1}H NMR spectrum of complex **1** in DCM-d_2 – MeOD

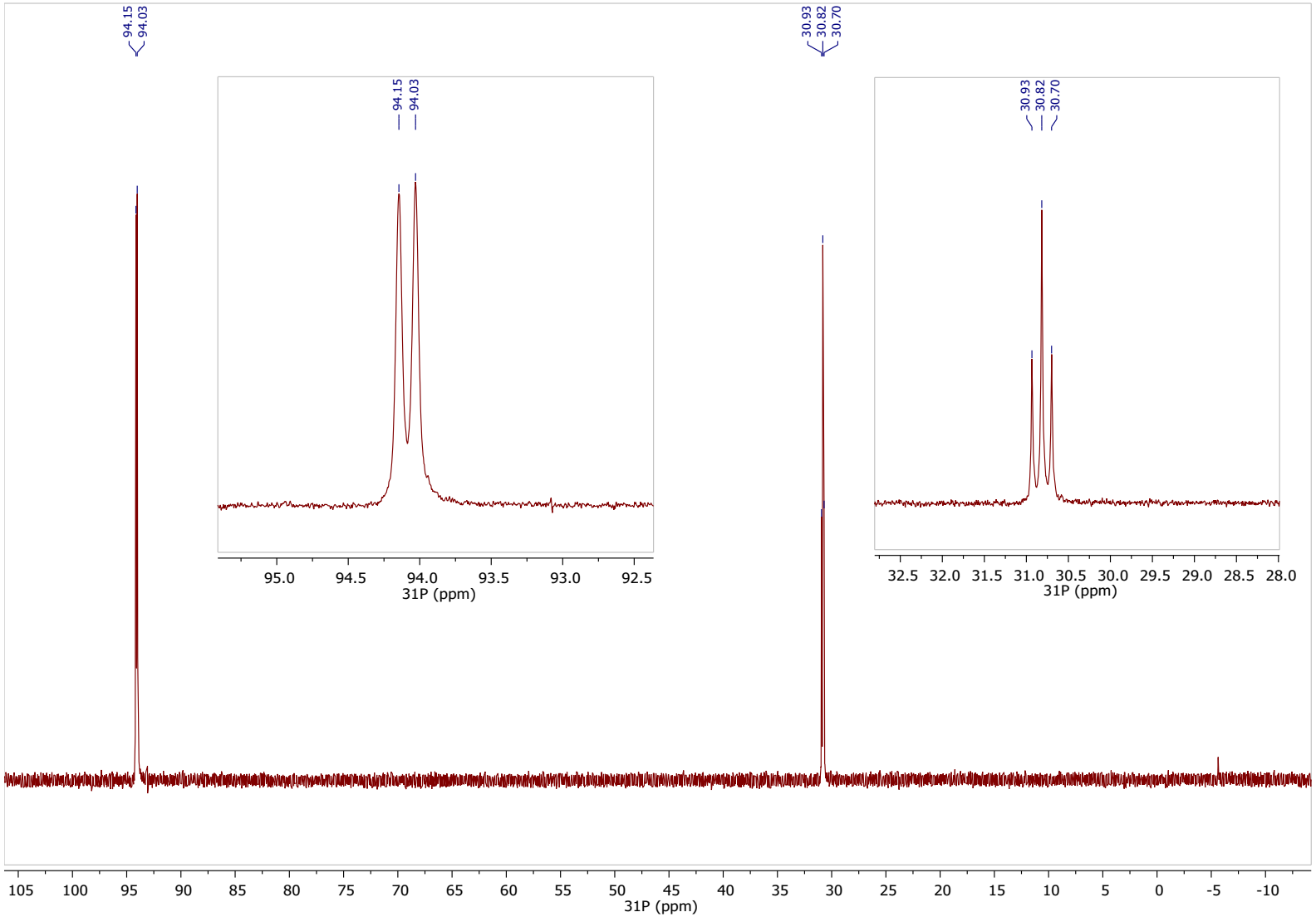

Figure S3. ^{31}P NMR spectrum of complex **1** in DCM-d_2 – MeOD

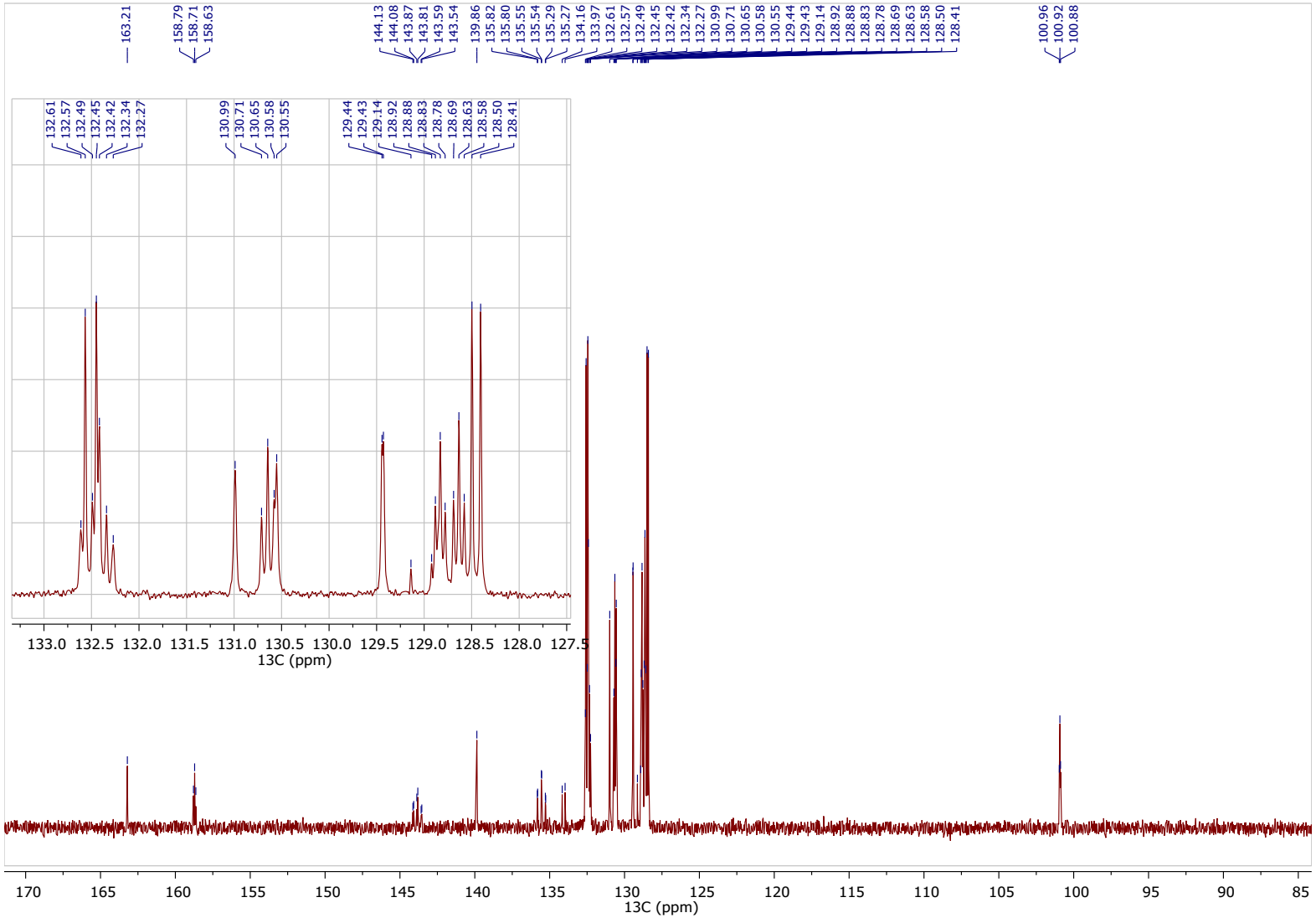

Figure S4. ^{13}C NMR spectrum of complex **1** in DCM-d_2 – MeOD

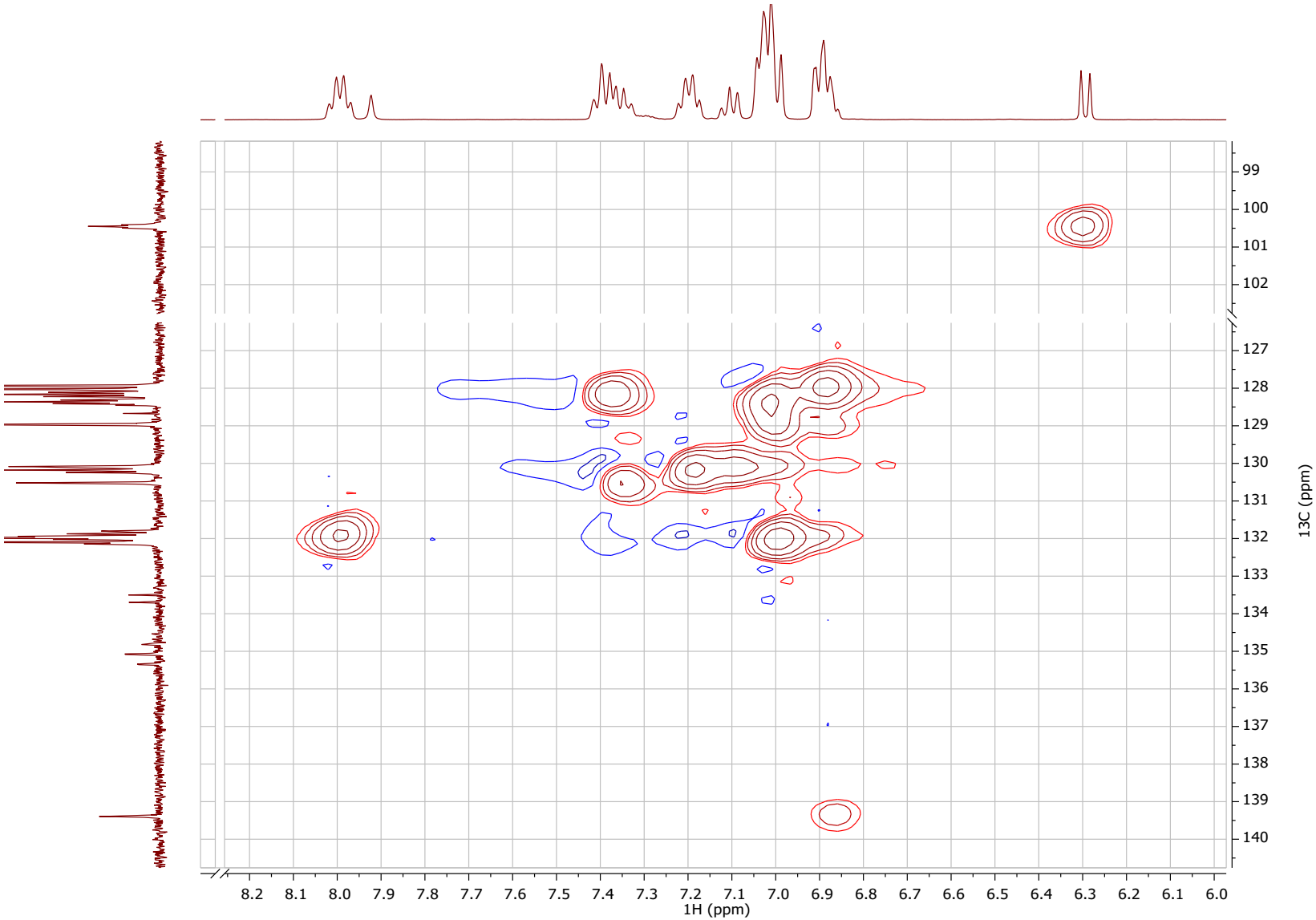

Figure S5. ASAPHMQC NMR spectrum of complex **1** in DCM-d_2 – MeOD

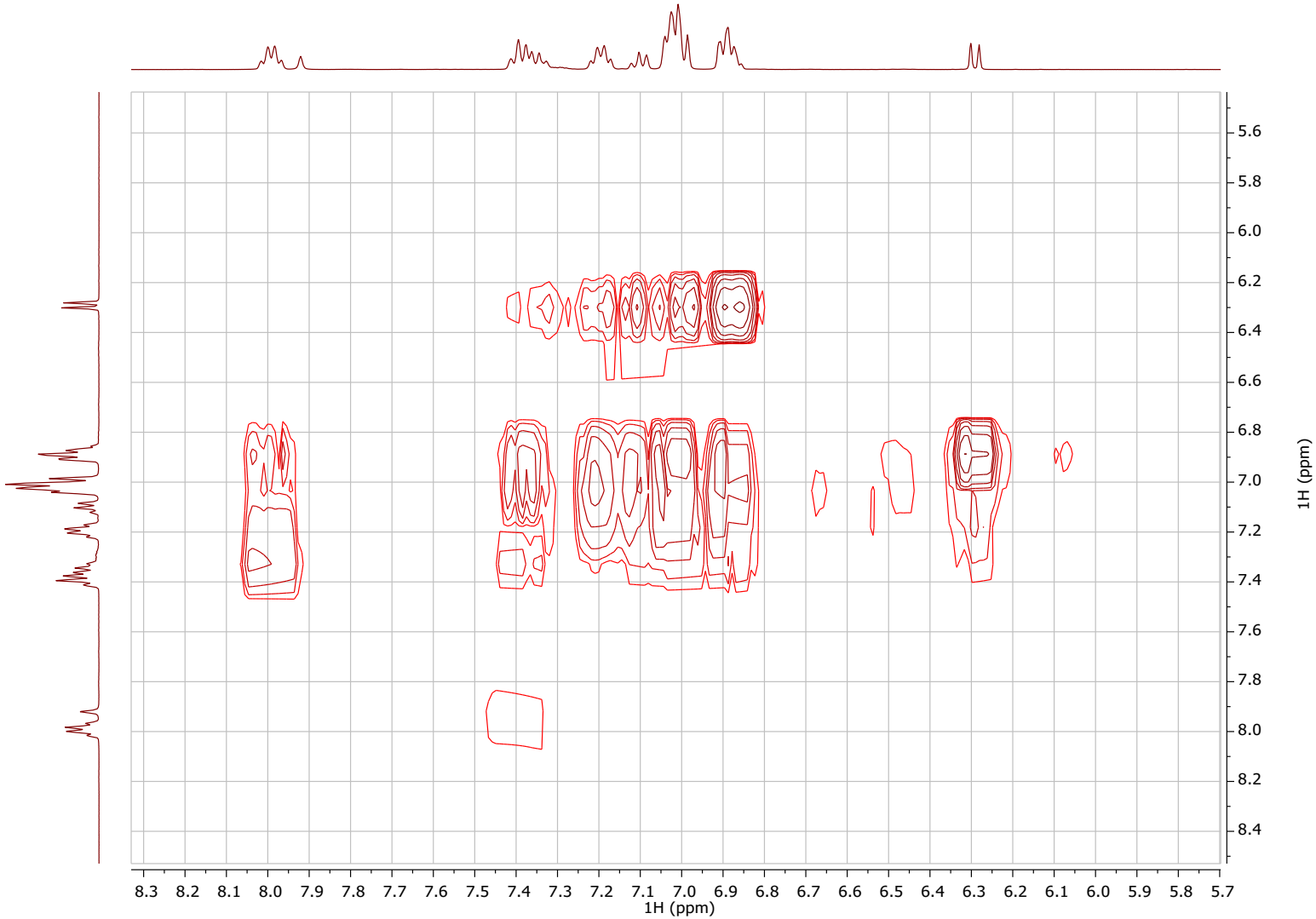

Figure S6. gCOSY spectrum of complex **1** in DCM-d_2 – MeOD

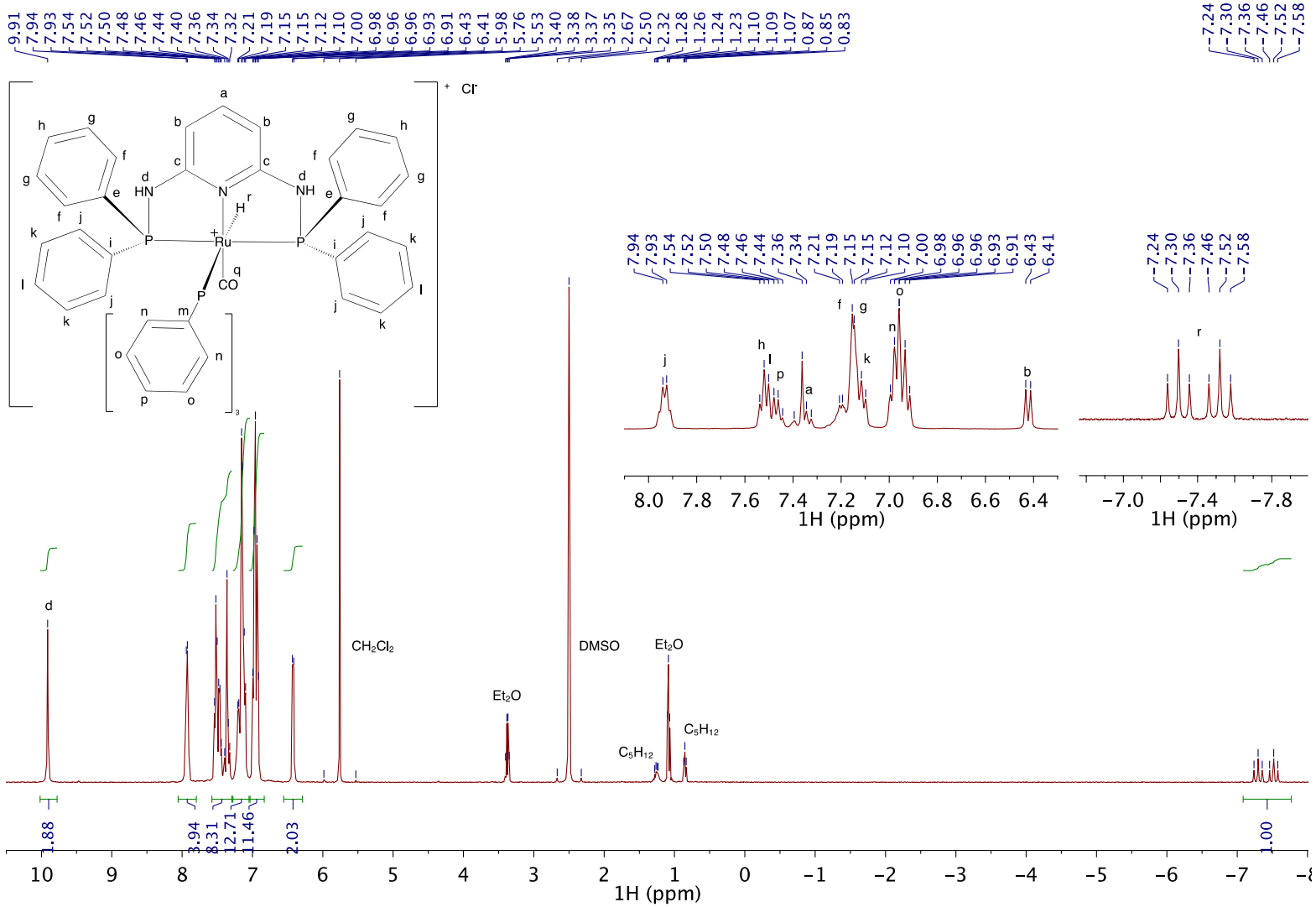

Figure S7. ^{1}H NMR spectrum of complex **1** in DMSO-d_6.

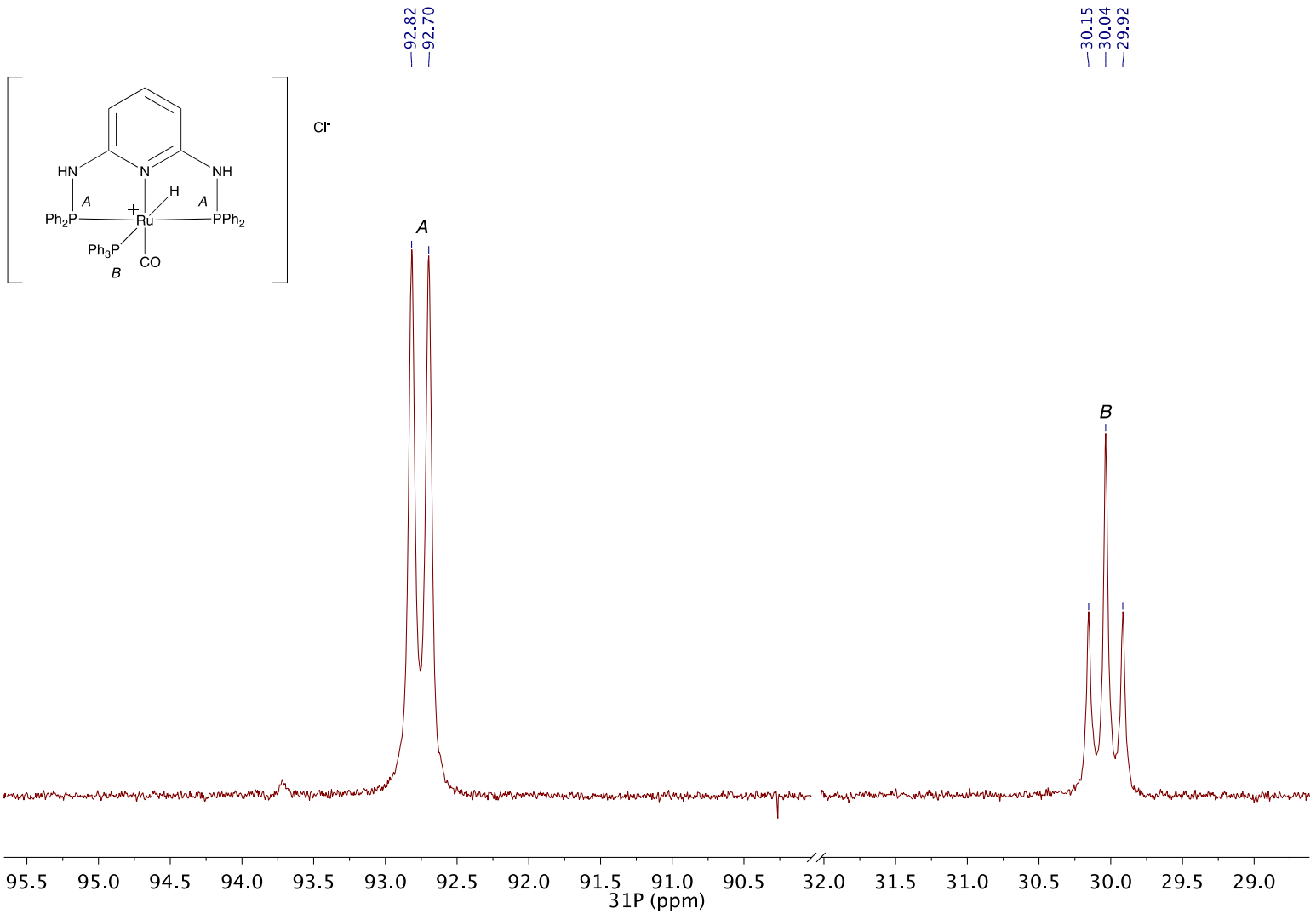

Figure S8. ^{31}P NMR spectrum of complex **1** in DMSO-d_6.

Single deprotonation of 1 - generation of complex 2

Single deprotonation of **1** can be performed in several ways all providing results consistent with findings of Huang and co-workers for this compound.[1]

A) Reaction with KO^{t}Bu in DMSO

(5 mg, 5.52 µmol, 1 eq.) is suspended in DMSO-d_6 and treated with KOtBu (0.6 mg, 5.52 µmol, 1 eq as a stock solution). Reaction mixture is shaken in the NMR tube and analysed immediately.

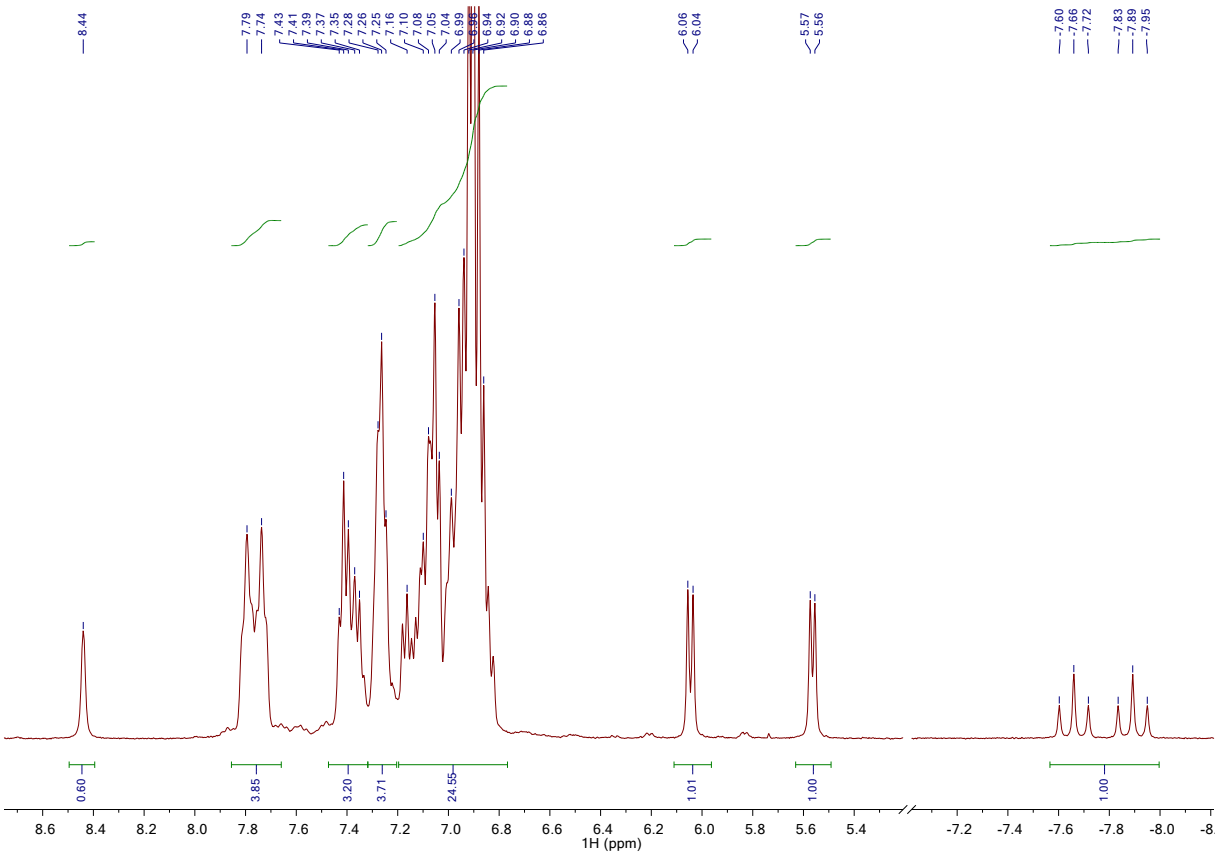

Figure S9. ^{1}H NMR spectrum of complex **2** generated in DMSO-d_6 via reaction with KO^{t}Bu. Note the remaining NH resonance at 8.44 ppm and the loss of equivalence between pyridine backbone protons.

B) Reaction with KHMDS or KO^{t}Bu in THF

(5 mg, 5.52 µmol, 1 eq.) is suspended in THF-d_8 and treated with KHMDS (1.1 mg, 5.52 µmol, 1 eq as a stock solution) or KOtBu (0.6 mg, 5.52 µmol, 1 eq as a stock solution) in a separate experiment. Reaction mixture is shaken in the NMR tube and analysed (See spectra below). Unlike in DMSO, we noted that complex **2** was dynamic in THF, a behaviour resulting in broadening of the pyridine proton resonances and those of pincer phosphorus donors in 31P NMR.

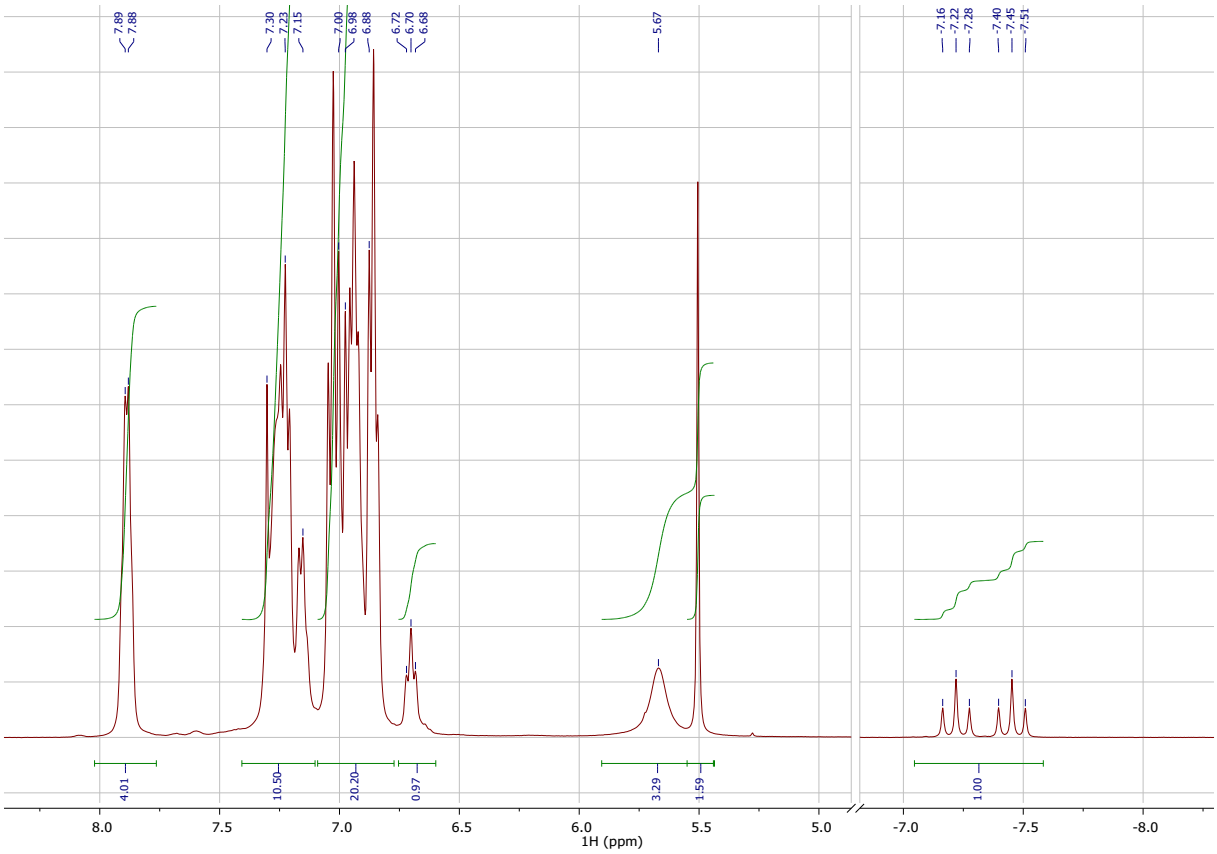

Figure S10. ^{1}H NMR spectrum of complex **2** generated in THF-d_8 via reaction with KO^{t}Bu. Note the coalescence of pyridine backbone proton resonances appearing as a broad peak at 5.67 ppm.

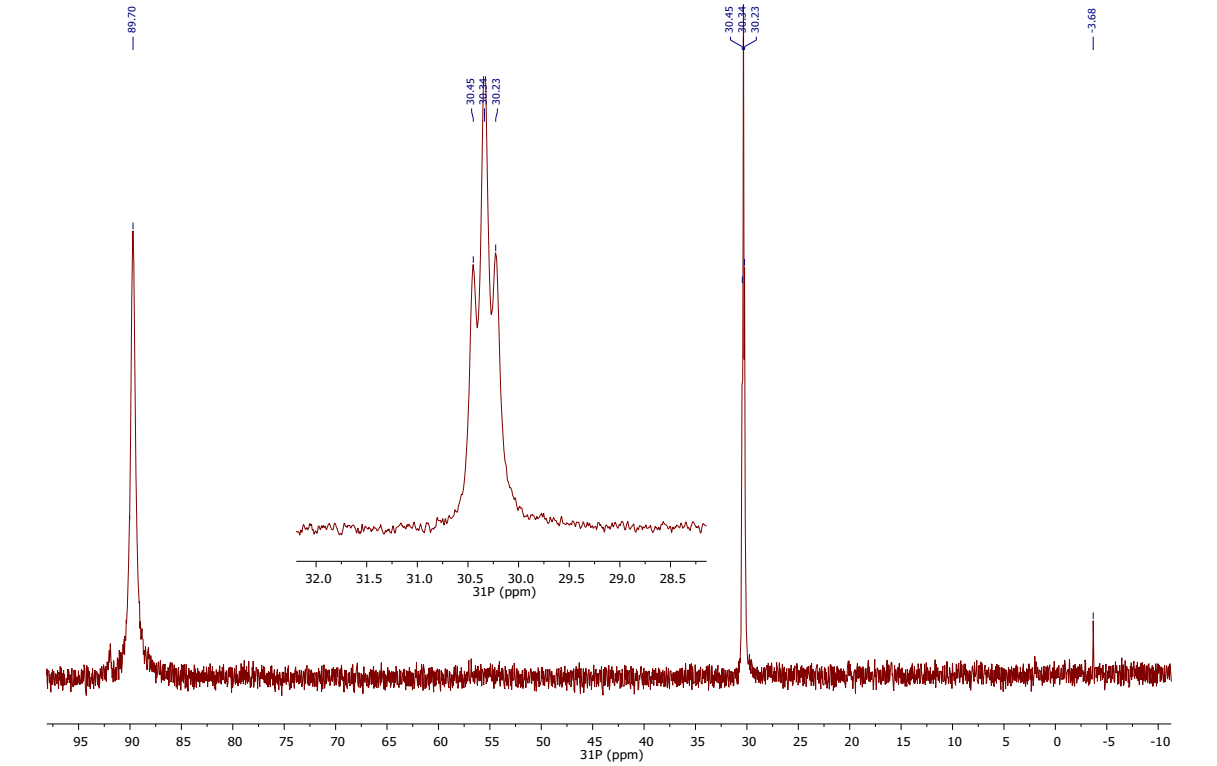

Figure S11. ^{31}P NMR spectrum of complex **2** generated in THF-d_8 via reaction with KO^{t}Bu. Note the low field peak appearing as broad singled due to the exchange.

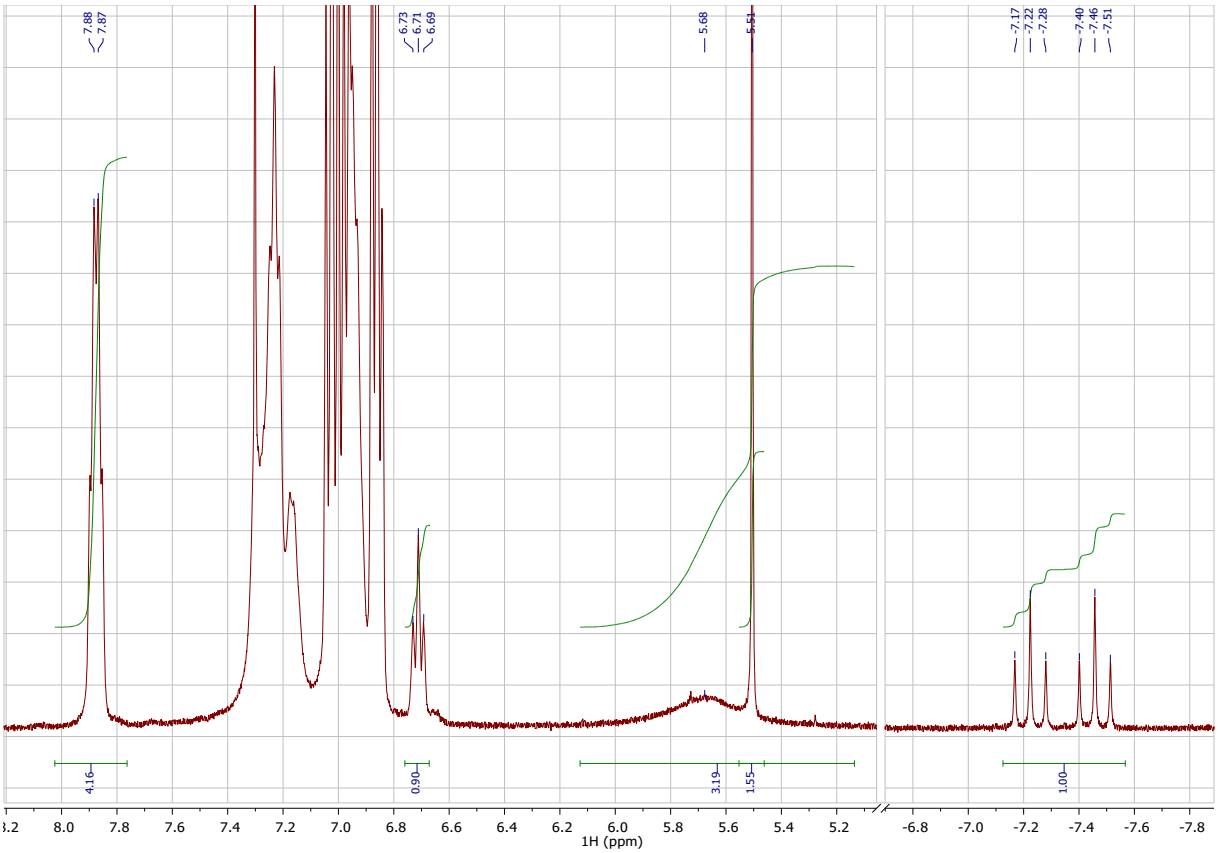

Figure S12. ^{1}H NMR spectrum of complex **2** generated in THF-d_8 via reaction with KHMDS. Note the coalescence of pyridine backbone proton resonances appearing as a broad peak at 5.68 ppm.

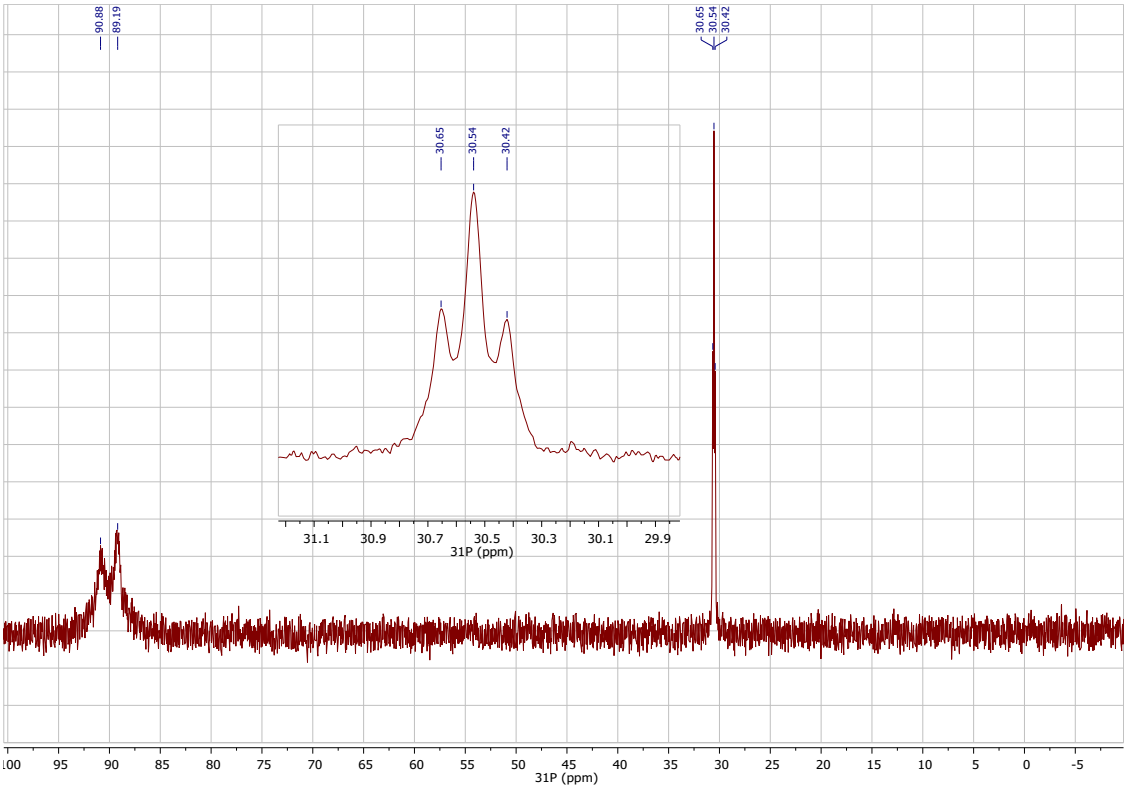

Figure S13. ^{31}P NMR spectrum of complex **2** generated in THF-d_8 via reaction with KHMDS. Note the broadening of a low field resonance due to the exchange.

We assumed that the chemical exchange observed in THF to be accelerated by the protic side products originating from the basic reagents used for deprotonation. A small scale isolation of **2** was performed to obtain pure complex suitable for spectroscopy and diffraction analysis. For this, the solution of **2** generated using procedure B above was diluted with pentane (1/1 ratio with THF), filtered and crystallised using pentane vapour diffusion method. The obtained crystalline material was confirmed to be complex **2** by diffraction methods and NMR spectra of these sample did not show chemical exchange noted for in situ generated **2**.

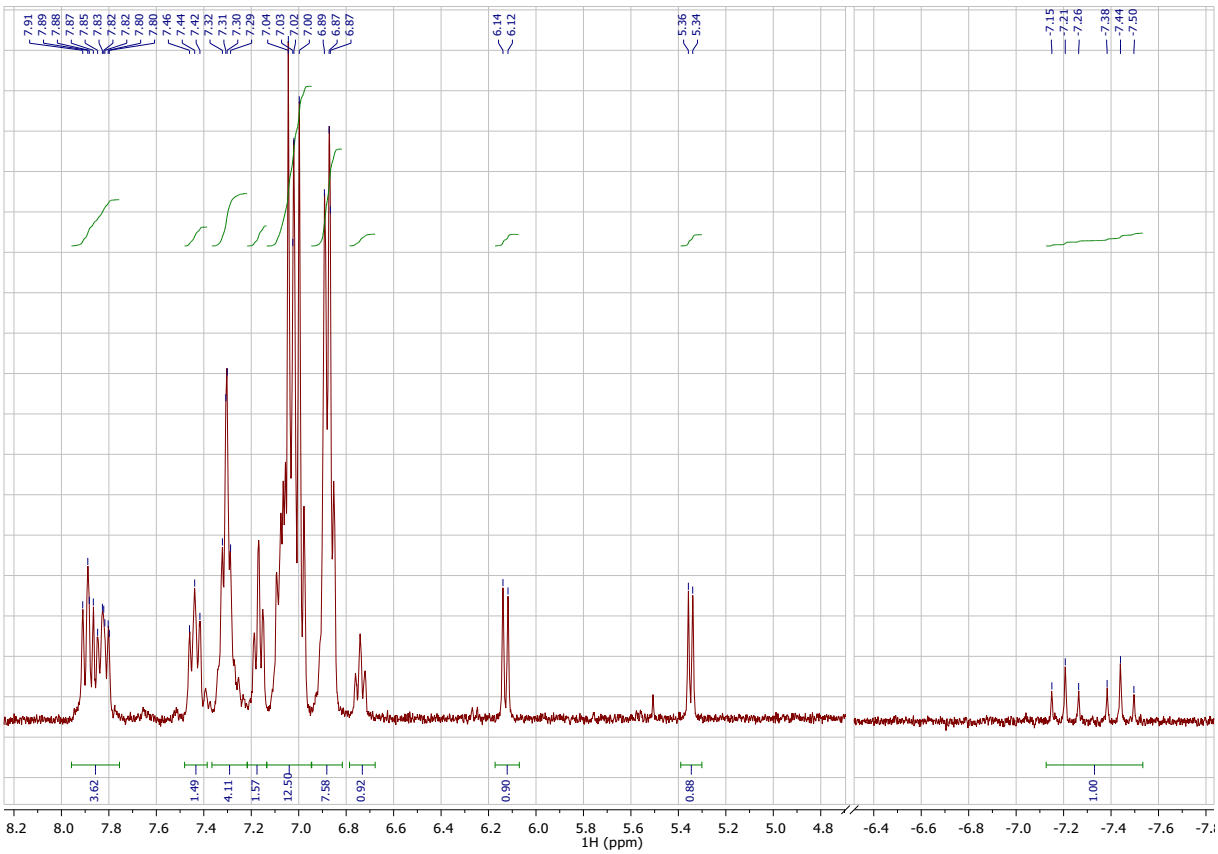

Figure S14. ^{1}H NMR spectrum of crystalline complex **2** in THF-d_8. Note the absence of exchange and pyridine backbone proton resonances appearing as two doublets.

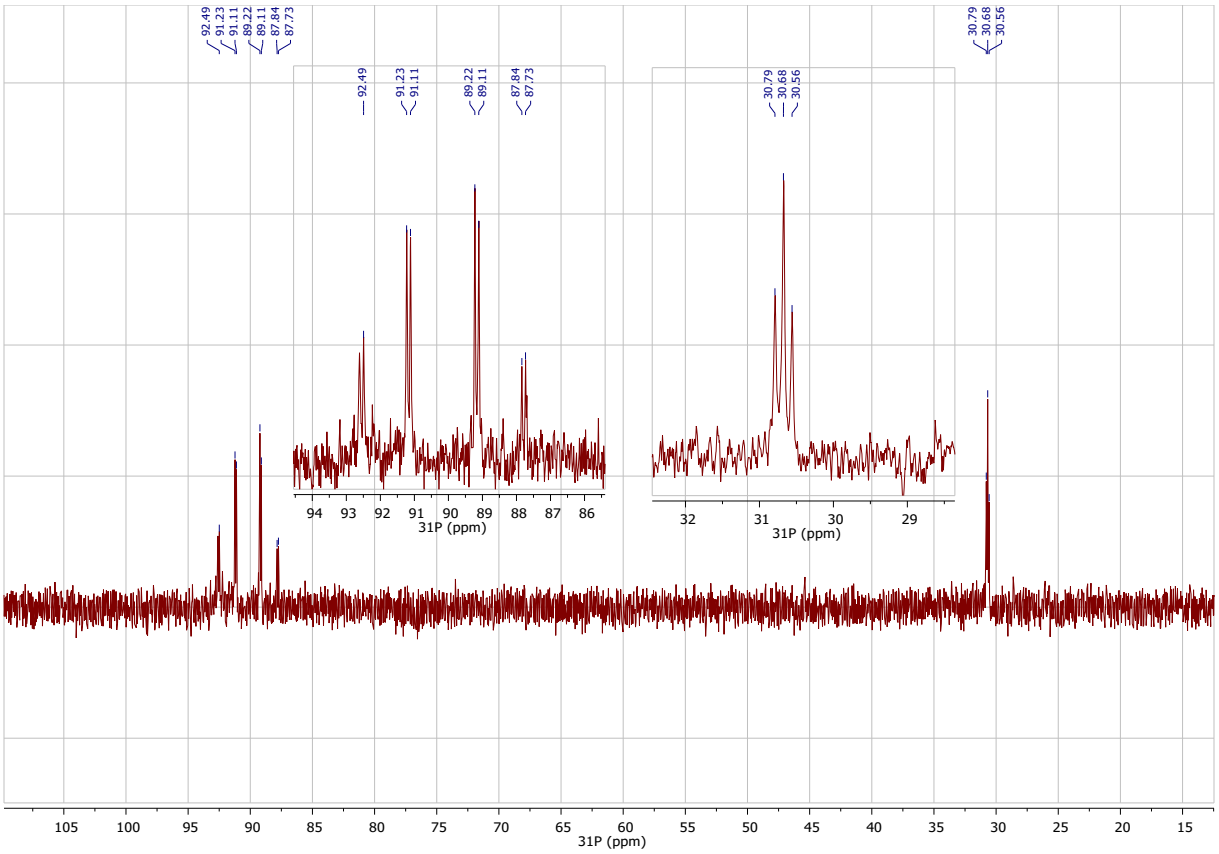

Figure S15. ^{31}P NMR spectrum of crystalline complex **2** in THF-d_8. Note the absence of exchange evidenced by the coupling pattern of the low field ^{31}P resonance.

Double deprotonation of 1 - generation of complex 3

Complex **1** (12.9 mg, 0.01425 mmol) was suspended in THF-d_8 (0.6 mL) and loaded into an NMR tube. A solid lump of KO^{t}Bu (3.2 mg, ca 2.05 eq) was added and the sealed tube was shaken for 2 minutes and spectral characterization was performed.

IMPORTANT: Please note that spectral assignments in ^{1}H spectra are done using **31P decoupled data**. Comparison with the coupled spectrum is given below.

^{1}H{31P} NMR (400 MHz, THF-d_8) δ 7.95 (d, *J* = 7.5 Hz, 4H, -PPh_2 C**H**-*ortho set 1*), 7.29 (br s, 4H, -PPh_2 C**H**-*ortho set 2*), 7.17 (t, *J* = 7.5 Hz, 4H, -PPh_2 C**H**-*meta set 1*), 7.02 (m, overlap of -PPh_2 C**H**-*meta set 2* 4H, -PPh_2 C**H**-*para* 4H, total 8H), 6.91 (t, *J* = 7.3 Hz, 3H, PPh_3 C**H**-para), 6.81 (m, overlap of PPh_3 C**H**-ortho and meta total 12H), 6.58 (t, *J* = 7.7 Hz, 1H, py-C**H**-para), 5.46 (d, *J* = 7.7 Hz, 2H, py-C**H**-meta), -7.42 (s, 1H, Ru-**H**).

^{13}C NMR (101 MHz, THF-d_8) δ 210.89 (q, *J* = 9.2, 8.7 Hz, Ru-***C***O), 172.93 (t, *J* = 7.6 Hz, py-$\boldsymbol{C_q}$), 153.93 and 146.97 (apparent dt, -PPh_2-$\boldsymbol{C_q}$), 138.82 (d, *J* = 28.4 Hz, PPh_3, $\boldsymbol{C_q}$), 137.45 (s, py-***C***H-para), 134.93 (d, *J* = 11.7 Hz, -PPh_2 ***C***H- *meta*), 133.34 (t, *J* = 6.3 Hz, -PPh_2 ***C***H- *ortho set 1*), 132.66 (t, *J* = 5.9 Hz, -PPh_2 ***C***H- *ortho set 2*), 128.8-128.0 (overlap , -PPh_2 ***C***H- *meta and 2 para* ***C****H, PPh_3* – **C**H, total 5 resonances), 96.24 (t, *J* = 11.4 Hz, py-***C***H-meta).

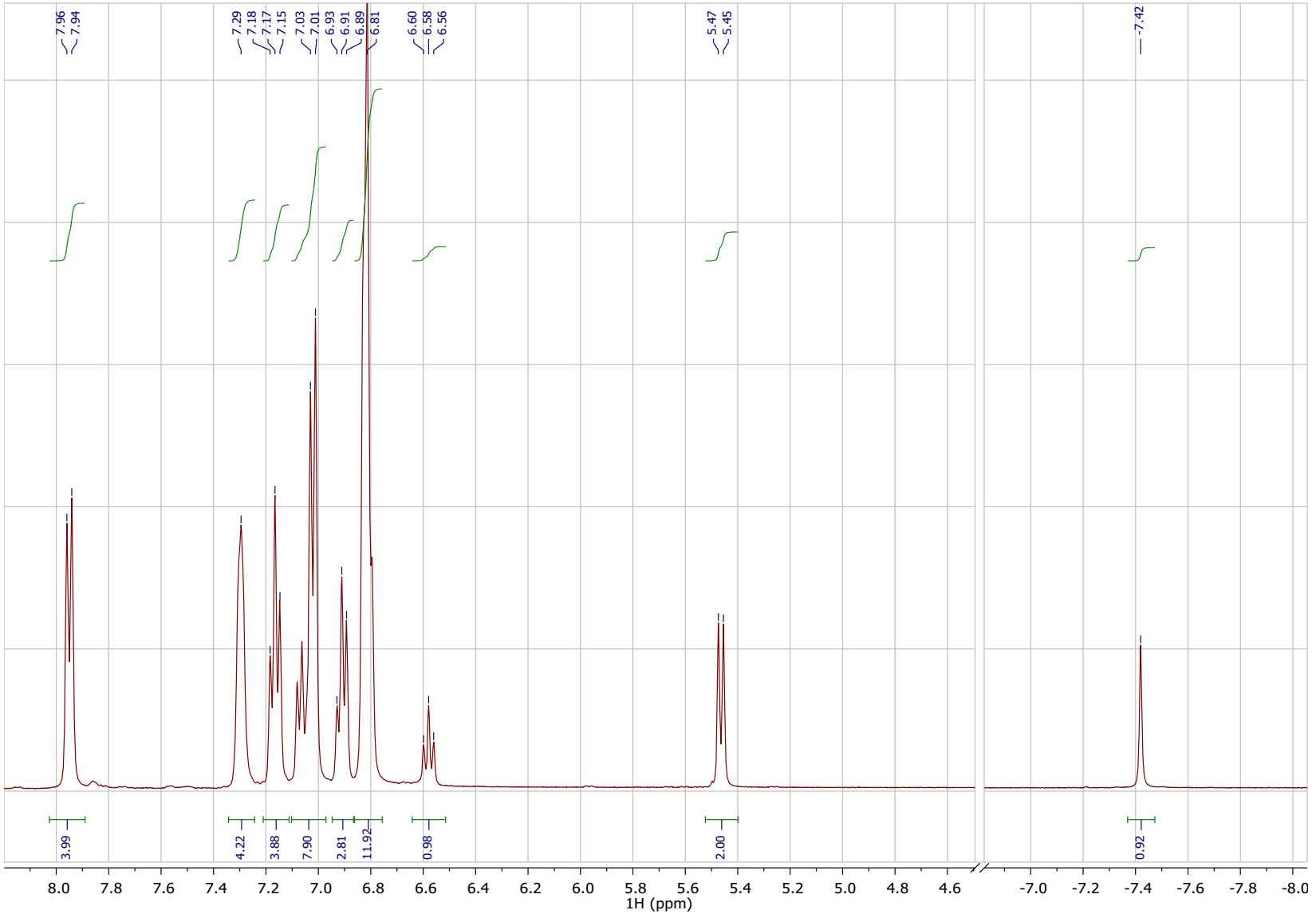

Figure S16. $^{1}H\{31P\}$ NMR spectrum of complex **3** generated in THF-d_8

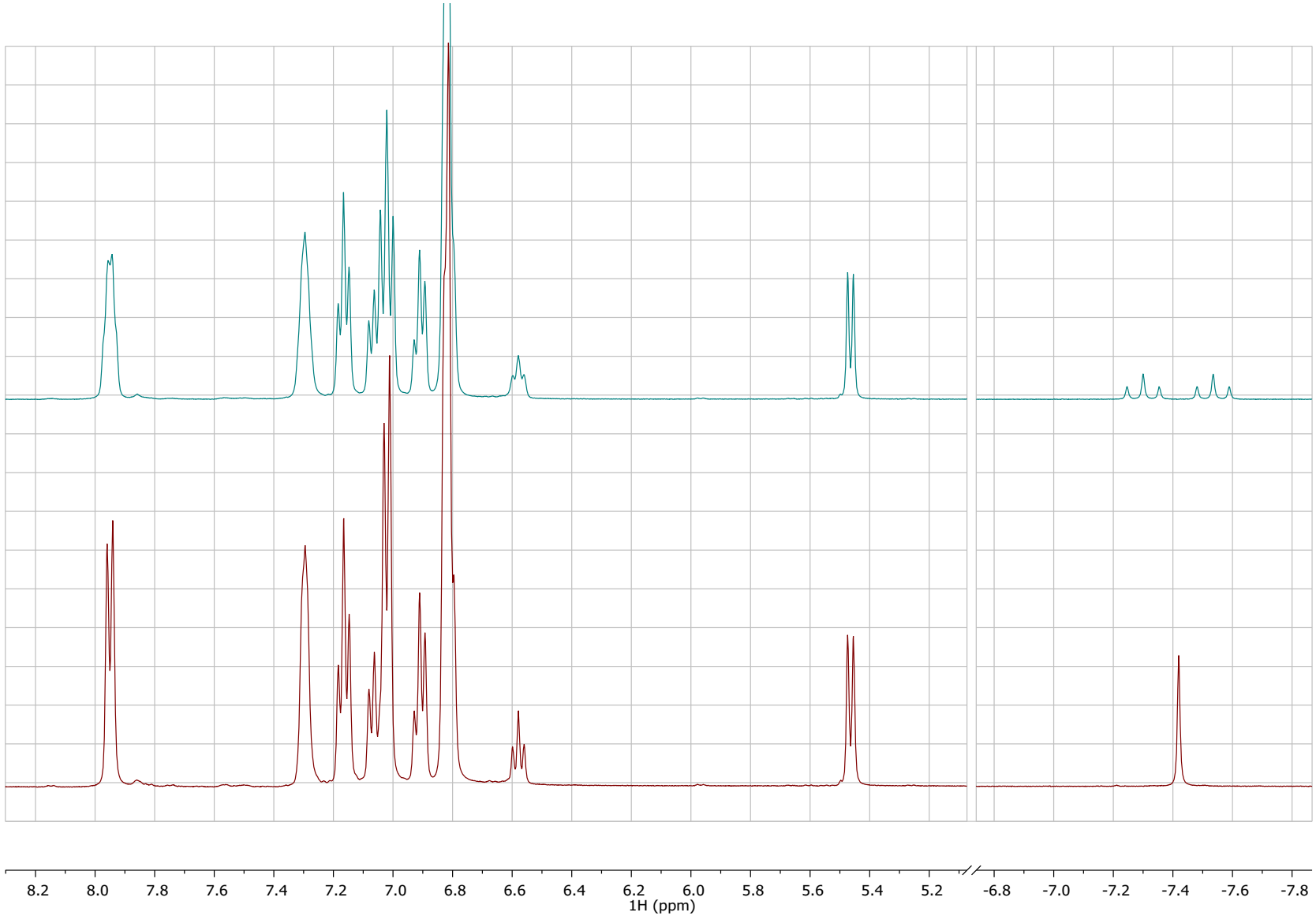

Figure S17. Comparison between ^{1}H NMR spectra with (bottom) and without (top) ^{31}P decoupling for complex **3** generated in THF-d_8

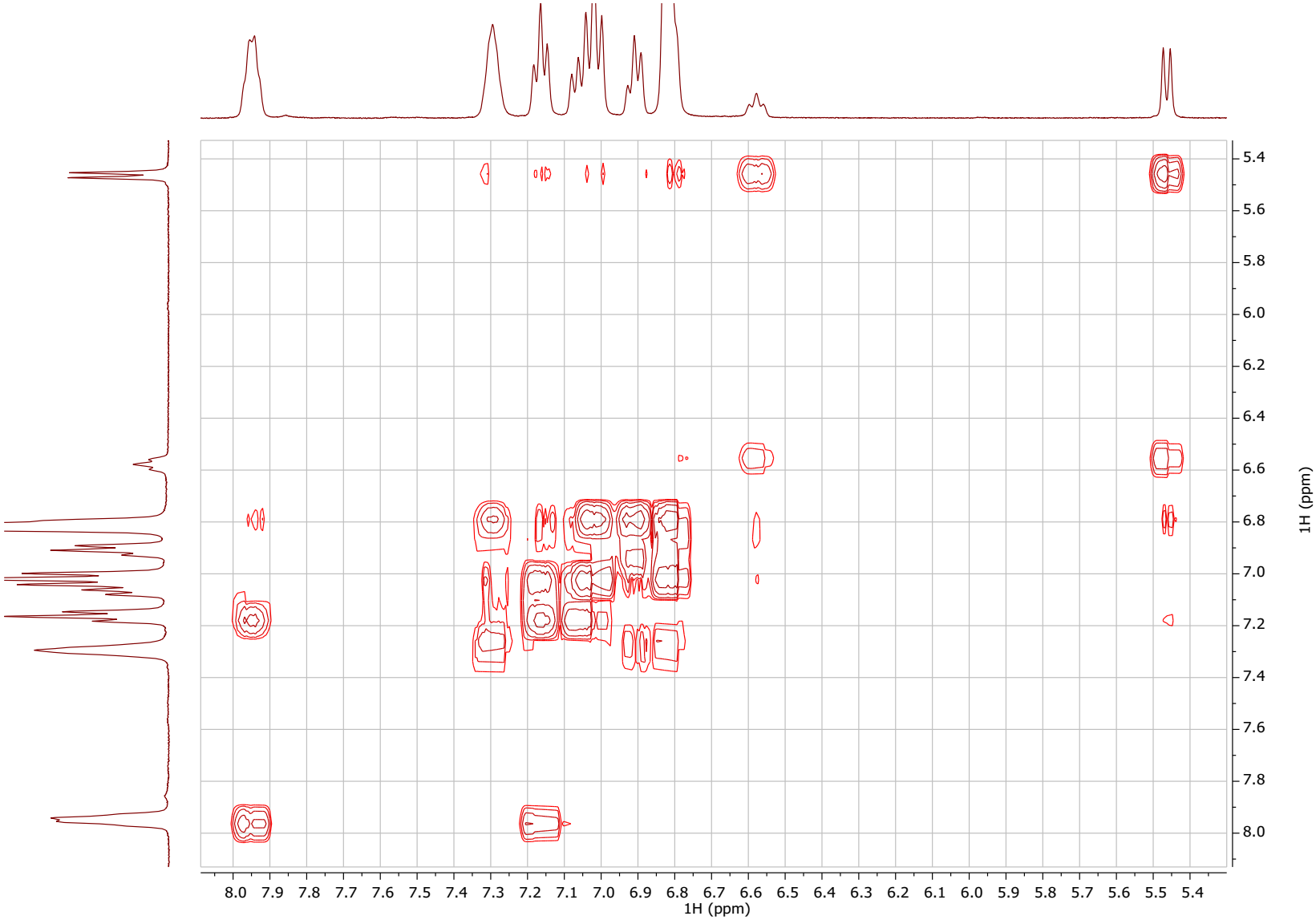

Figure S18. gCOSY spectrum of complex **3** generated in THF-d_8

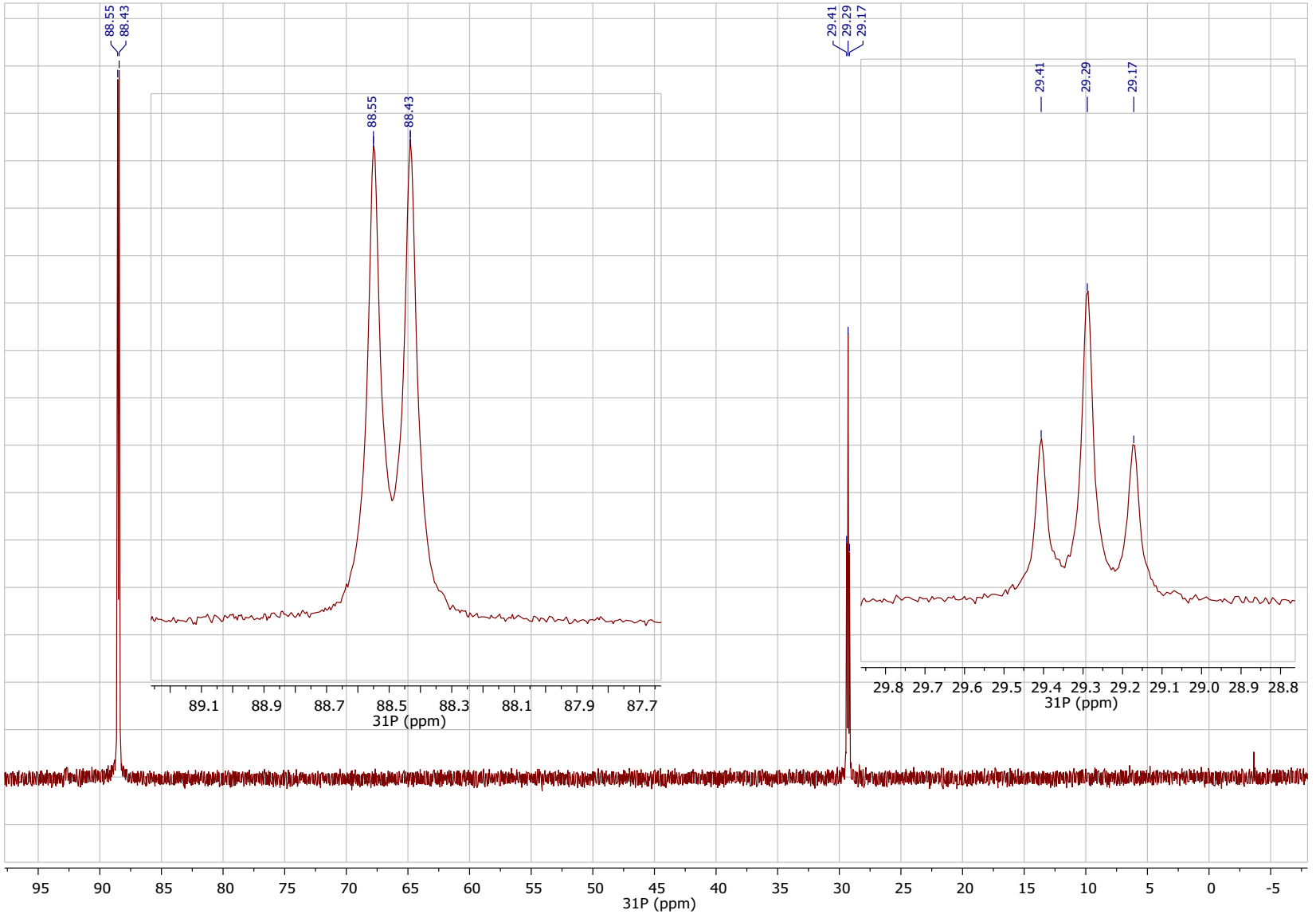

Figure S19. $^{31}P\{^{1}H\}$ spectrum of complex **3** generated in THF-d_8

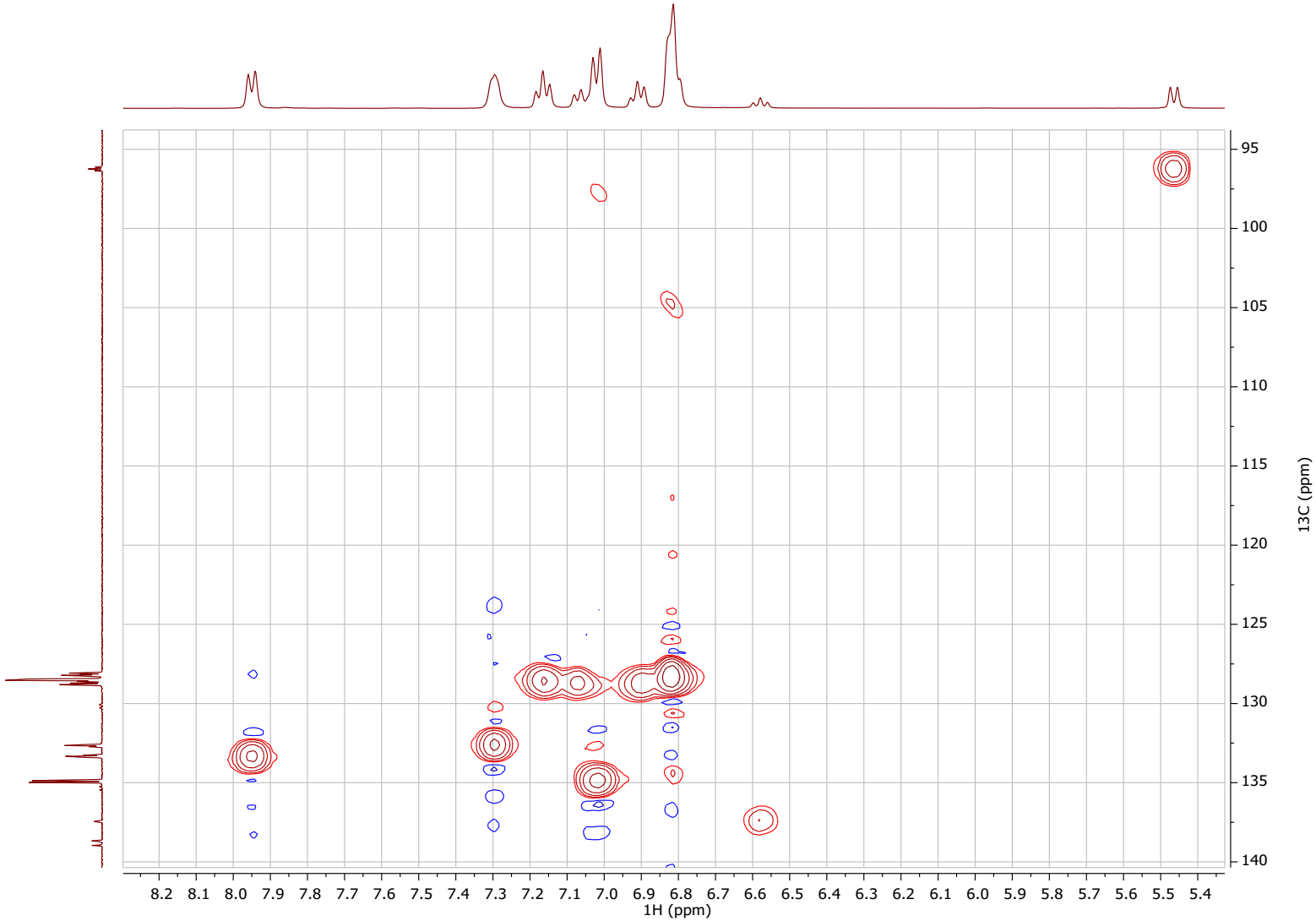

Figure S20. gHMQC spectrum of complex **3** generated in THF-d_8

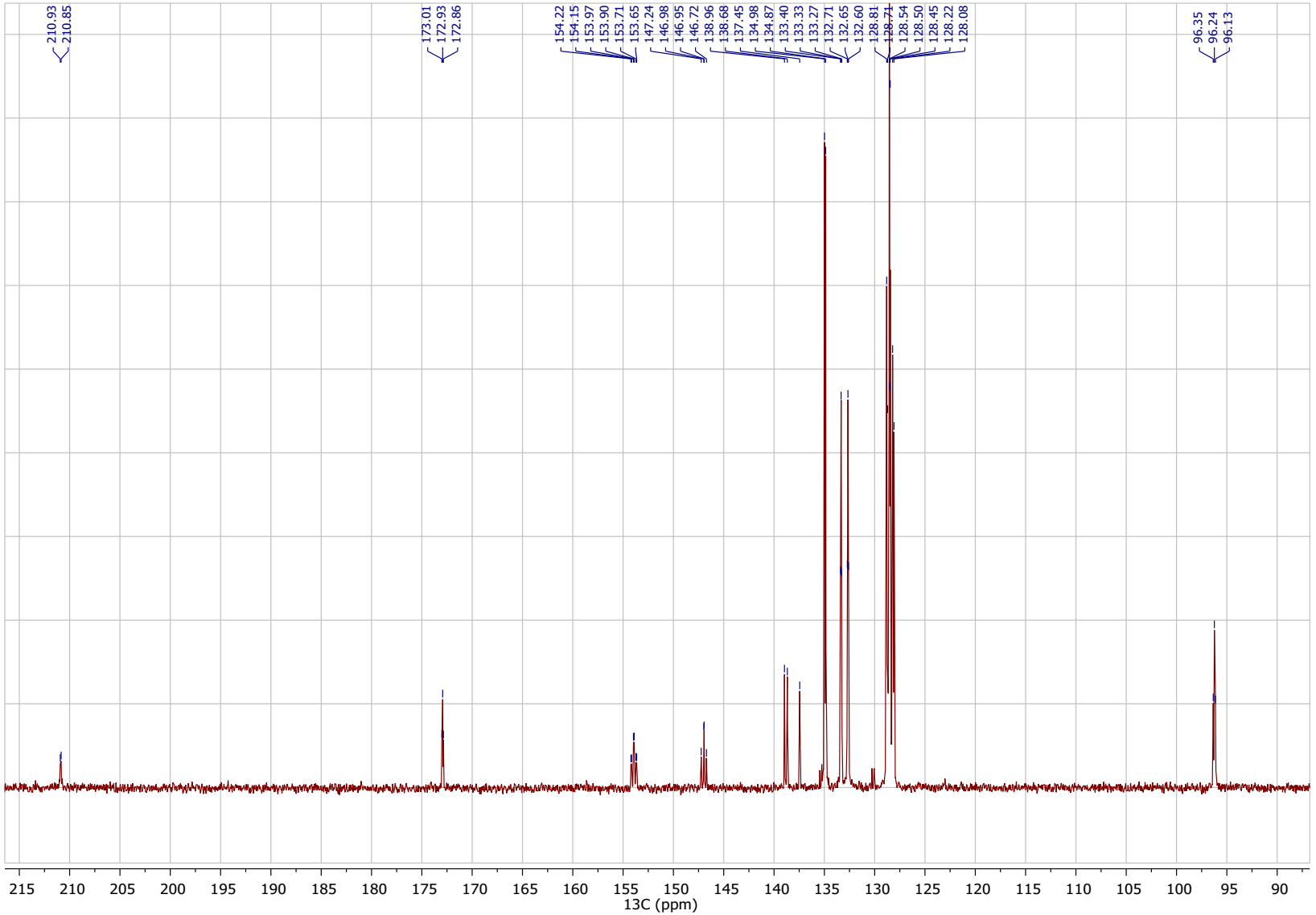

Figure S21. ^{13}C spectrum of complex **3** generated in THF-d_8

Ligand exchange in complex 3 – generation of 3DMSO

Complex **3** generated as above in THF was treated with 50 mkl DMSO, the tube was shaken and the NMR spectra were recorded at 5 and 120 minute intervals.

Ligand exchange can be observed by the disappearance of additional H-P coupling of Ru-H resonance and notable shift of ortho-C***H*** resonances of $-PPh_2$ groups and those of pyridine backbone.

Complex **3DMSO** produced in this way was crystallized from THF using diethyl ether vapour diffusion method.

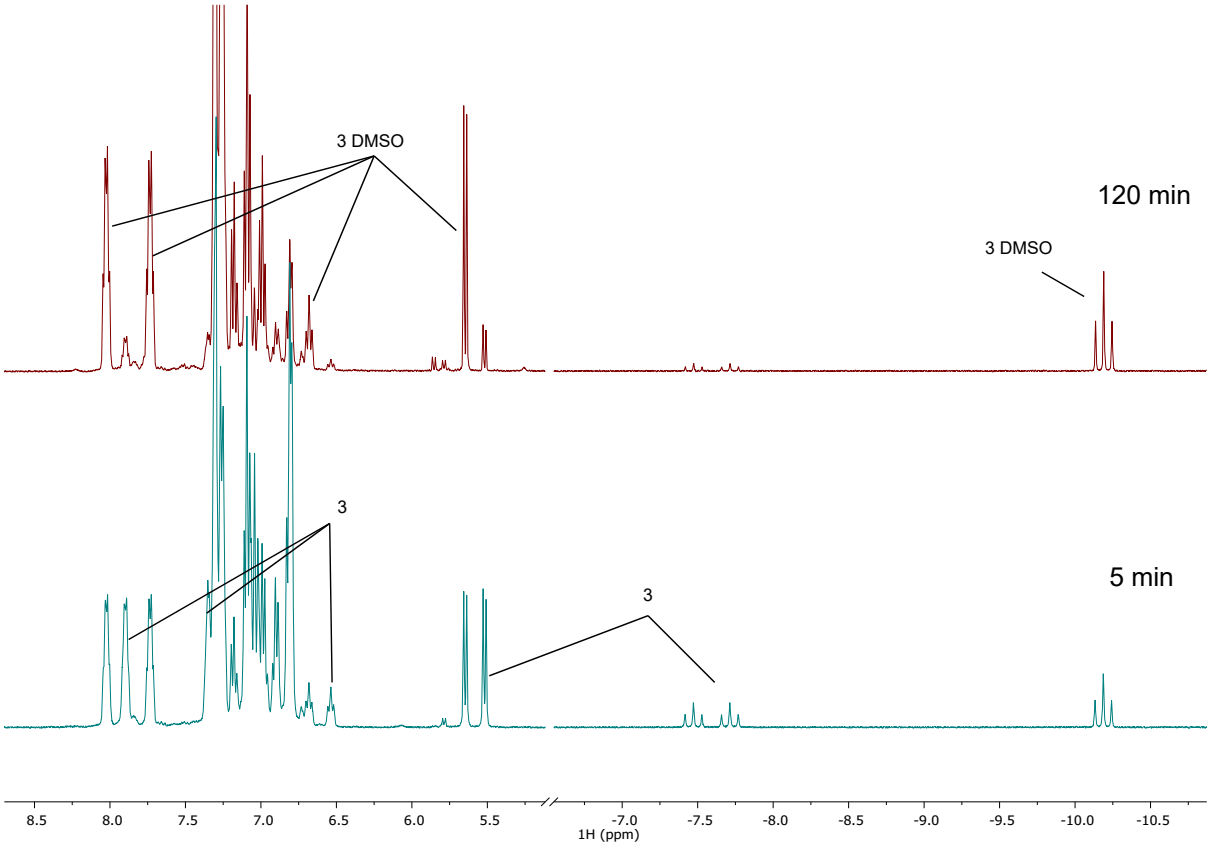

Figure S22. ^{1}H NMR follow up of ligand exchange in complex **3** generated in THF-d_8 in the presence of DMSO

Sequential deprotonation of complex 1 in DMSO – evidence for PPh_3 ligand exchange.

The procedure for generation of complex **3** was replicated in DMSO-d_6 solvent with KO^{t}Bu loaded in two portions to produce **2** and **3** sequentially. Neutral complex **2** was stable in DMSO while complex **3** immediately underwent ligand exchange forming **3-DMSO** under these conditions.

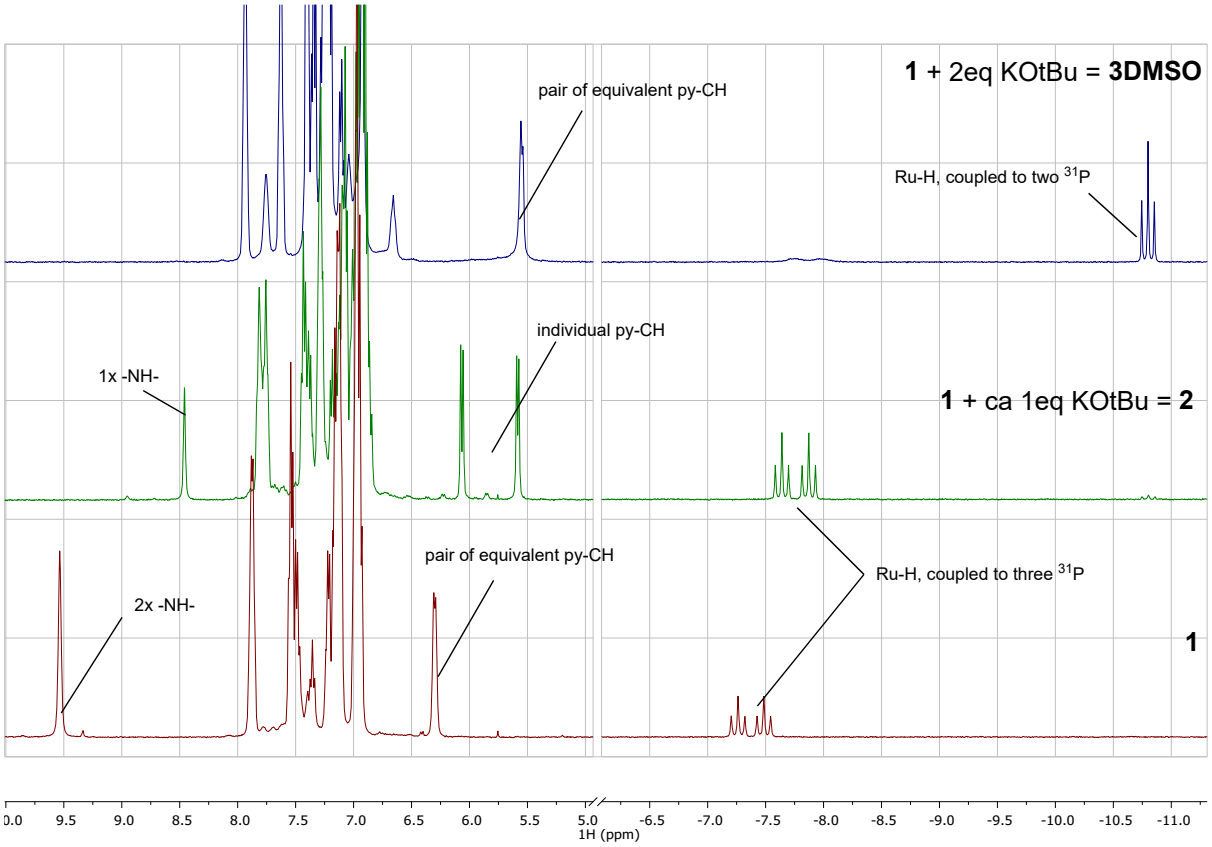

Figure S23. ^{1}H NMR follow up of sequential deprotonation of complex **1** in DMSO.

Note the disappearance of NH resonance in the 8-10 ppm region, changes in molecular symmetry indicated by the pyridine backbone proton resonances (5.5-6.5 ppm) and substitution of PPh_3 ligand in **3** ligand evidenced by the change of the H-P coupling pattern for Ru-H resoncance.

Interaction of complex 3 with H_2: dihydride complex 4:

Complex **3** generated as above in THF was placed into the NMR Quick pressure tube and exposed to 3 bar H_2. The tube was gently shaken before the measurement. It was noted that addition of hydrogen to **3** takes ca 60 minutes at room temperature and proceeds within 5 minutes at 50°C.

IMPORTANT: The presence of trace amounts of free KO^{t}Bu was found to be critical for generation of **4**. For example, if solution of **3** is generated using 1.95 eq of base with respect to **1**, no formation of **4** is observed under H_2.

^{1}H{^{31}P} NMR (400 MHz, THF-d_8) δ 8.08 (d, J = 7.7 Hz, 8H, -PPh_2 C**H**-*ortho)*, 7.29 (m, 15H, free PPh_3), 7.14 (t, J = 7.3 Hz, 8H, -PPh_2 C**H**-*meta*), 7.02 (t, J = 7.1 Hz, 4H, -PPh_2 C**H**-*para*), 6.60 (t, J = 7.8 Hz, 1H, Py-CH para), 5.55 (d, J = 7.9 Hz, 2H, Py-CH meta), -7.40 (s, 2H, Ru-$(H)_2$).

^{13}C NMR (101 MHz, THF-d_8) δ 213.63 (t, insufficient sensitivity to accurately determine the coupling constant, Ru-***C***O), 170.05 (t, J = 9.6 Hz, py-$\boldsymbol{C_q}$), 151.73 (t, J = 22.7 Hz, -PPh_2-$\boldsymbol{C_q}$), 134.55 (t, J = 3.3 Hz, py-***C***H-para), 131.04 (t, J = 7.2 Hz, -PPh_2 **C**H-*ortho*), 126.42 (t, J = 4.6 Hz, , -PPh_2 **C**H-*meta*), 126.26 (s, , -PPh_2 **C**H-*para*), 92.96 (t, J = 10.4 Hz, py-***C***H-meta).

Additional peaks observed for free PPh_3: 137.52 (d, J = 12.1 Hz, free PPh_3, $\boldsymbol{C_q}$), 133.50 (d, J = 19.7 Hz, ortho **C**H), 128.41 (s, para **C**H), 128.23 (d, J = 6.9 Hz, meta **C**H),

NOTE: Generation of complex **4** was attempted in DMSO-d_6 solvent using the identical procedure, however no conversion into **4** was observed over the course of 3 hours.

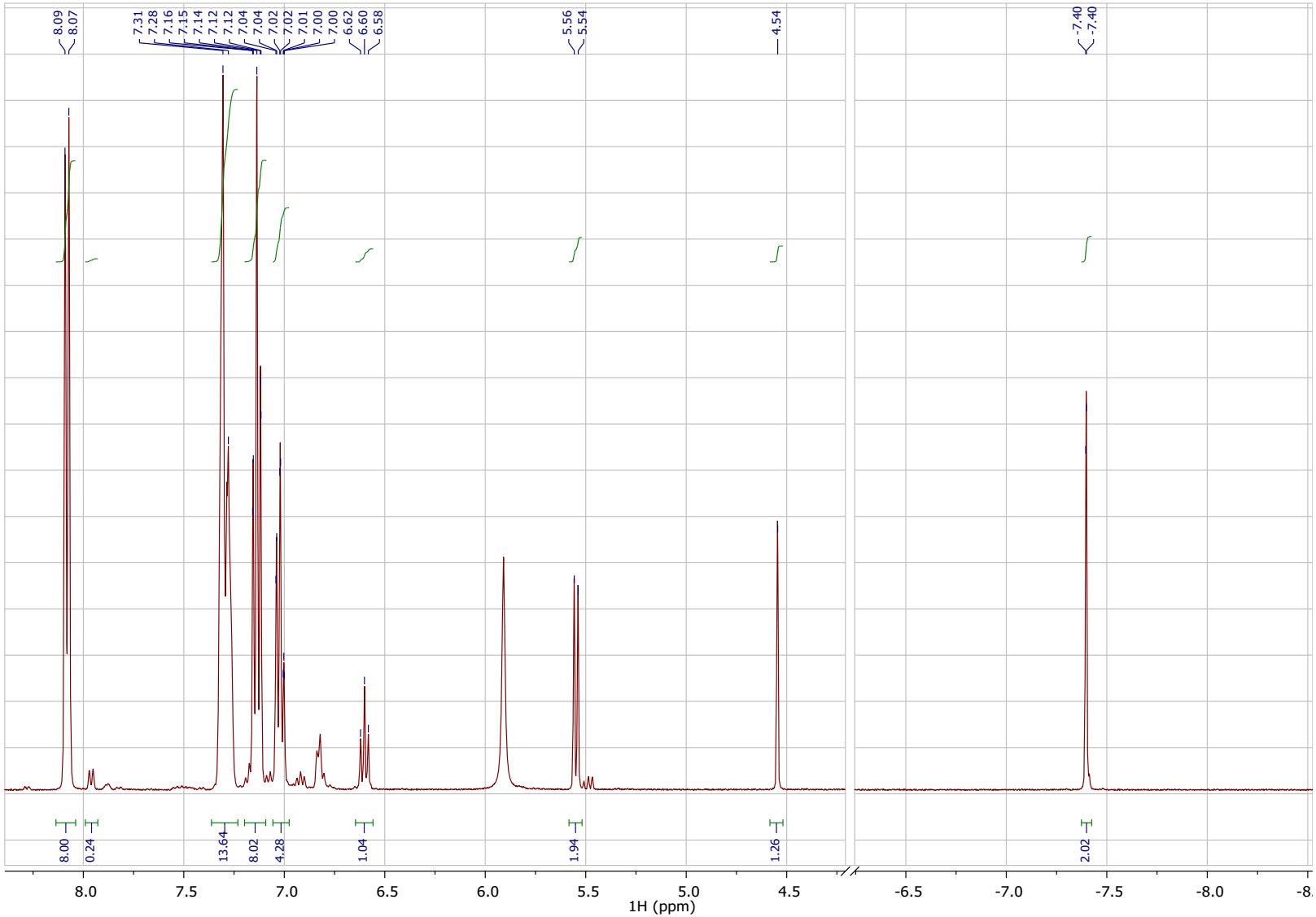

Figure S24. $^{1}H\{31P\}$ NMR of complex **4** generated in THF-d_8.

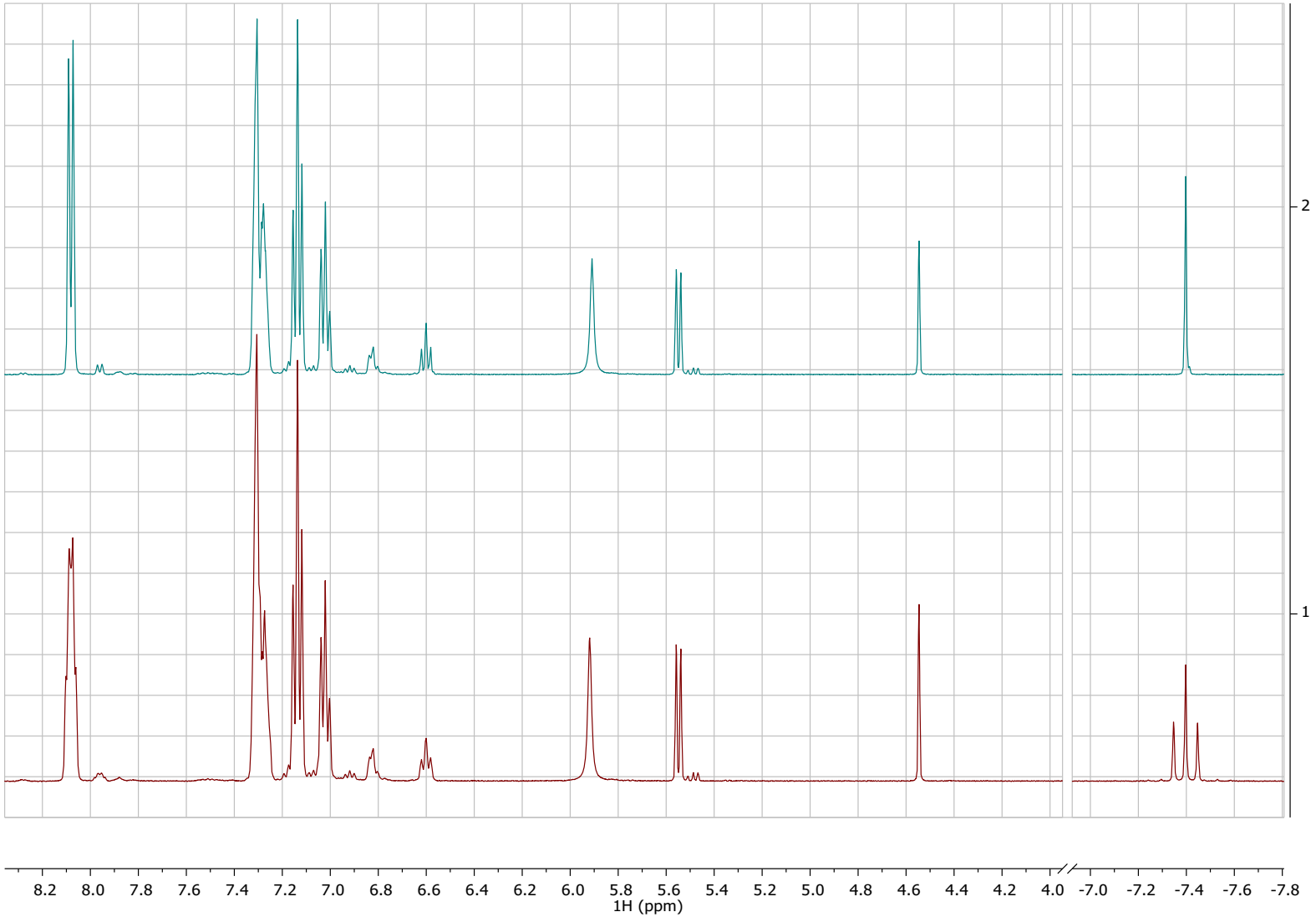

Figure S25. Comparison between ^{1}H and $^{1}H\{31P\}$ NMR of complex **4** generated in THF-d_8.

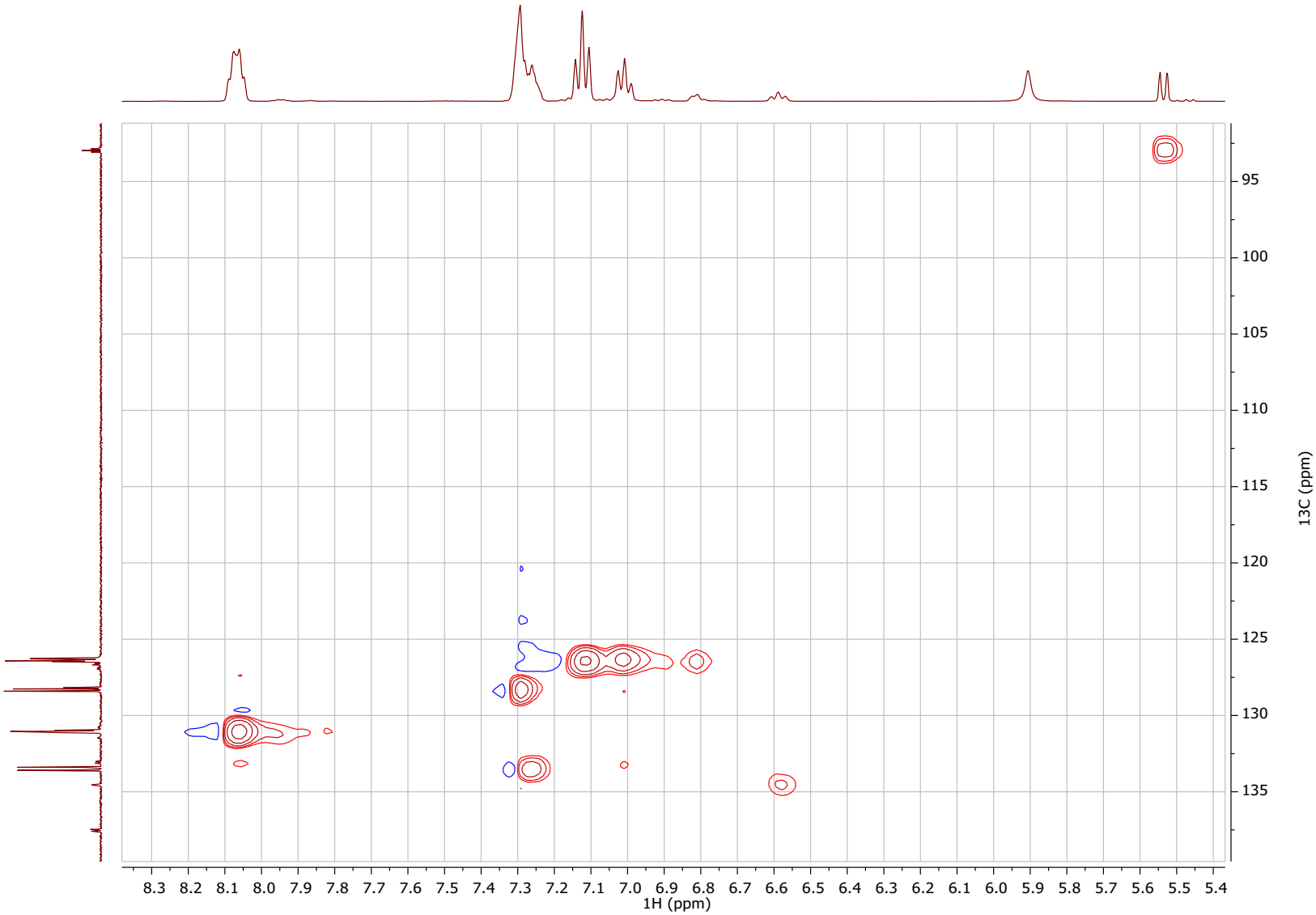

Figure S26. gHMQC spectrum of complex **4** generated in THF-d_8.

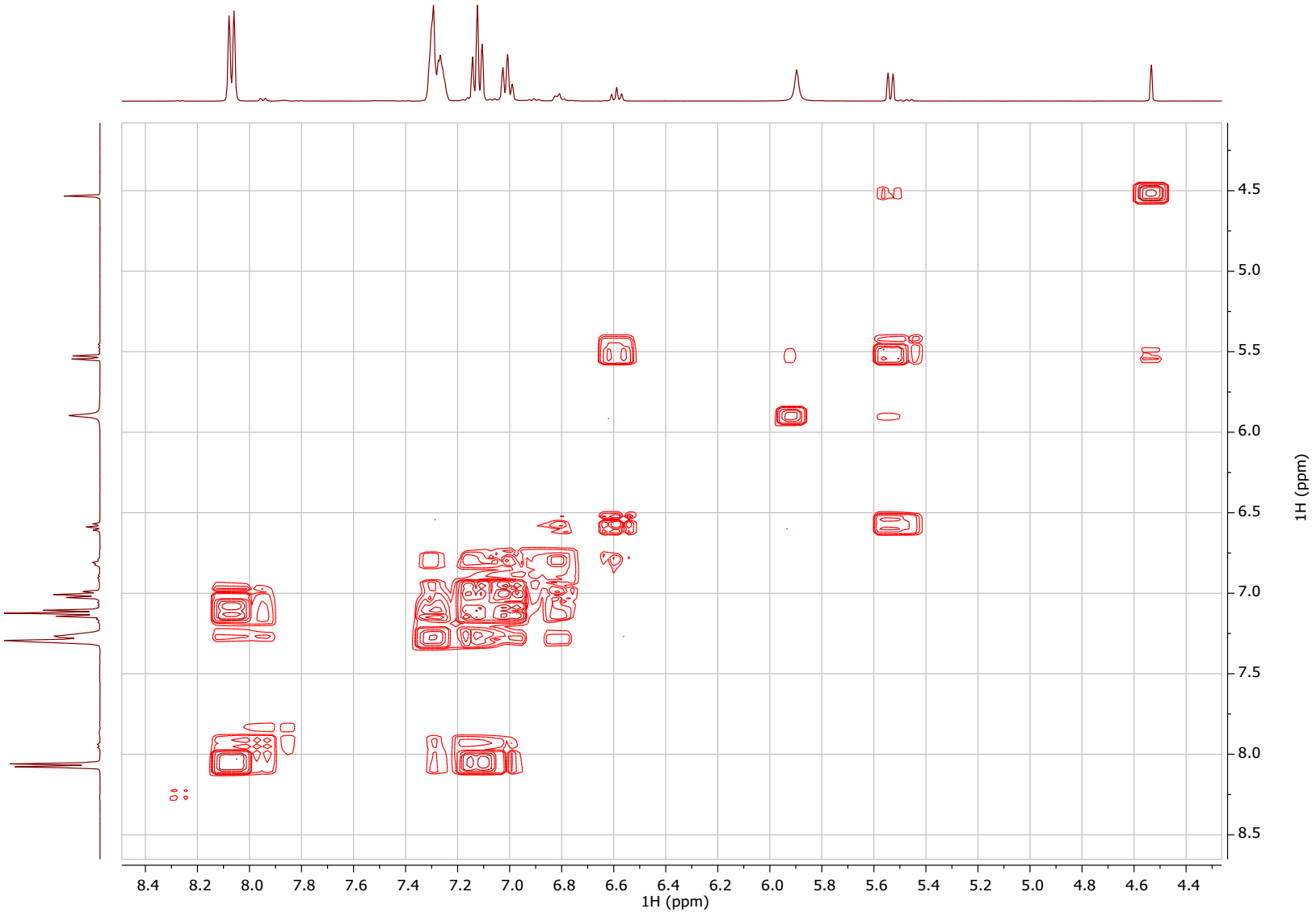

Figure S27. gCOSY spectrum of complex **4** generated in THF-d_8.

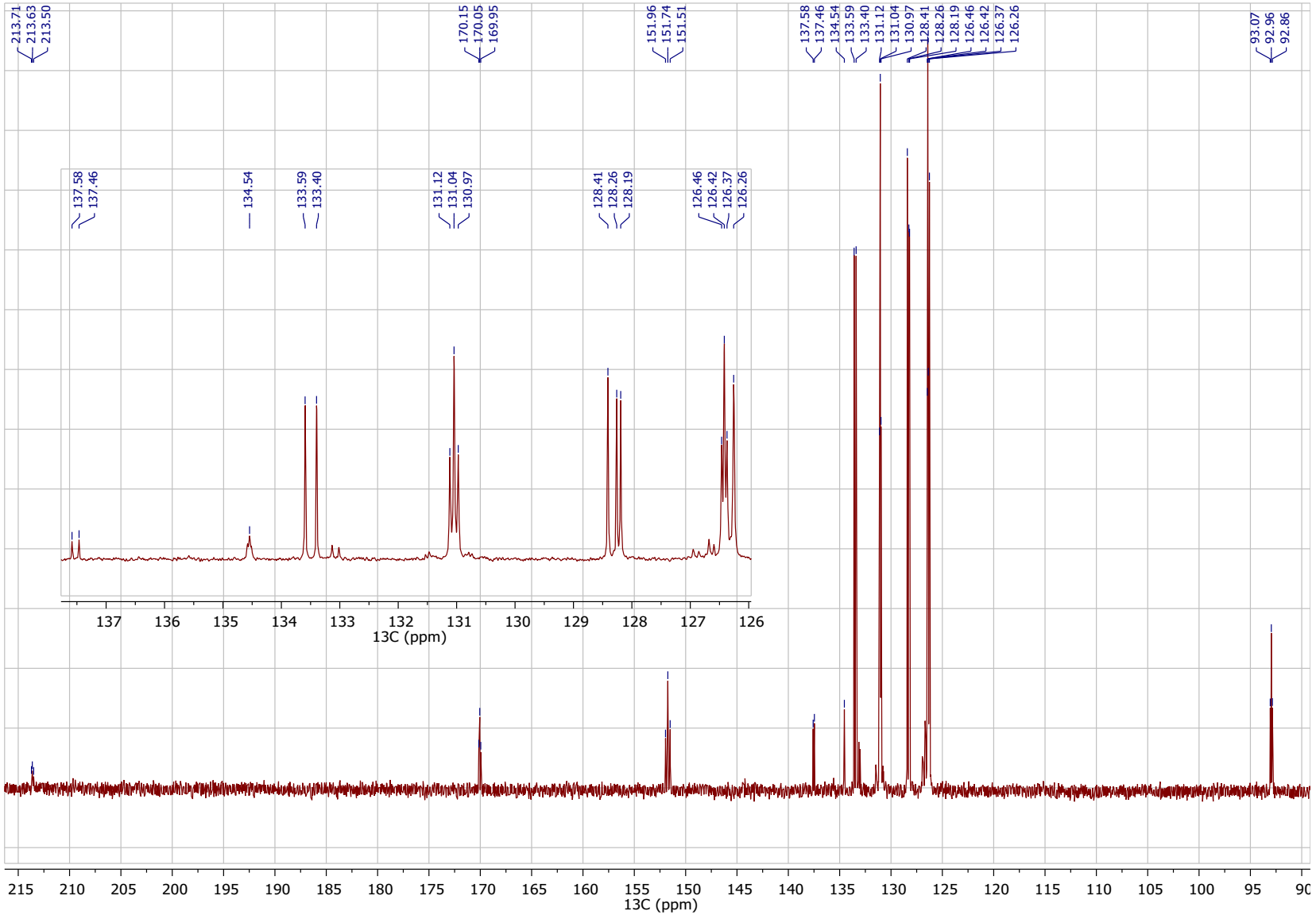

Figure S28. ^{13}C NMR spectrum of complex **4** generated in THF-d_8.

Interaction of dihydride complex 4 with CO_2:

Dihydride complex **4** generated as above in THF in the NMR Quick pressure tube was connected to the gas manifold and the atmosphere in the tube was quickly exchanged for 3 bar CO_2. This led to immediate formation of gel-like solid. The tube was gently shaken before the measurement that confirmed that singly deprotonated complex **2** was the sole soluble product of this reaction.

To identify the precipitate this experiment was repeated using $^{13}CO_2$ gas. THF solution was filtered off and the solids were dissolved in DMSO-d_6. ^{1}H and ^{13}C NMR confirmed the formation of potassium formate and potassium tert-butyl carbonate as the main species containing the ^{13}C label.

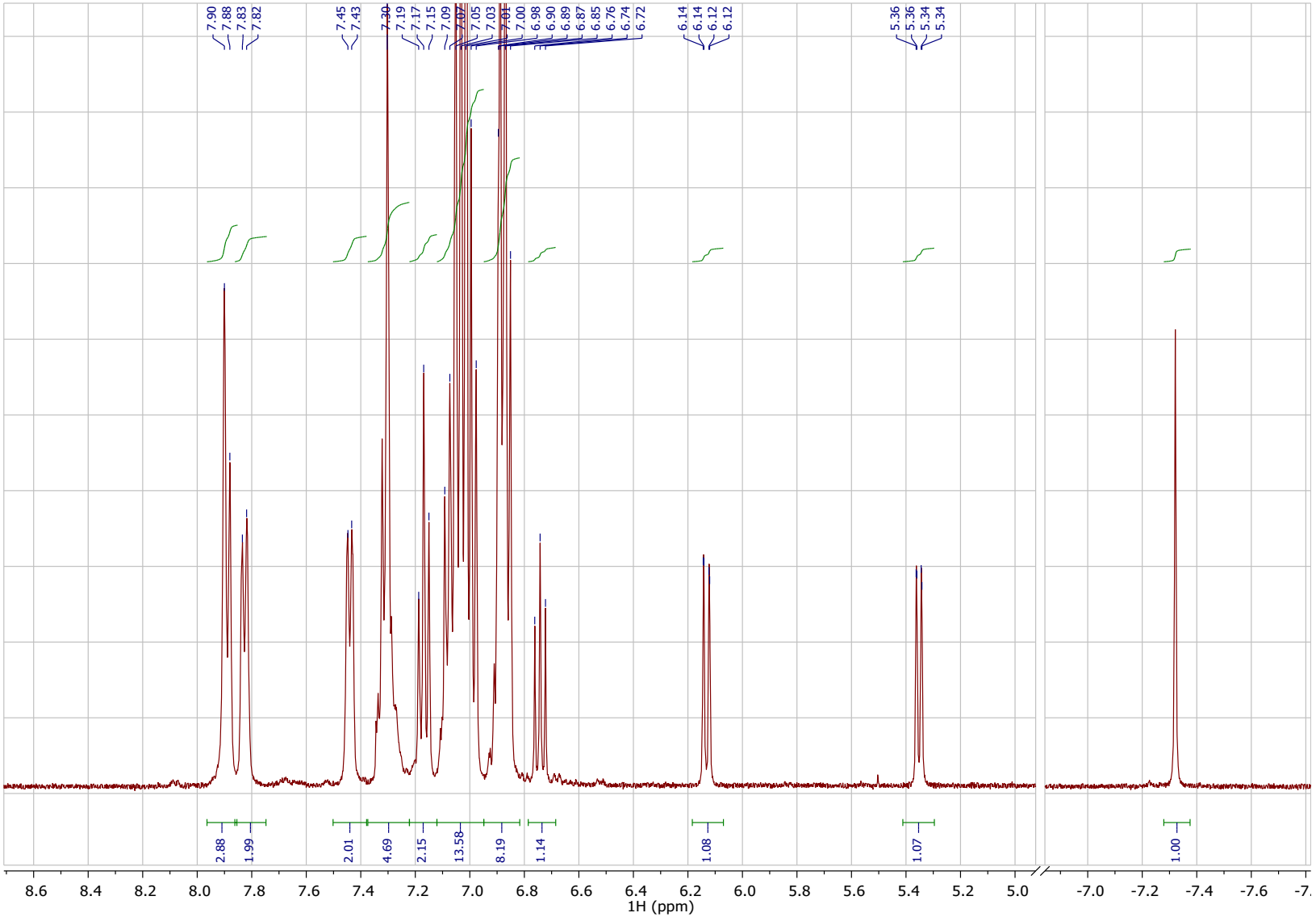

Figure S29. $^{1}H\{^{31}P\}$ NMR spectrum of complex **2** generated in THF-d_8 in reaction of complex **4** with CO_2

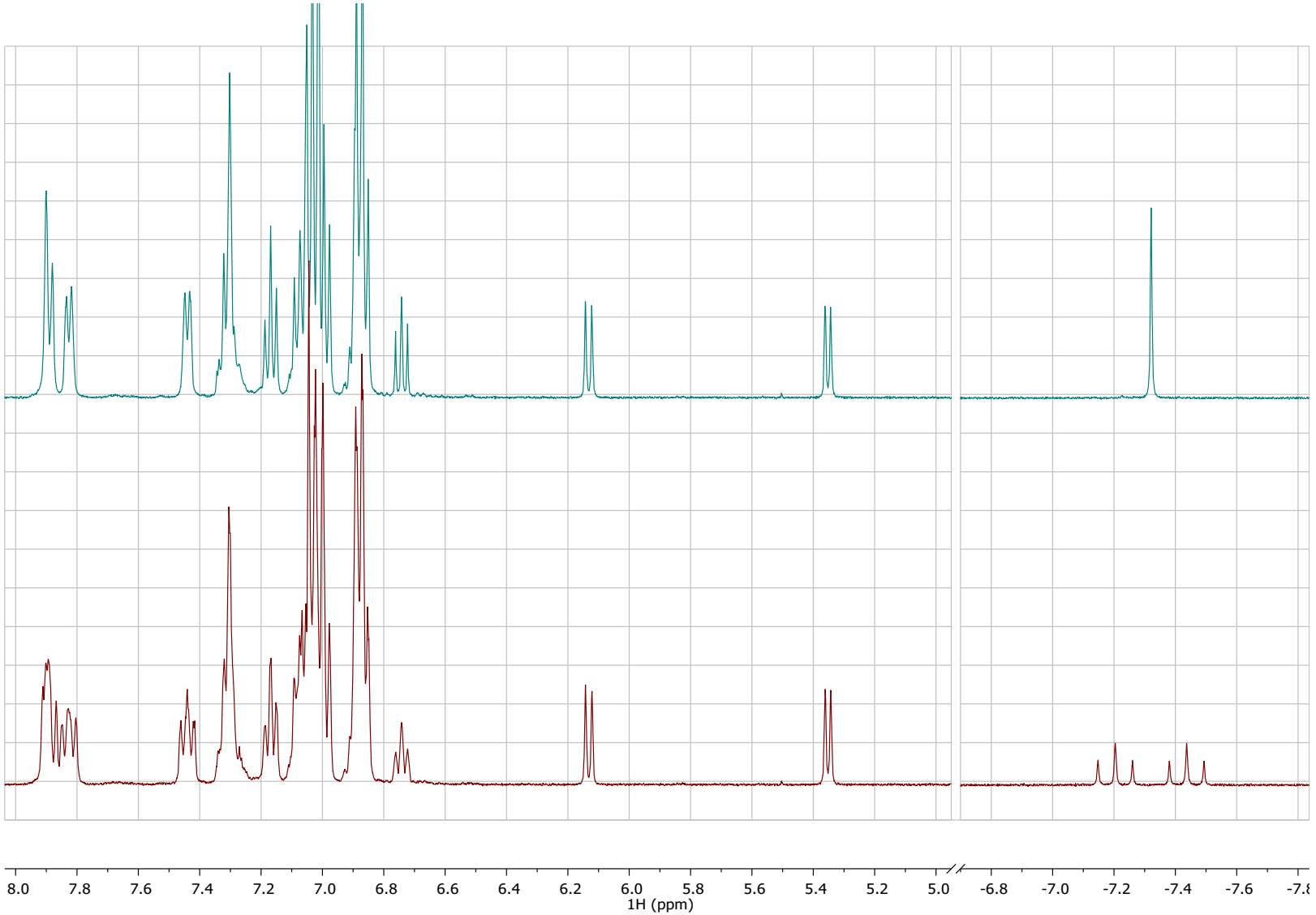

Figure S30. Comparison of ^{1}H and $^{1}H\{^{31}P\}$ NMR spectra of complex **2** generated in THF-d_8 in reaction of complex **4** with CO_2

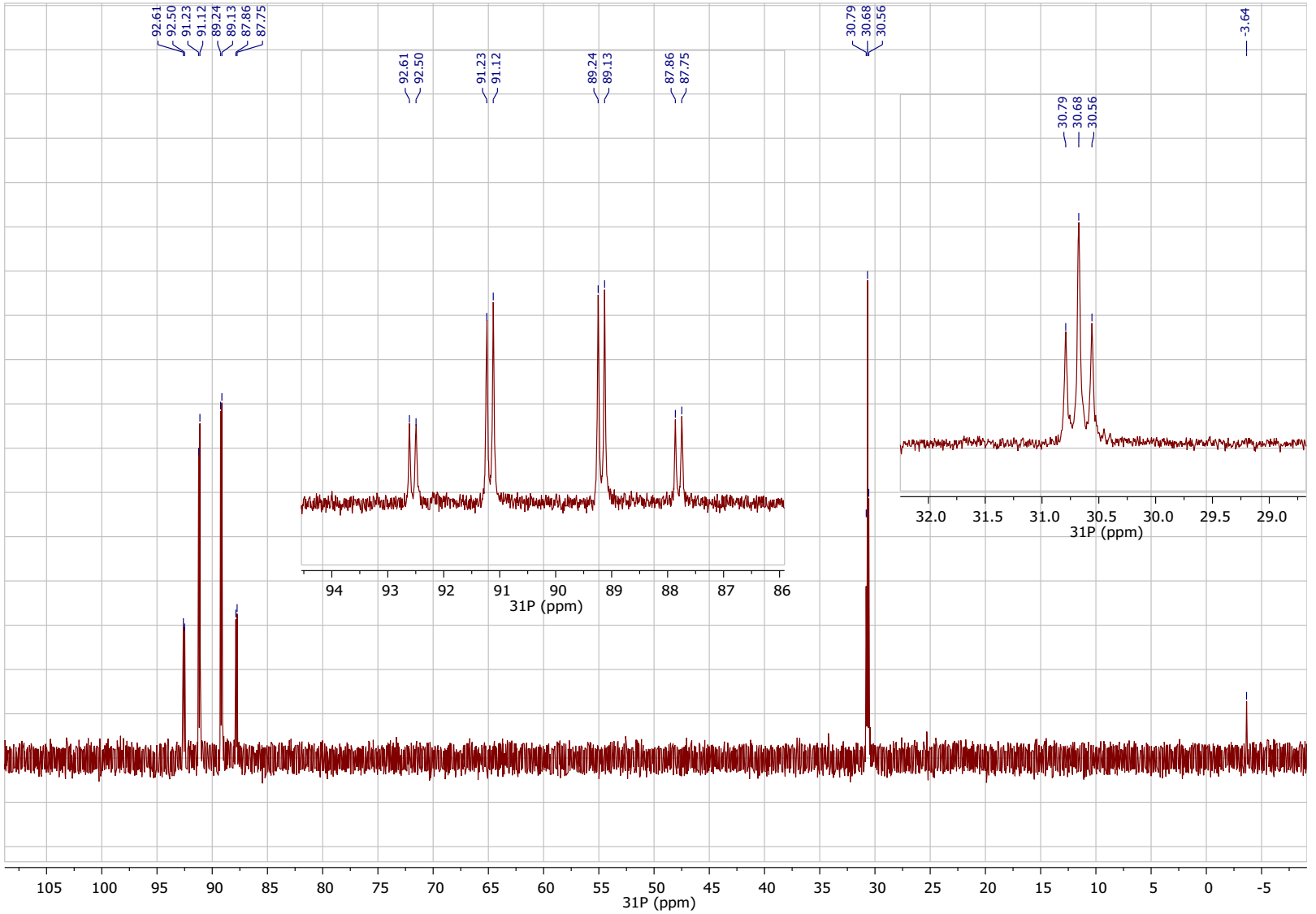

Figure S31. ^{31}P NMR spectrum of complex **2** generated in THF-d_8 in reaction of complex **4** with CO_2

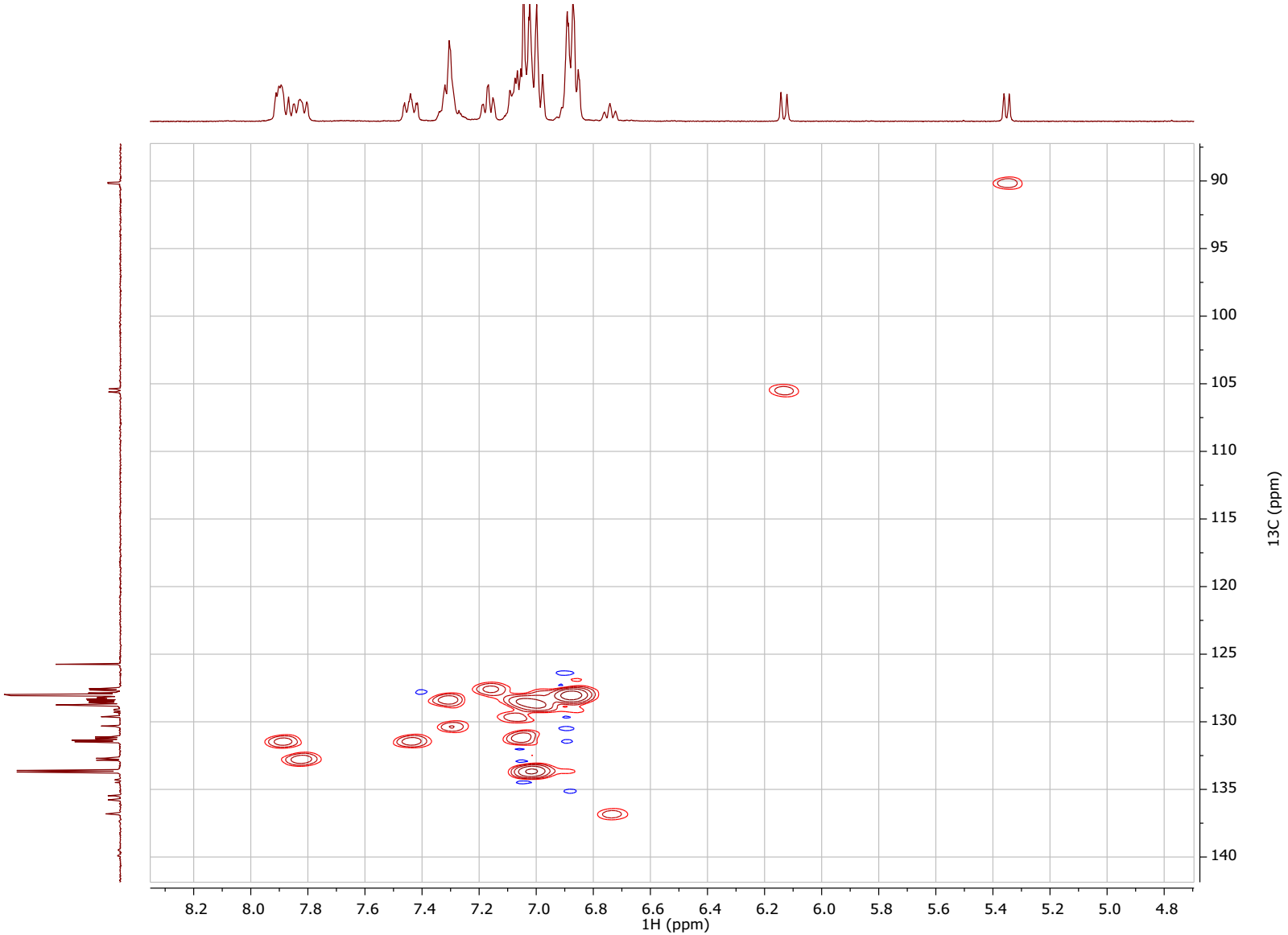

Figure S32. gHMQC spectrum of complex **2** generated in THF-d_8 in reaction of complex **4** with CO_2

Figure S33. gCOSY spectrum of complex **2** generated in THF-d_8 in reaction of complex **4** with CO_2

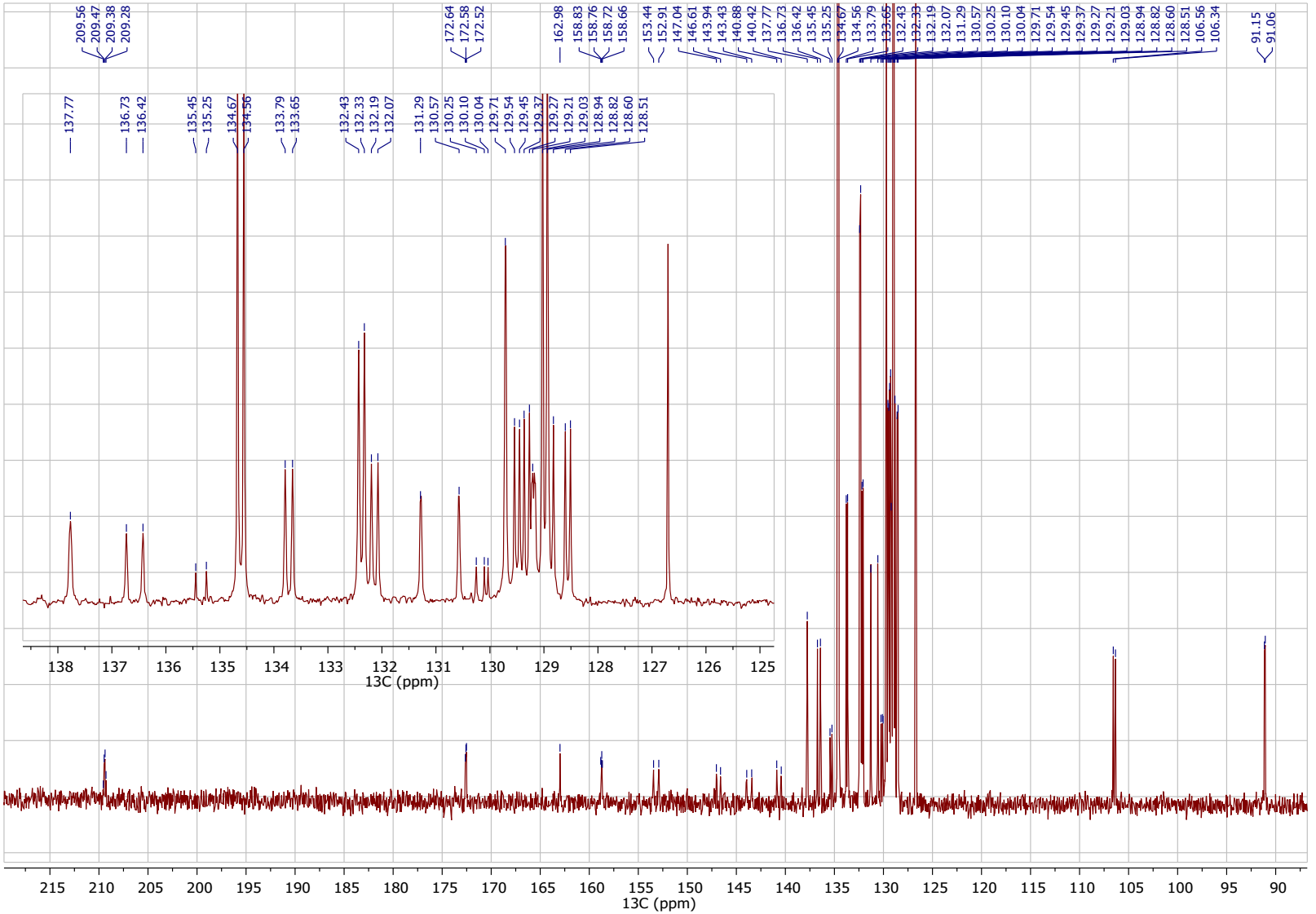

Figure S34. ^{13}C NMR spectrum of complex **2** generated in THF-d_8 in reaction of complex **4** with CO_2

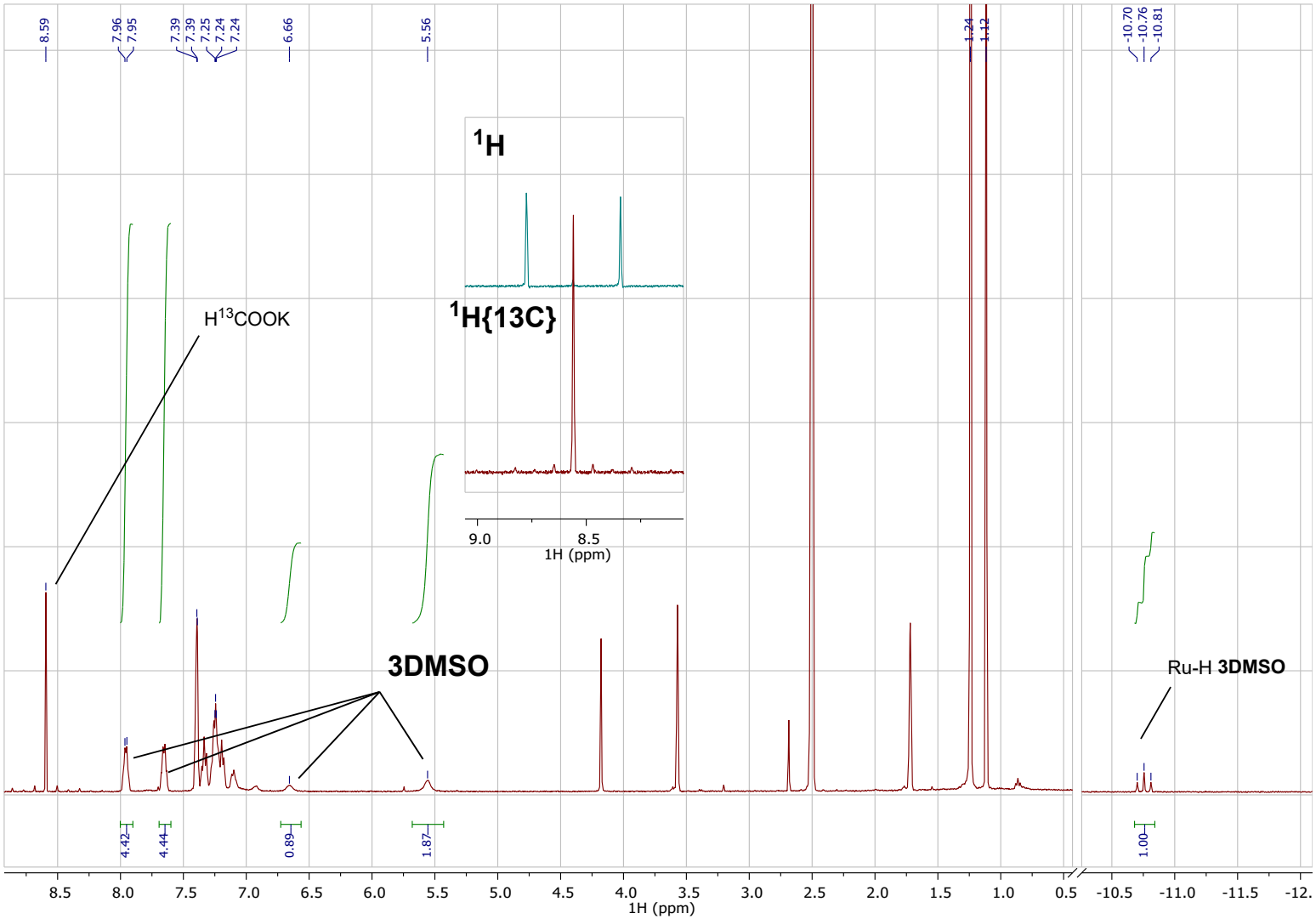

Figure S35. $^{1}H\{^{13}C\}$ NMR spectrum of precipitate generated in THF-d_8 in reaction of **4** with $^{13}CO_2$ atmosphere. Note residual complex **3** and a potassium formate peak at 8.59 ppm. Insert shows comparison of ^{1}H and $^{1}H\{^{13}C\}$ decoupled spectra.

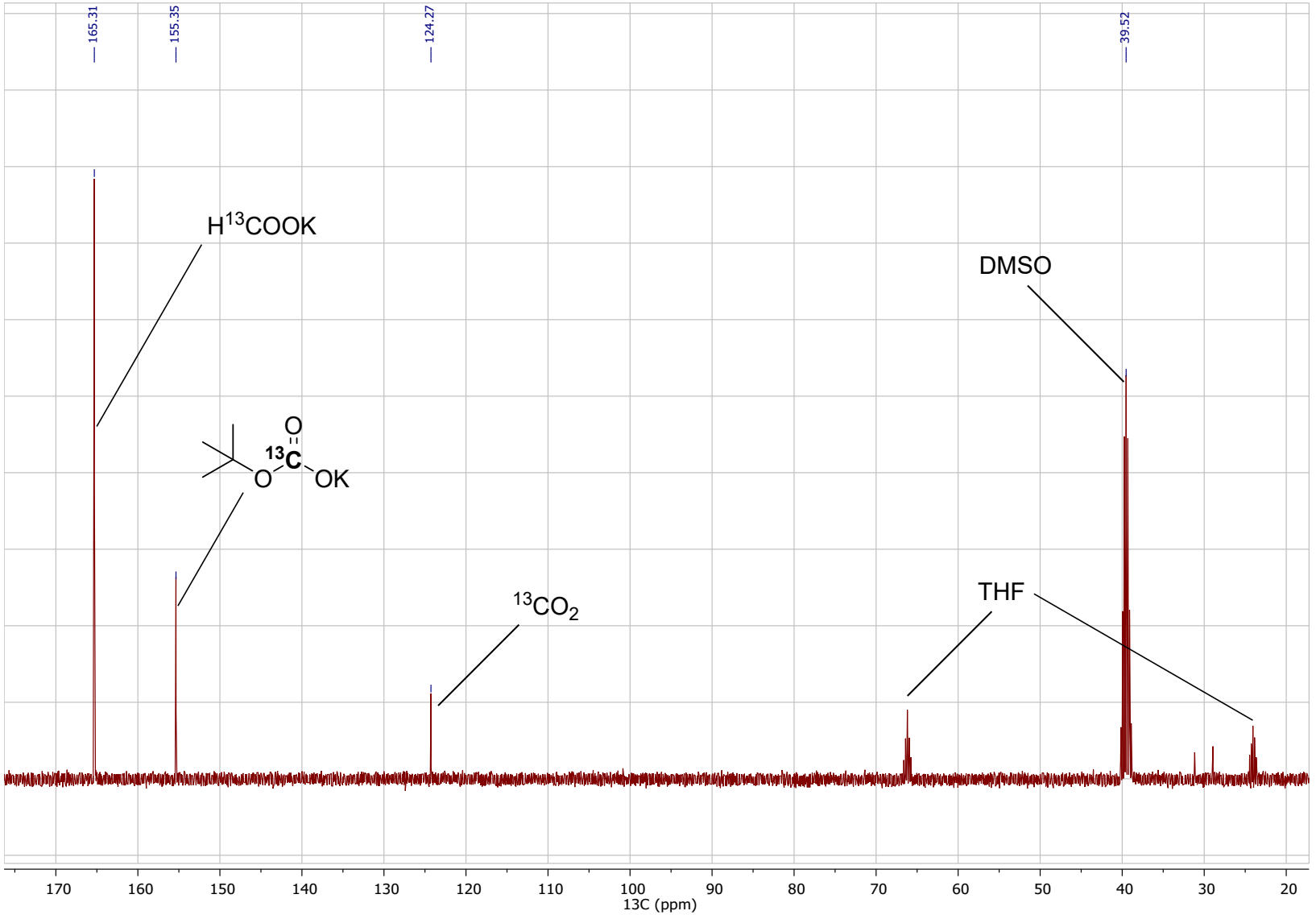

Figure S36. ^{13}C NMR spectrum of precipitate generated in THF-d_8 in reaction of **4** with $^{13}CO_2$ atmosphere.

Generation of formate from singly deprotonated complex 2 in the NMR tube:

Complex **2** generated by reacting **4** with CO_2 as described above was placed into the NMR tube and pressurized with equimolar H_2/CO_2 gas mixture to 3 bar and gently shaken and set aside at room temperature. NMR measurements were performed at 16 and 40 h intervals.

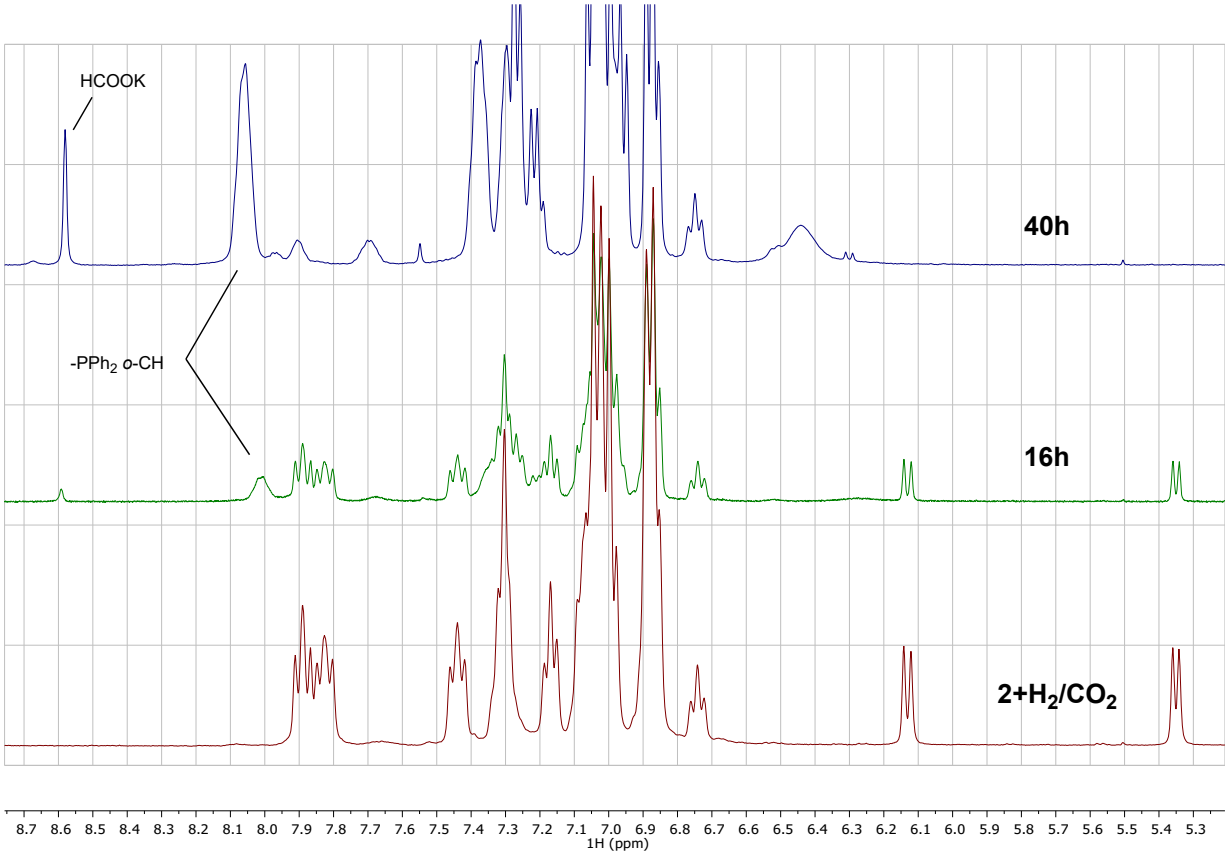

Figure S37. Stacked ^{1}H NMR spectra (aromatic region) for the transformation of complex **2** under H_2/CO_2 gas in THF-d_8. Note the appearance of formate product and formation of new Ru-PN^{3}P species.

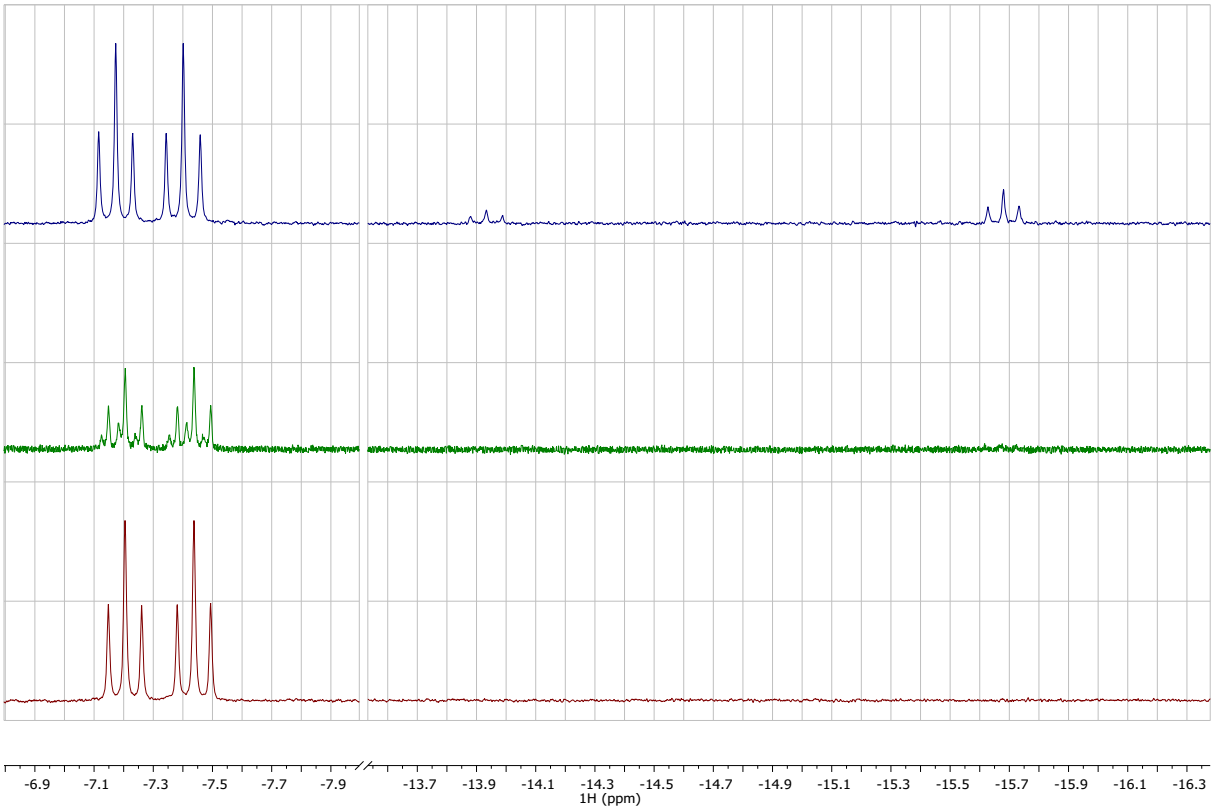

Figure S38. Stacked ^{1}H NMR spectra (hydride region) for the transformation of complex **2** under H_2/CO_2 gas in THF-d_8. Note the gradual transformation of **2**

Reaction of complex 1 with DBU base and KOH in the presence of water

Complex **1** (5.6 mg, 6.18 µmol, 1eq) was dissolved in DMSO-d_6 and 10 eq DBU was added (9.4 mg, 9.2 µL) and the solution was transferred to the NMR tube, set aside at room temperature for 2 h and analysed using NMR spectroscopy.

Complexes **2** and **3DMSO** were identified by their respective hydride and ^{31}P resonance positions.

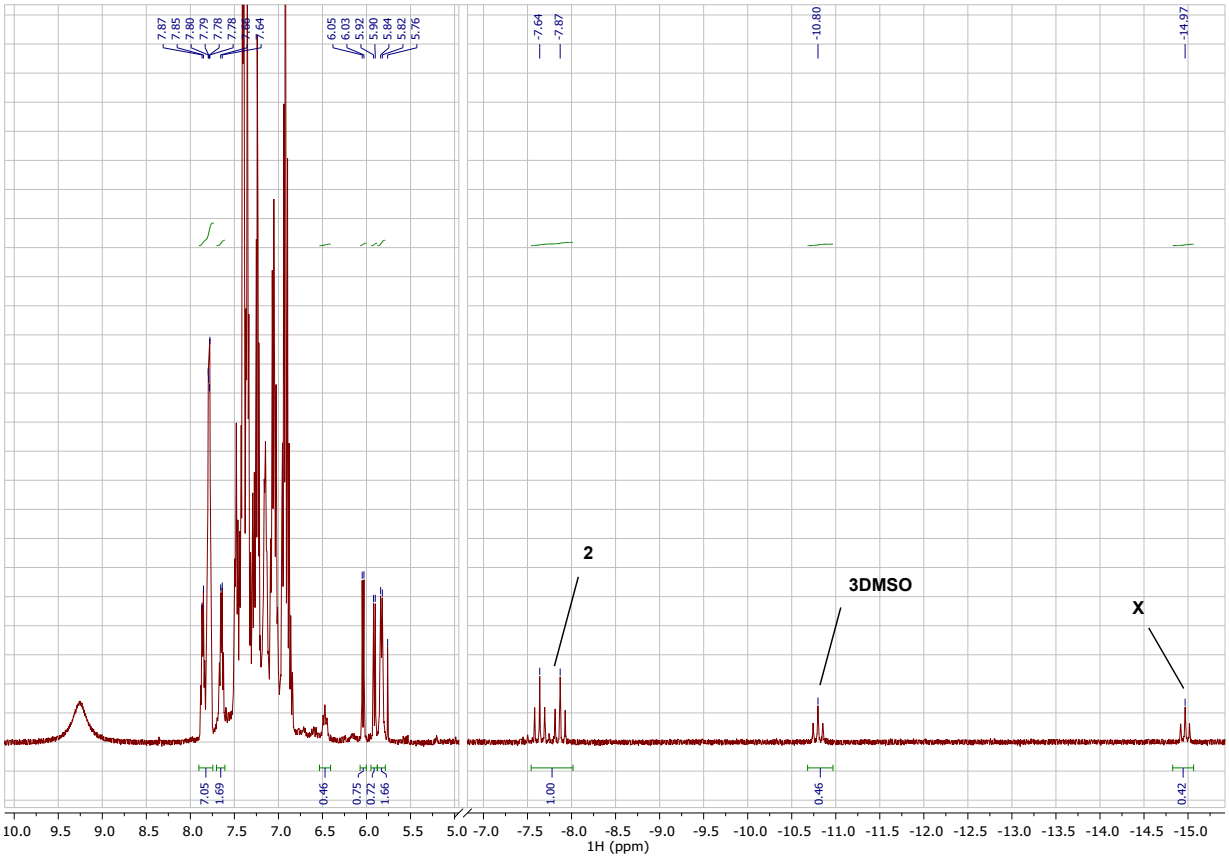

Figure S39. ^{1}H NMR spectrum for reaction between complex **1** and DBU base in DMSO-d_6. Note the hydride resonances consistent with formation of **2** and **3DMSO**. Minor species **X** could not be assigned.

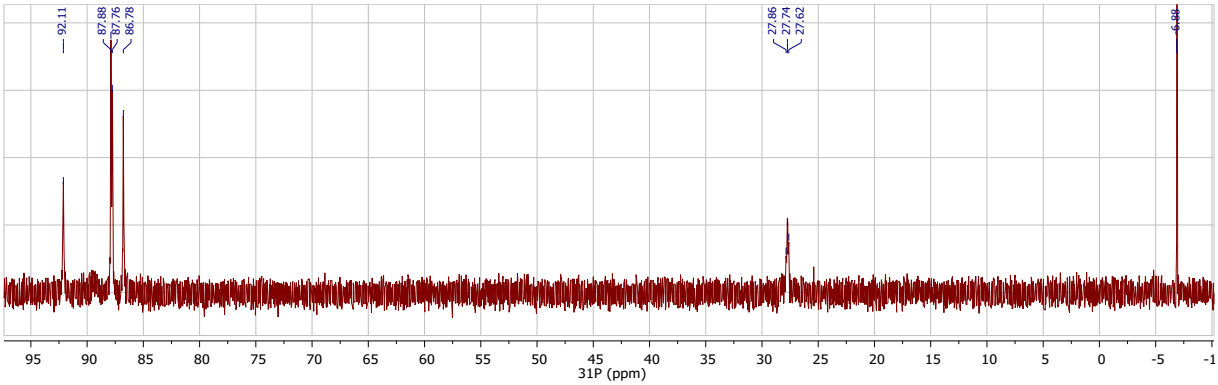

Figure S40. ^{31}H NMR spectrum for reaction between complex **1** and DBU base in DMSO-d_6. Note the free PPh_3 consistent with formation of **3DMSO** and resonance set at 87.8 and 27.7 characteristic of **2**.

Complex **1** (5.6 mg, 6.18 μmol, 1eq) was suspended in THF-d_8 and 20 mkl of 20% KOH solution were added to the suspension. The tube was vigorously shaken and suspended solids dissolved within several minutes. ^{1}H NMR evidenced consumption of **1** and formation of highly dynamic species. Performing the characterization at -50°C we confirmed dearomatization of the PN^{3}P ligand, presence of a single NH proton and assigned the reaction product as a singly deprotonated complex **2**. Additional analysis using IR spectroscopy confirmed the assignment.

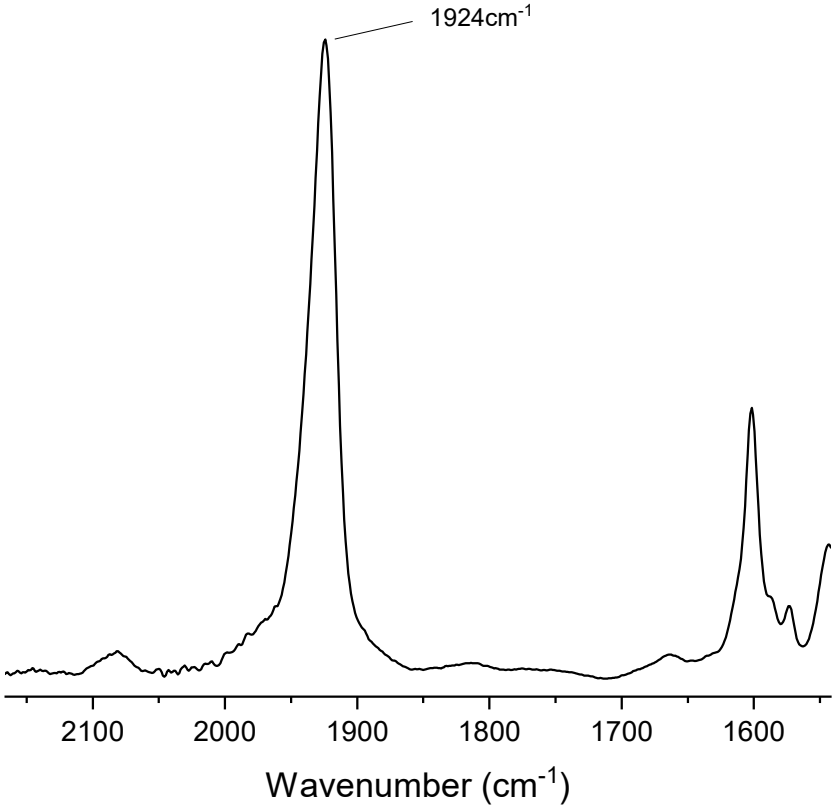

Figure S41. IR spectrum for deprotonation of complex **1** with aqueous KOH. Note the carbonyl band frequency matching that of a singly deprotonated complex 2 prepared in reaction with KO^{t}Bu (Figure S41 below)

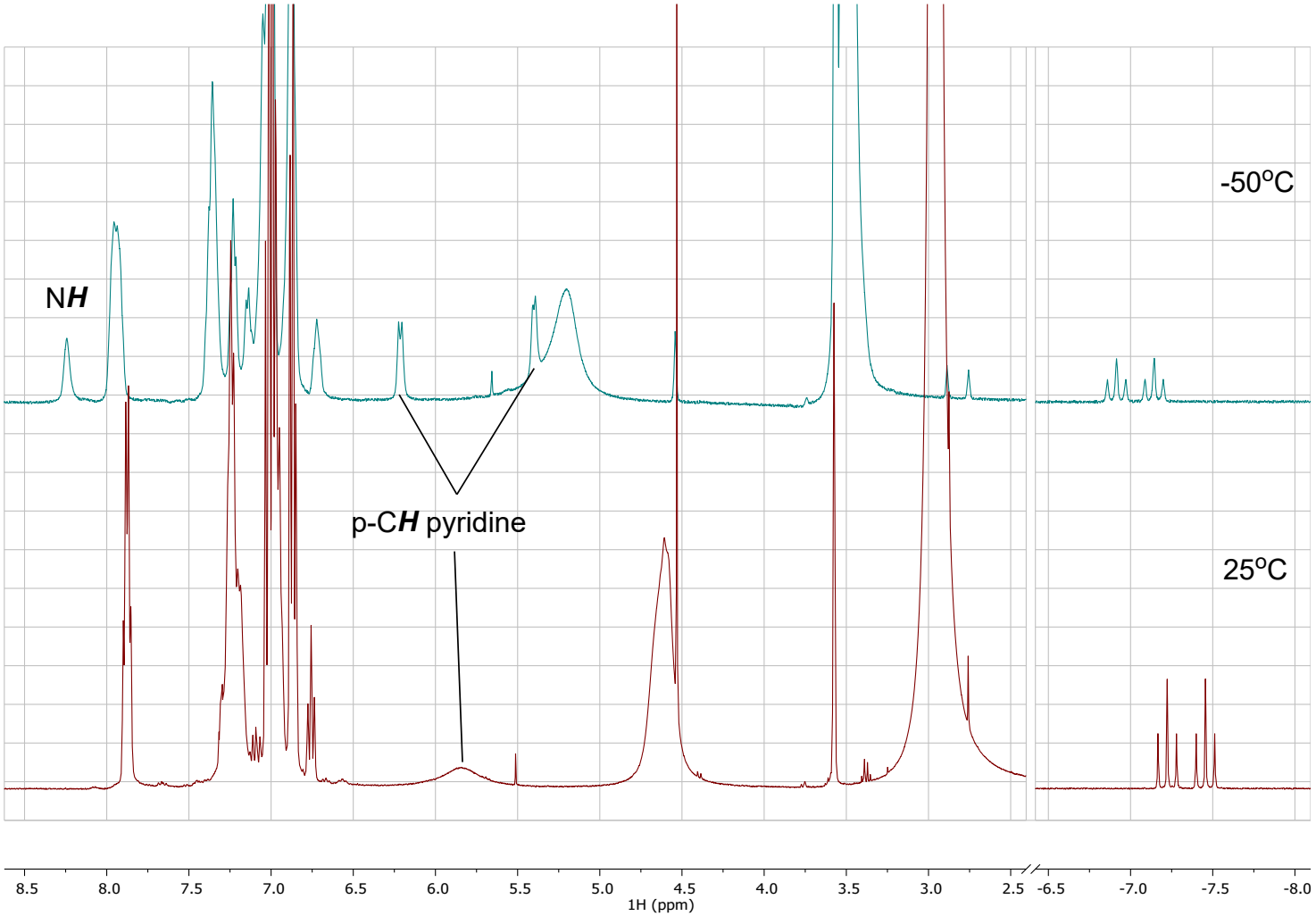

Figure S42. ^{1}H NMR spectra for deprotonation of complex **1** with aqueous KOH in THF-d_8. Note the dynamic nature of formed **2** in THF containing water and the appearance of distinct resonances for pyridine backbone protons at lower temperature indicating backbone dearomatization and inequivalency of *para* positions within the ring.

IR spectroscopy data

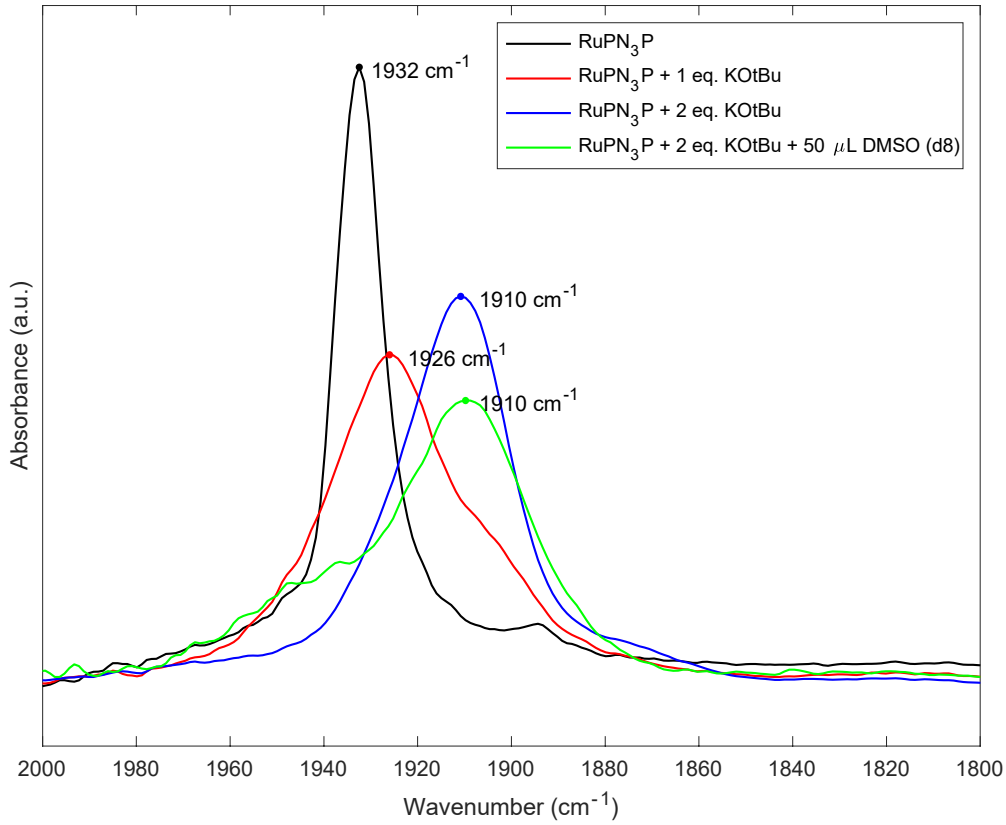

Figure S43. Evolution of IR spectra for sequential deprotonation of complex **1**. Complex **1** was measured as solid, the remaining complexes measures as thin films cast from THF-d8 solutions on the ATR crystal in the Ar-filled glovebox.

S2 Catalytic hydrogenation

General procedure for catalytic hydrogenation of CO_2 in presence of DBU

Stock solutions of **1** (0.013-0.014 M) were prepared in dimethylformamide solvent. In a typical run, DMF (2 mL), DBU (333 µL) and appropriate amount of the stock solution of complex **1** were combined in this order in a 4 mL glass vial equipped with a rare-earth stirring bar and transferred into a stainless steel autoclave in the glovebox. The system was purged with argon (5 × 8 bar) and 1:1 H_2:CO_2 mixture (7 × 10 bar), pressurized with H_2:CO_2 mixture to the desired initial pressure and further tuned with H_2 to reach the final pressure, then heated to specified temperature. After the desired reaction time, the autoclave was cooled with ice and the pressure released, after which DMSO was added as an internal standard (100 µL, 1.408 mmol). A 100 µL aliquot of the sample was dissolved in D_2O and the yield determined by ^{1}H NMR analysis.

General procedure for catalytic hydrogenation of potassium bicarbonate

Stock solutions of **1** (0.013-0.014 M) were prepared in dimethylformamide solvent. In a typical run, potassium bicarbonate, methyltrioctylammonium chloride (24 mg, 55 µmol), toluene (1 mL), water (1 mL) and appropriate amount of the stock solution of complex **1** were combined in this order in a 4 mL glass vial equipped with a rare-earth stirring bar and transferred into a stainless steel autoclave in the glovebox. The system was purged with argon (5 × 8 bar) and H_2 (7 × 10 bar), pressurized with H_2 to 5 bar, and heated to specified temperature, after which the H_2 was regulated to the desired pressure. After the desired reaction time, the autoclave was cooled with ice and the pressure released, after which DMSO was added as an internal standard (100 µL, 1.408 mmol). A 100 µL aliquot of the H_2O layer was dissolved in D_2O and the yield determined by ^{1}H NMR analysis.

NOTE: Reported TON and TOF values are calculated on the basis of the formate molecules produced in reaction run. Due to the low solubility, consumption of $KHCO_3$ should not be used as a main indicator of reaction progress.

Procedure for the bicarbonate hydrogenation at larger scale

In a glass vial insert (20 mL) 5.005g (50 mmol) $KHCO_3$ was weighed out and placed in an autoclave, of which the atmosphere was replaced with nitrogen by 5 sequential cycles of vacuum and refilling with nitrogen. Thereafter, 4 mL of toluene containing 120 mg (275 µmol) of methyltrioctylammonium chloride was added, followed by 5 mL of water. 0.696 µmol of catalyst in 1 mL toluene was added in the autoclave separated from the reaction solution by a valve. The autoclave was pressurized to 45 bar of H_2 and heated to 90 °C. When the desired temperature was reached the pressure was set at 50 bar and the valve containing the catalyst solution was opened, allowing a precise determination of reaction start (t_0).

After the desired reaction time, the autoclave was cooled and the pressure released, after which DMSO was added as an internal standard (500 µL, 7.04 mmol). A 100 µL aliquot of the H_2O layer was dissolved in D_2O and the read out using gas consumption data was corrected using ^{1}H NMR analysis.

Catalytic data provided in Table 1 of the manuscript

Table S1. Result of the catalytic hydrogenation of CO_2 in DMF (2 mL), in presence of DBU as a base (333 µL = 2.23 mmol). Conditions: T = 90 °C, p = 40 bar, t = 16h.

Catalyst	µmol	p_{H2}/p_{CO2}	TON	FA/Base
RuPNP**	0.107	20/20	19430	0.93
1	0.13	39/1	13029	0.75
1	0.13	20/20	11815	0.68

** IMPORTANT NOTE: Reference catalytic data for RuPNP complex is adopted from published report.[3]

^{1}H NMR data accompanying data provided in Table 1 of the manuscript

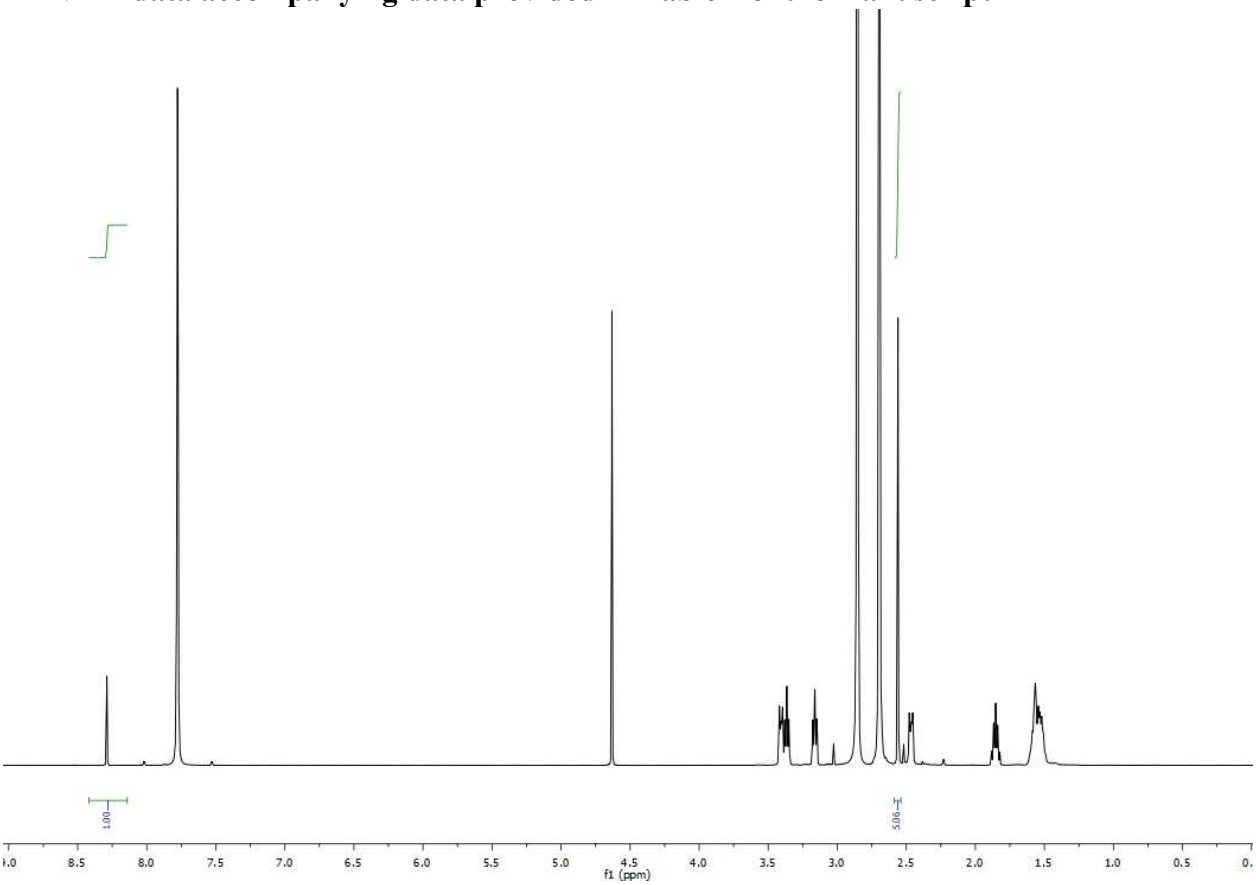

Figure S44. NMR Data belonging to Table S1, Entry 2.

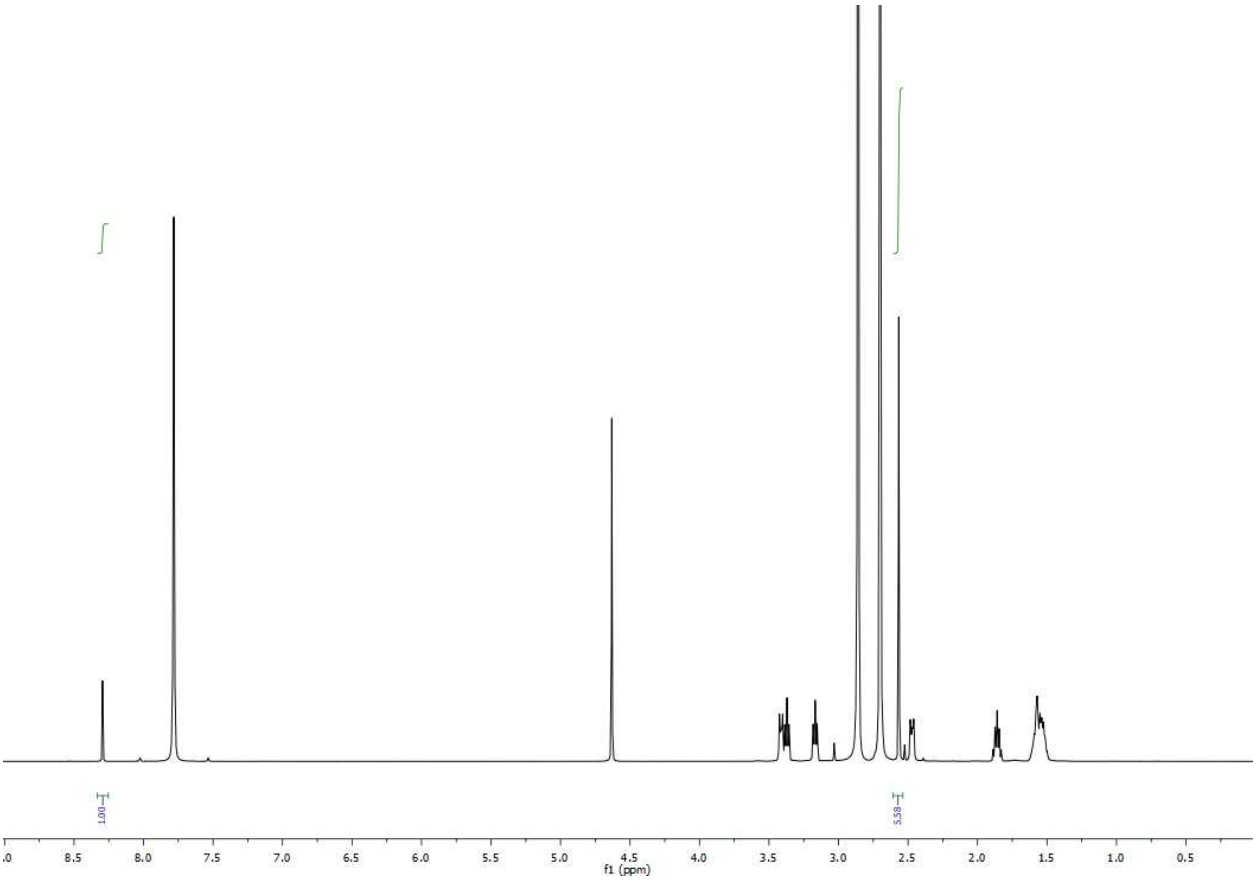

Figure S45. NMR Data belonging to Table S1, entry 3.

Table S2. ^{1}H NMR peak data belonging to TableS1 and Figures S44-S45.

Entry	**Ratio of DMSO to formate integral**
1	5.06
2	5.58

Table S3. Result of the catalytic hydrogenation of $KHCO_3$ in H_2O/toluene (1:1), in presence of methyltrioctylammonium chloride as a phase-transfer catalyst (± 54 µmol). Conditions: T = 90 °C, amount of KCO_3 = 5.00 mmol, p = 40 bar, t = 16h.

Catalyst	TON	Conversion (from $KHCO_3$)
RuPNP**	27728	66.4 %
1	25828	70.6 %

** IMPORTANT NOTE: Reference catalytic data for RuPNP complex is adopted from published report.[3]

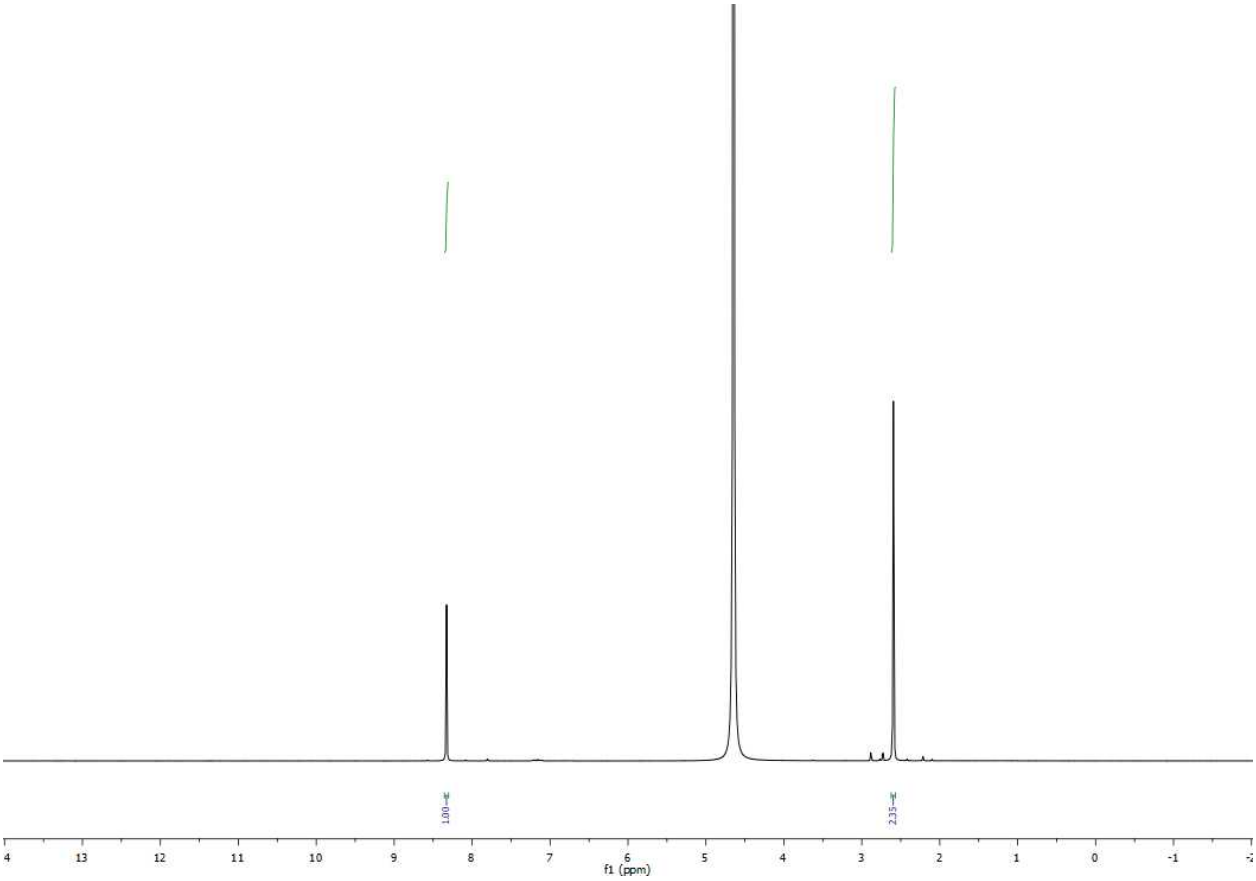

Figure S46. NMR Data belonging to Table S2, Entry 2

Table S3. ^1H NMR peak data belonging to Table S2 and Figure S46.

Entry	Ratio of DMSO to formate integral
2	2.35

Table S4. Comparison of a several solvent mixtures for bicarbonate hydrogenation. Conditions: T = 90 °C, amount of $KHCO_3$ = 5.00 mmol, p = 40 bar, t = 16h, methyltrioctylammonium chloride as a phase-transfer catalyst (± 54 µmol), catalyst **1** = 0.14 µmol.

Entry	Solvent	TON	Conversion
1	Toluene/water	25828	70.6 %
2	THF/water	21600	60.1 %
3	Dioxane/Water	26375	73.4 %

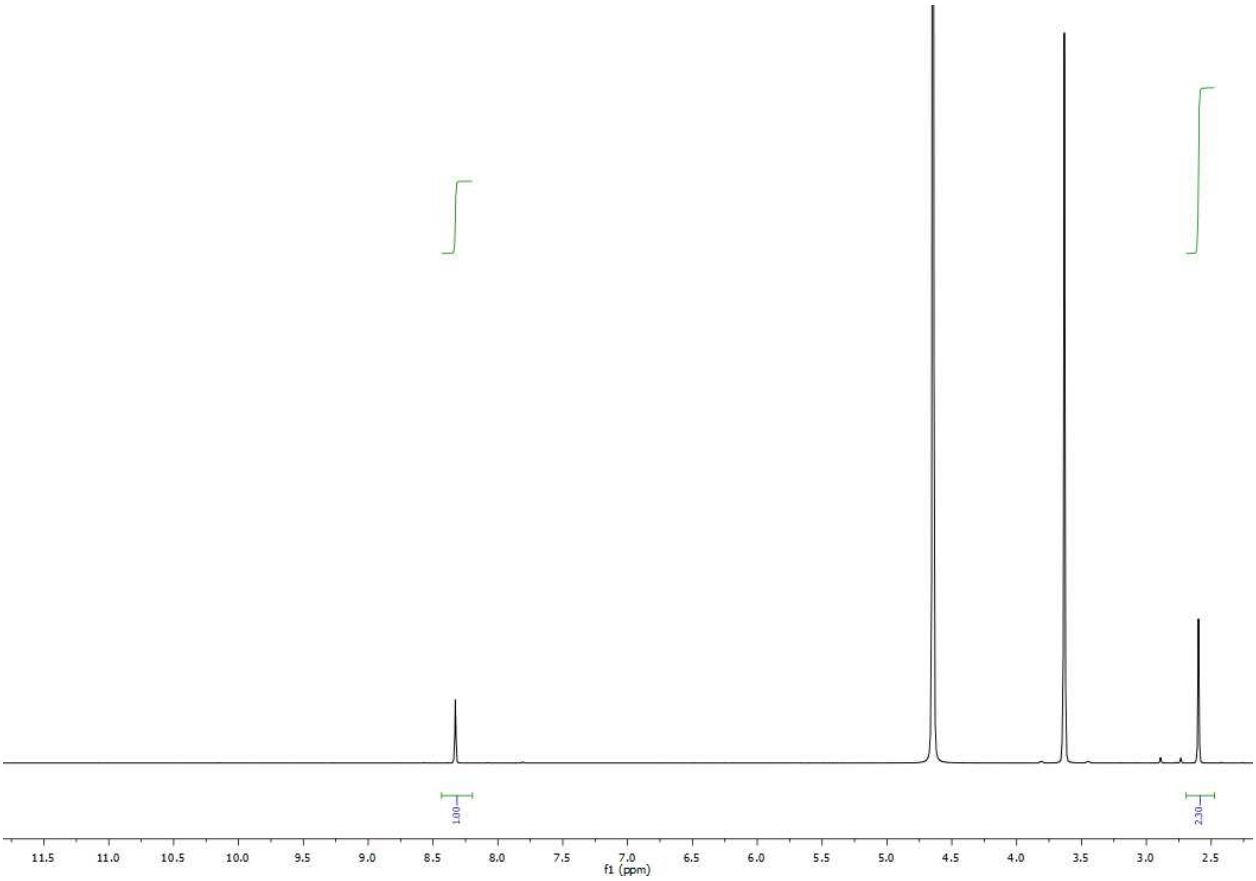

Figure S47. NMR Data belonging to Table S4, Entry 2.

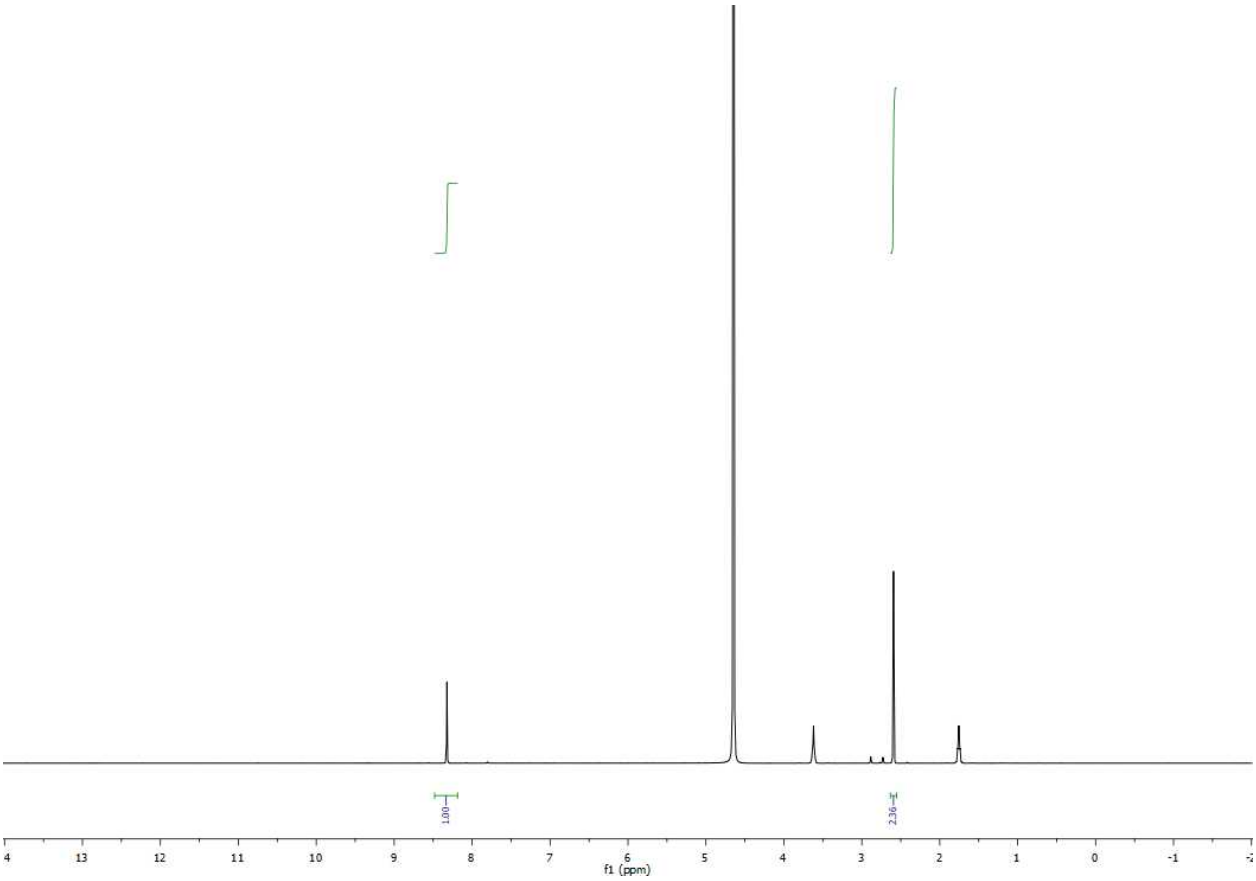

Figure S48. NMR Data belonging to Table S4, Entry 3.

Table S5. ^{1}H NMR peak data belonging to Table S4 and Figures S47-S48.

Entry	**Ratio of DMSO to formate integral**
1	2.35
2	2.36
3	2.30

Catalytic tests in the absence of phase transfer catalyst

Table S6 The influence of toluene and methyltrioctylammonium chloride on bicarbonate hydrogenation with complex **1.** Conditions: T = 90 °C, amount of KCO_3 = 5.00 mmol, p_{H2} = 40, t = 16h.

Entry	Solvent	Phase-transfer catalyst (54 µmol)	mmol $KHCO_3$	Yield	TON
1	water	no	10	7.1 %	5113
2	toluene-water (1:1)	no	5	1.3 %	450

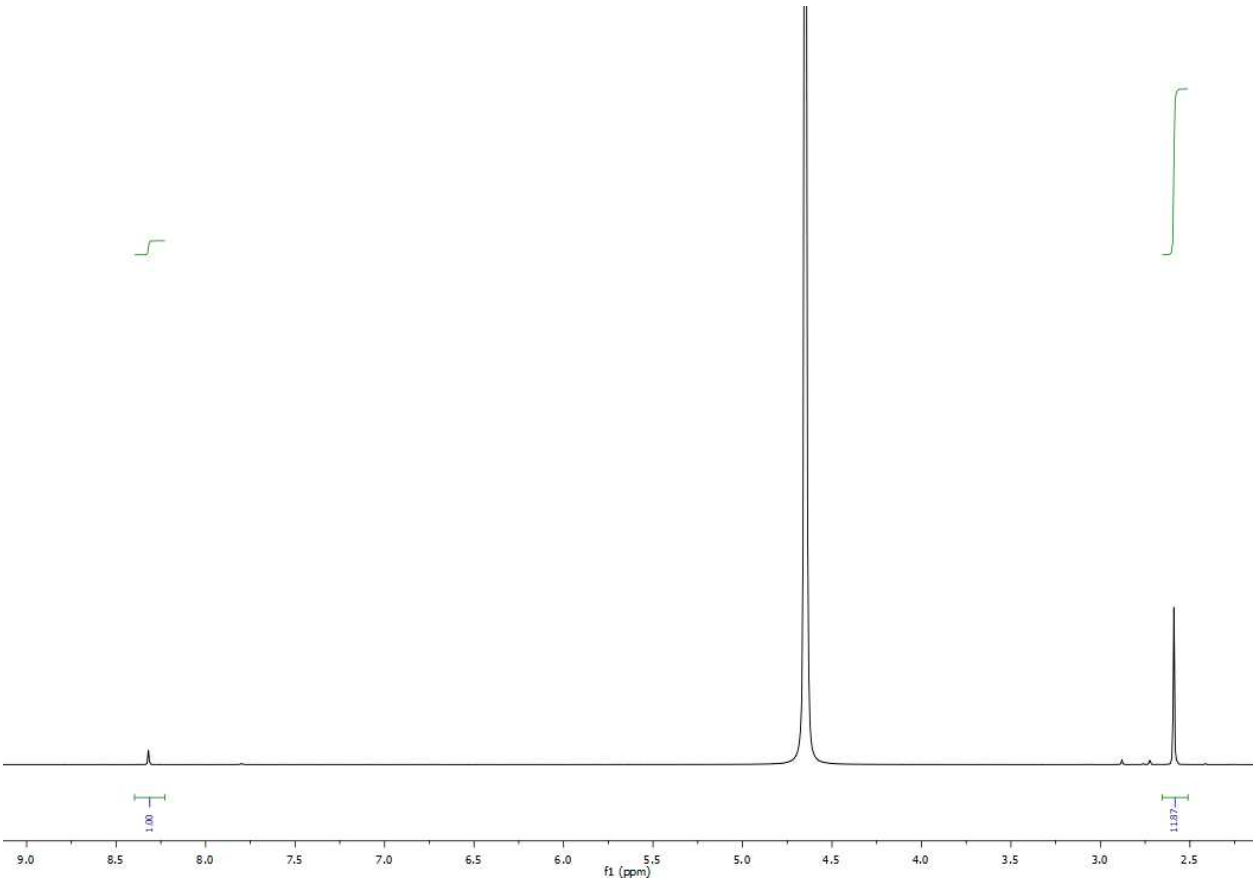

Figure S49. NMR Data belonging to Table S6, Entry 1.

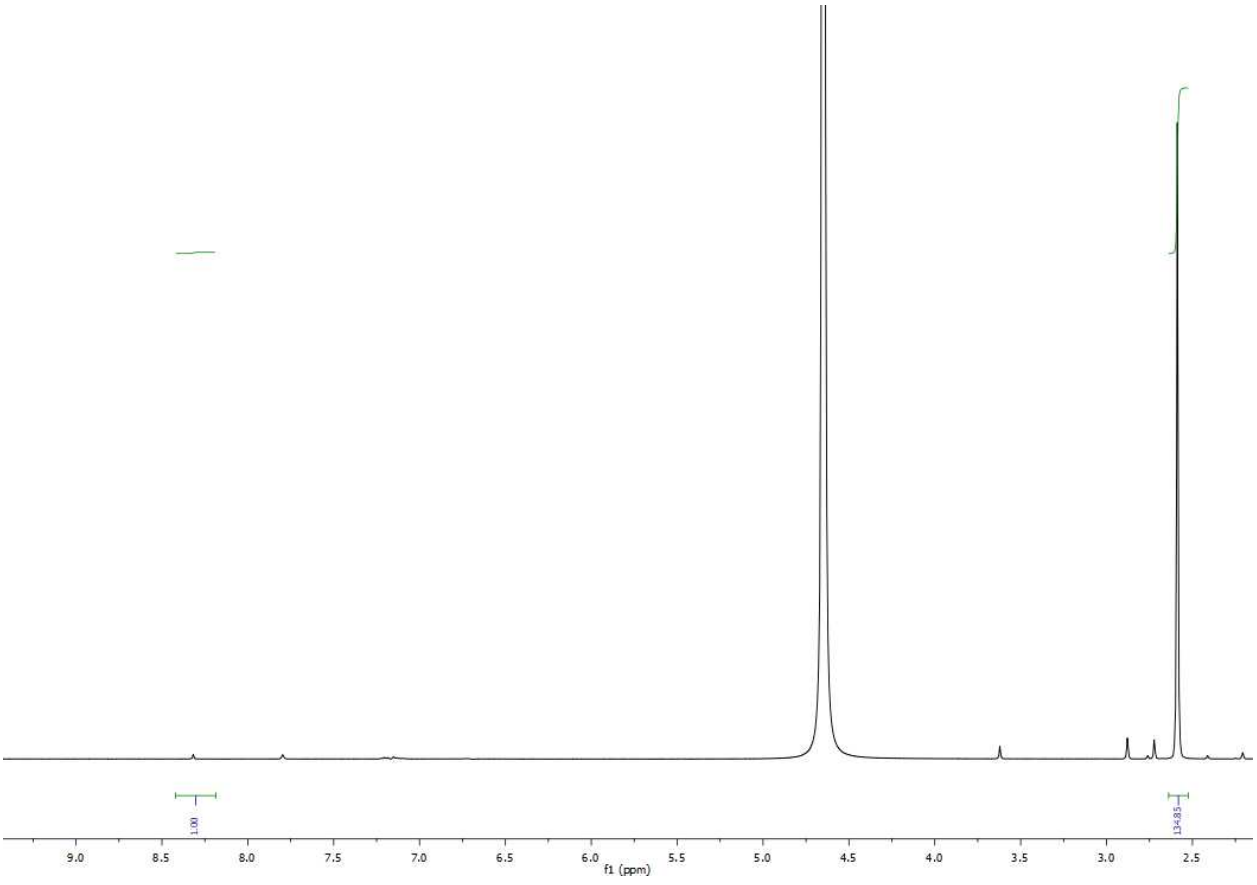

Figure S50. NMR Data belonging to Table S6, Entry 2.

Table S7. ^{1}H NMR peak data belonging to Table S6 and Figures S49-S50.

Entry	**Ratio of DMSO to formate integral**
1	11.87
2	134.85

Pressure and temperature dependence of formate yield in hydrogenation with complex 1

Table S8. Data accompanying Figure 4 in the main text, for T = 65 °.

Entry	Pressure (bar)	Ratio of DMSO to formate integral	Yield (%)	TON
1	5	15.73	10.7	3859
2	10	6.70	25.2	9059
3	20	2.82	60.0	21523
4	40	2.21	76.5	27464
5	60	2.32	73.0	26050

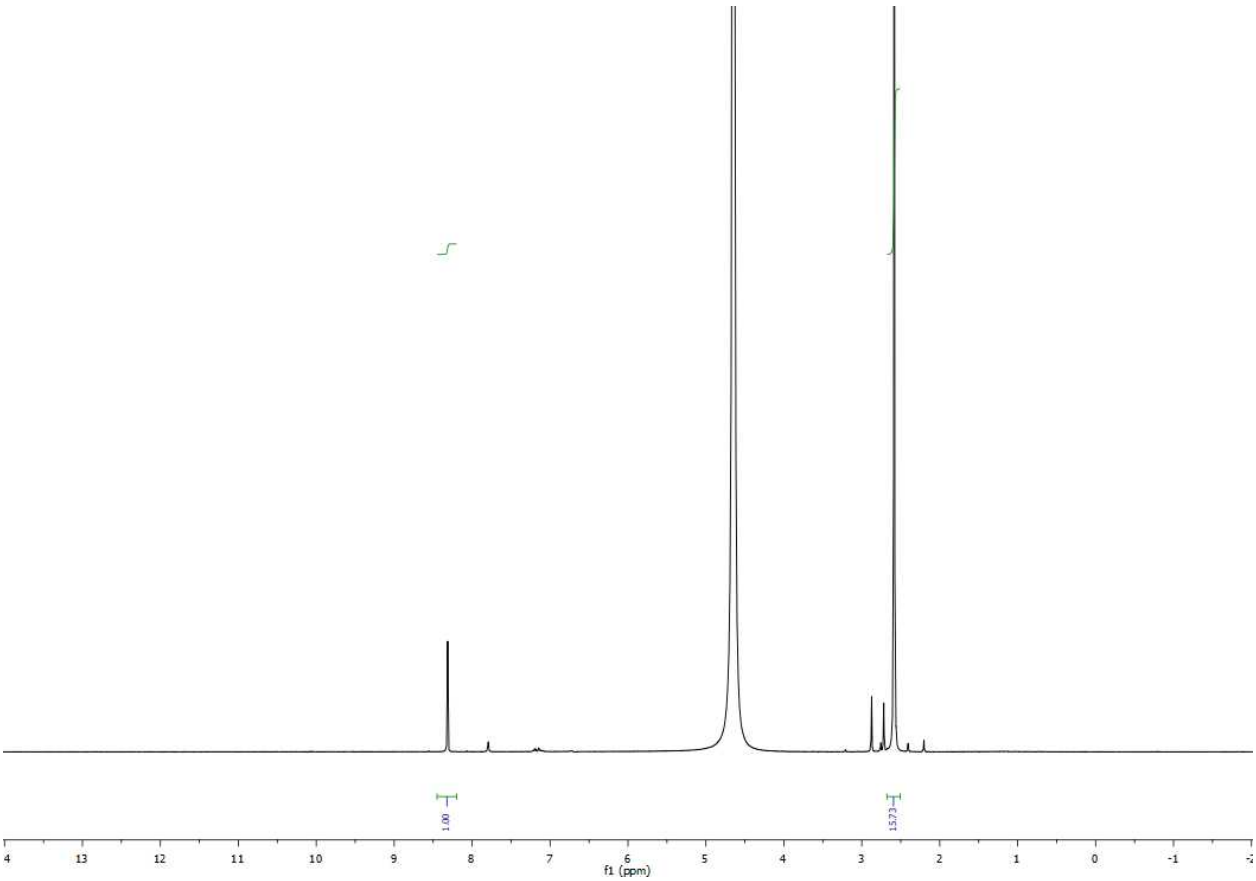

Figure S51. NMR Data belonging to Table S8, Entry 1.

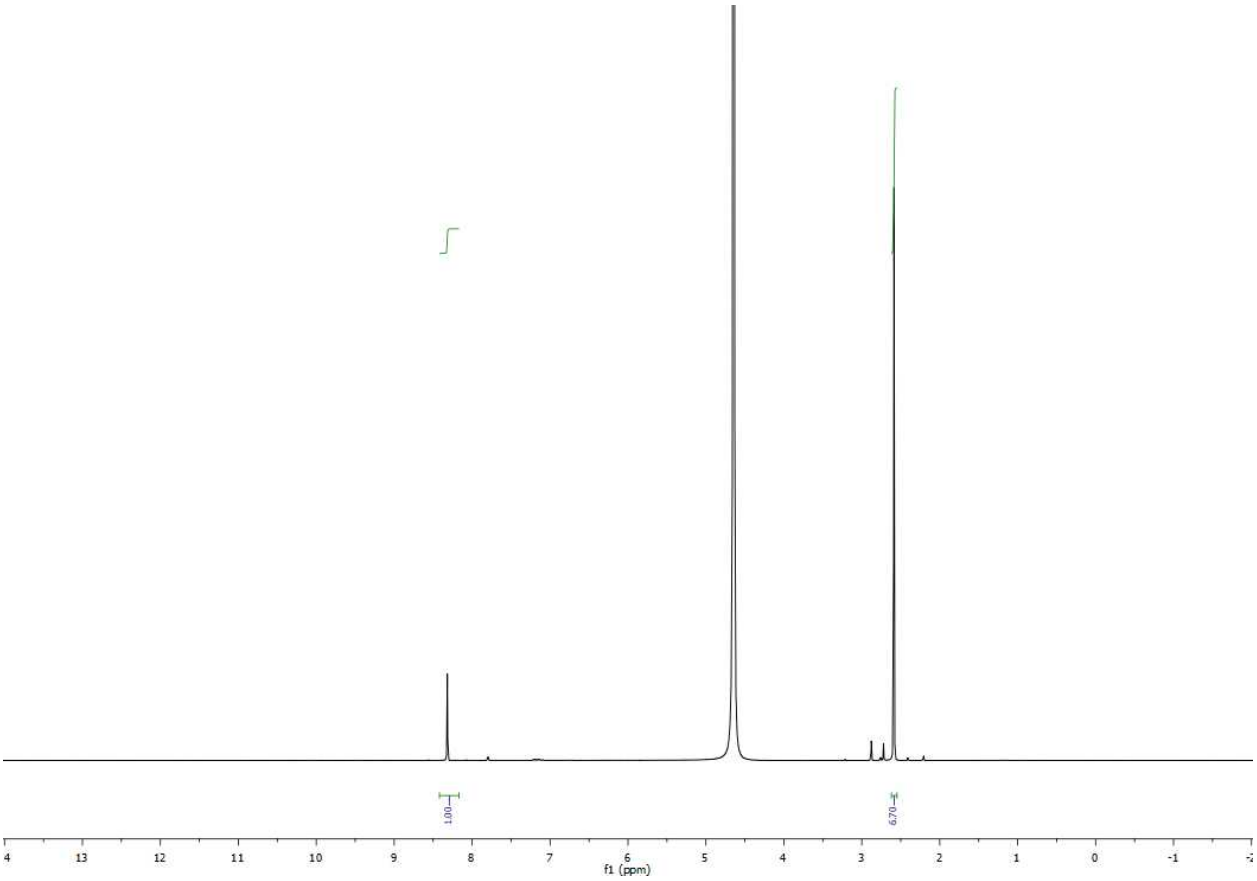

Figure S52. NMR Data belonging to Table S8, Entry 2.

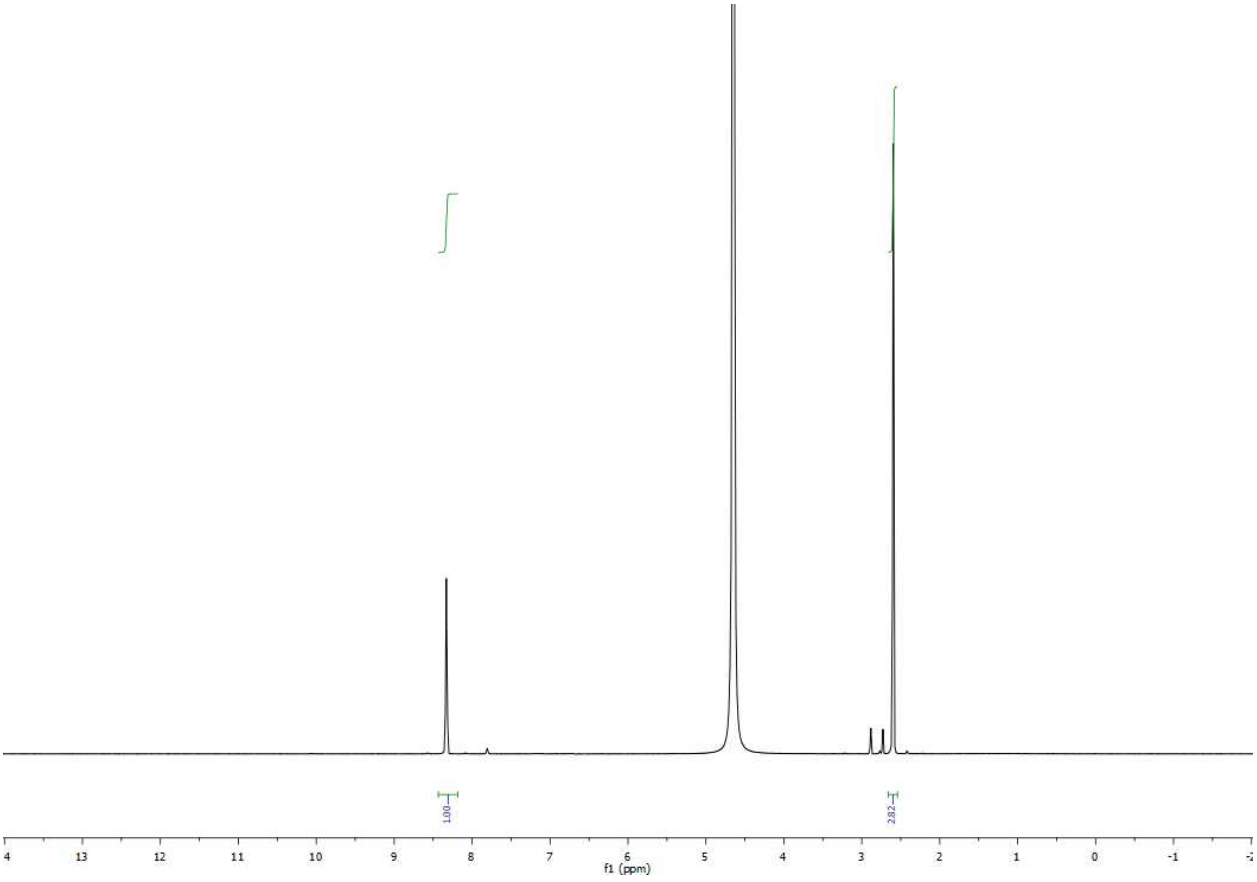

Figure S53. NMR Data belonging to Table S8, Entry 3.

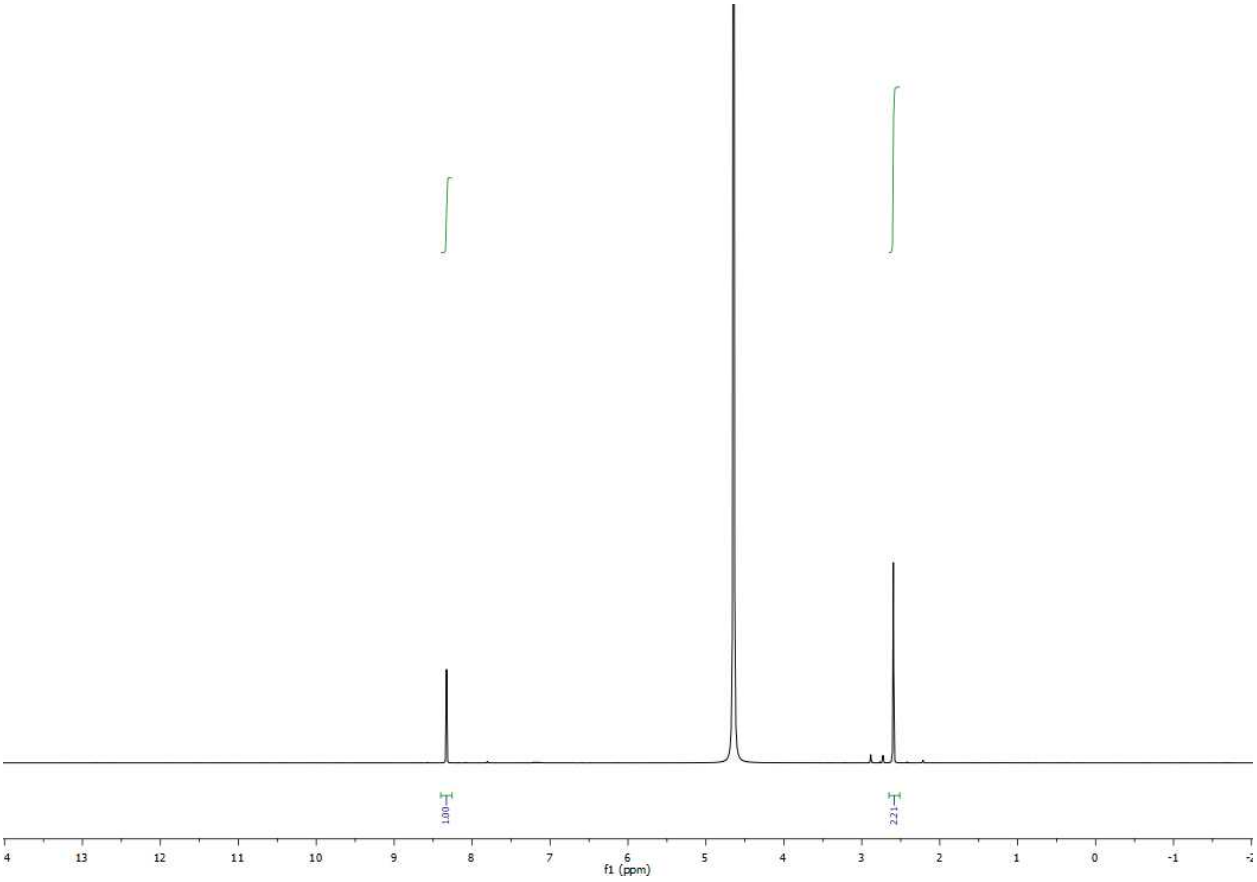

Figure S54. NMR Data belonging to Table S8, Entry 4.

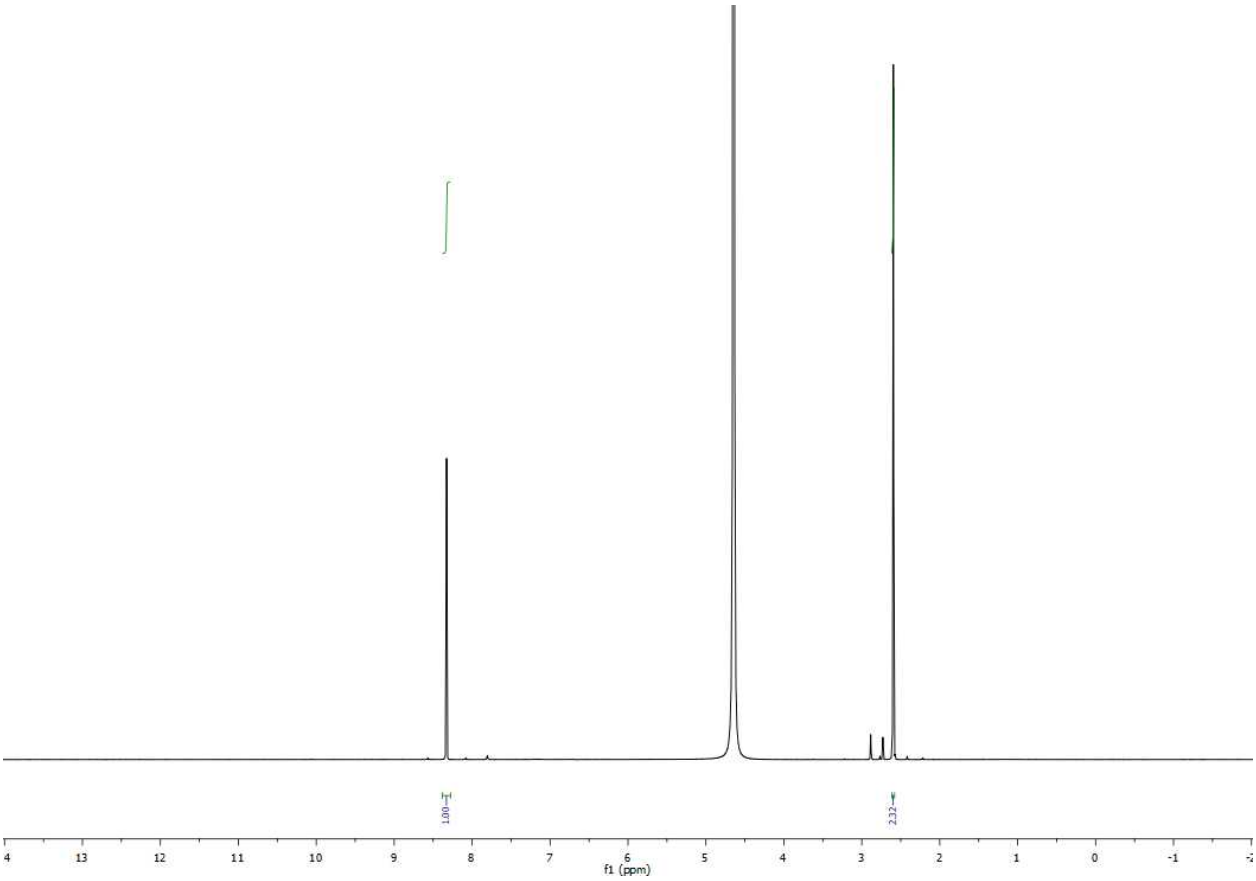

Figure S55. NMR Data belonging to Table S8, Entry 5.

Table S9. Data accompanying Figure 4 in the main text, for for T = 90 °.

Entry	**Pressure (bar)**	**Ratio of DMSO to formate integral**	**Yield (%)**	**TON**
1	5	10.51	15.8	5775
2	10	5.78	29.7	10877
3	20	3.72	44.6	16316
4	40	2.35	70.6	25828
5	60	2.31	71.8	26275

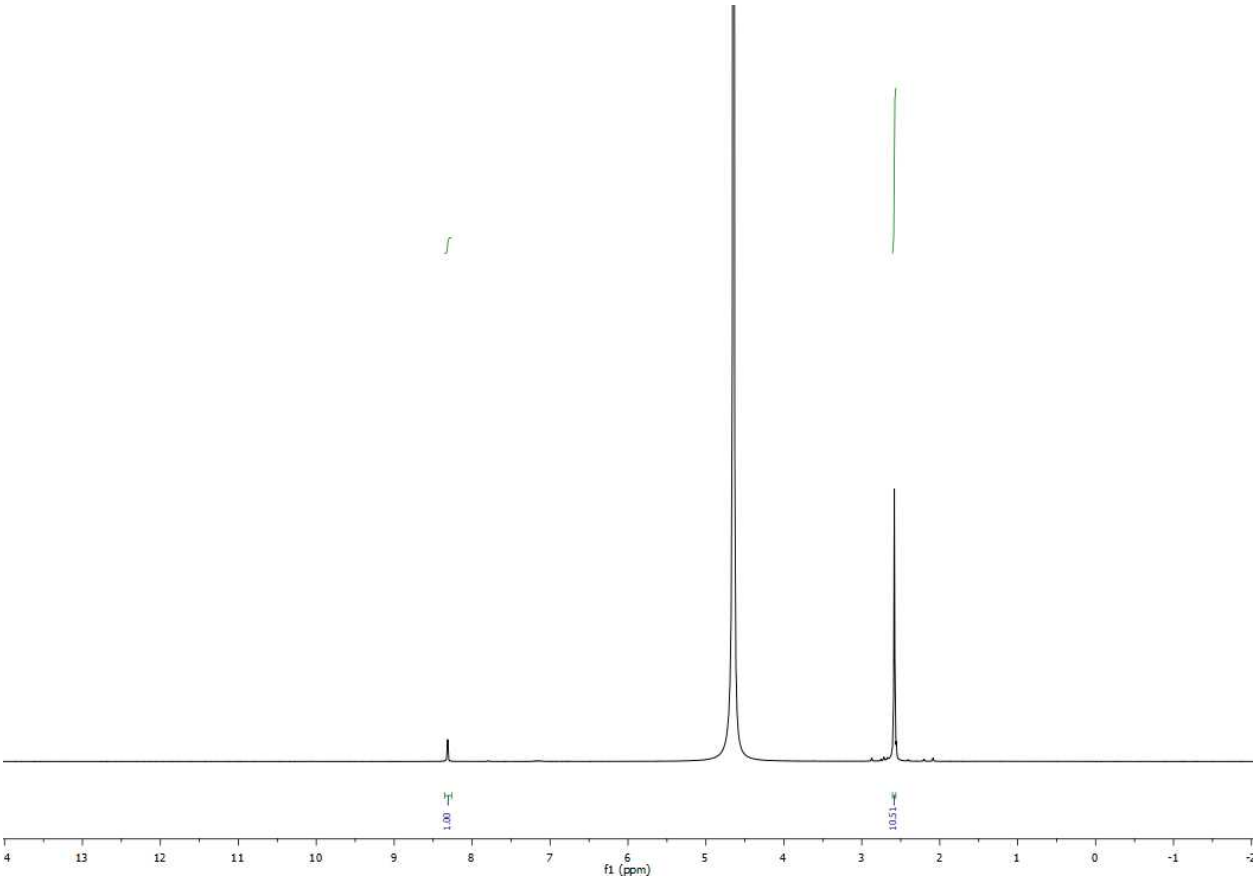

Figure S56. NMR Data belonging to Table S9, Entry 1.

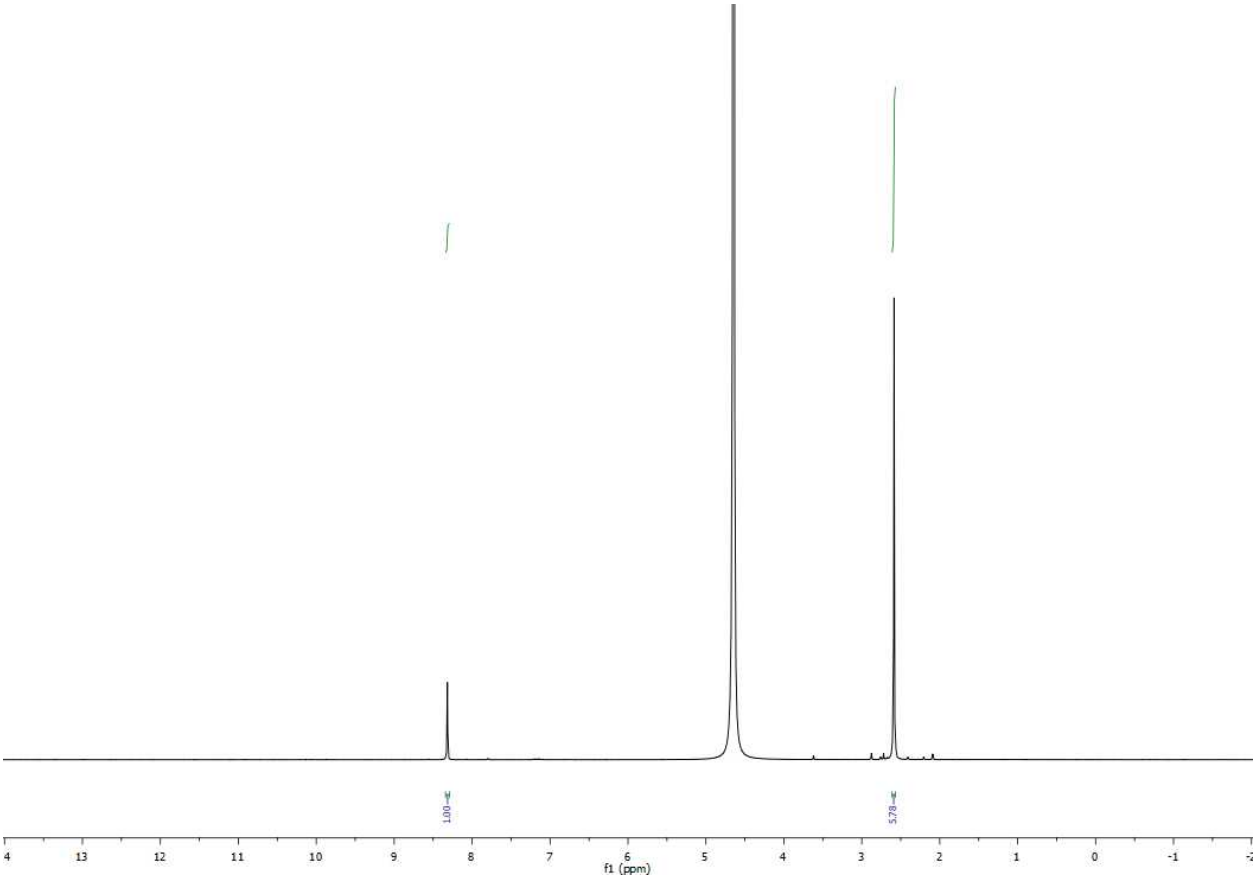

Figure S57. NMR Data belonging to Table S9, Entry 2.

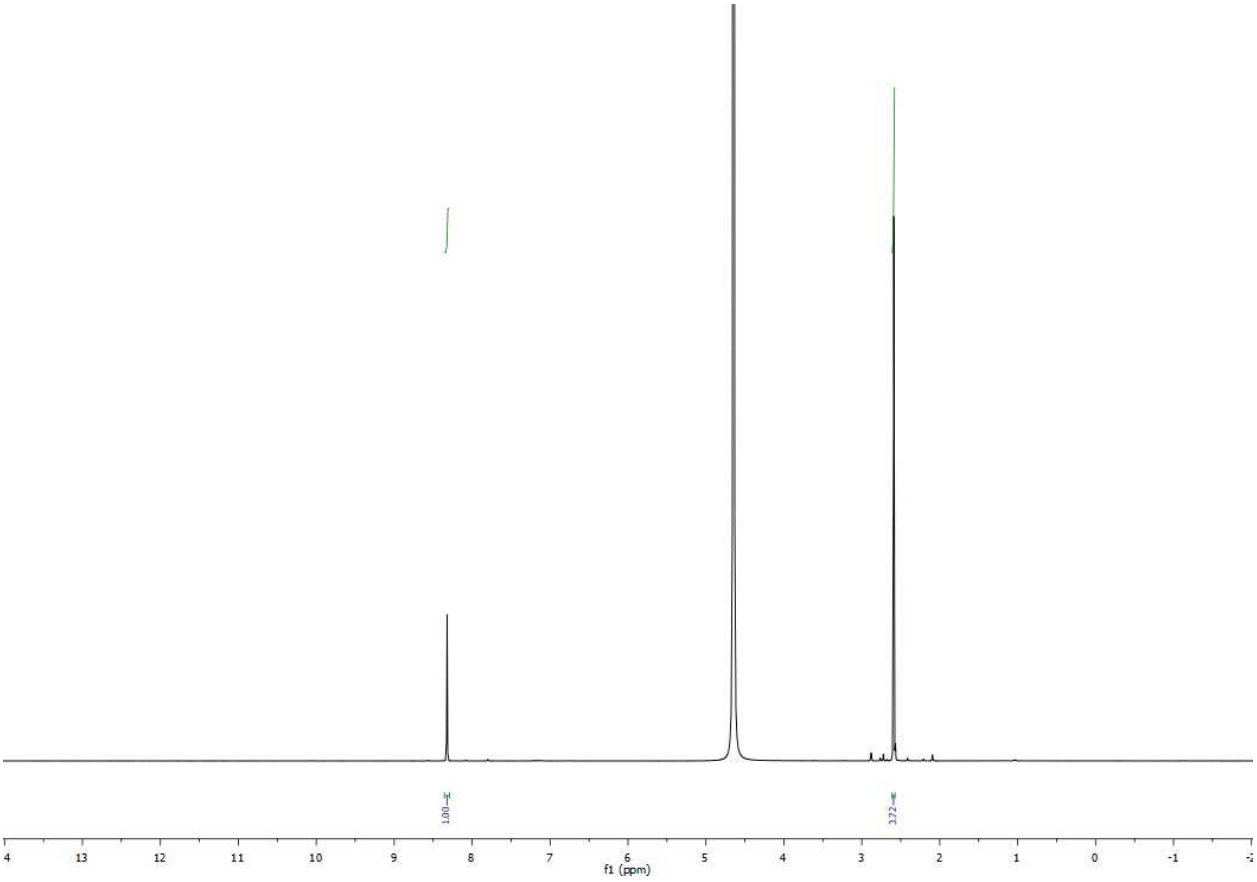

Figure S58. NMR Data belonging to Table S9, Entry 3.

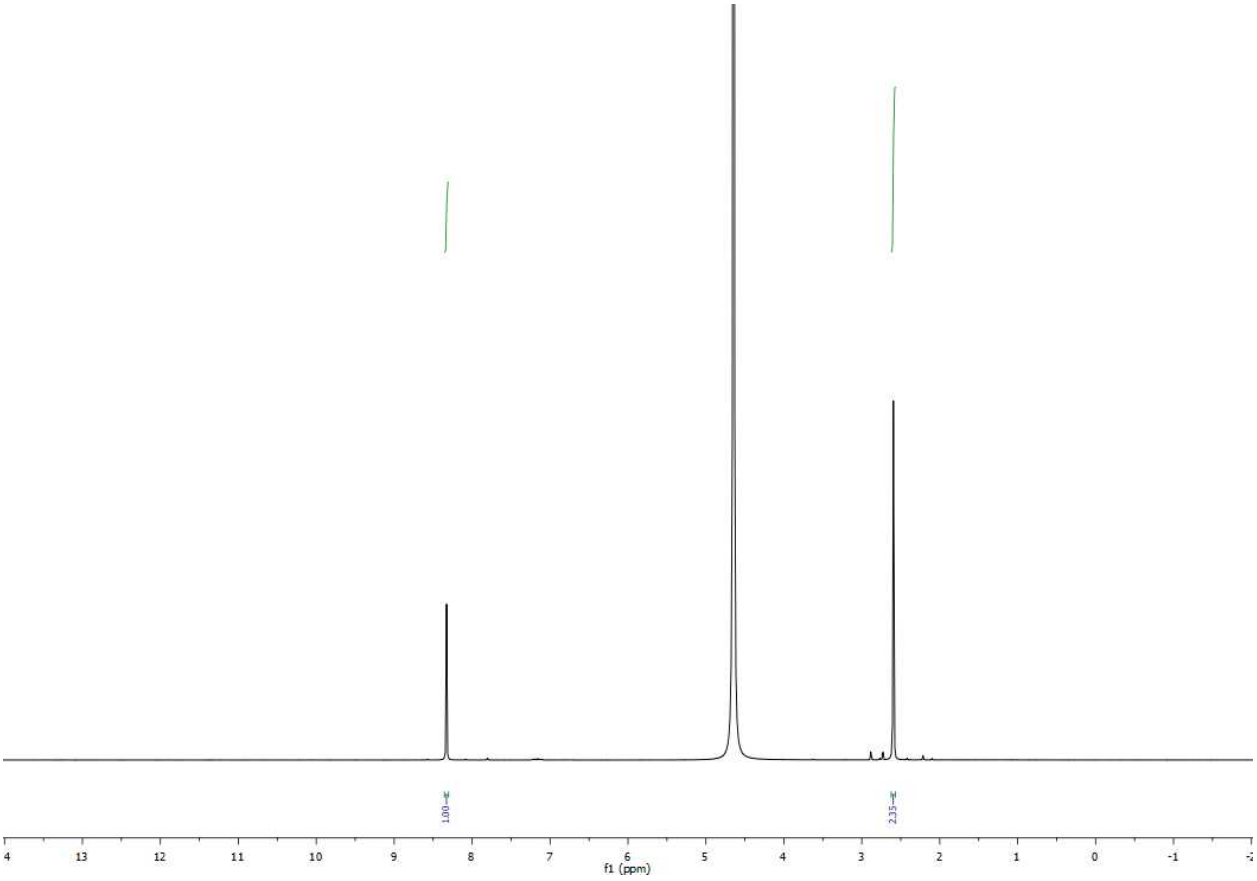

Figure S59. NMR Data belonging to Table S9, Entry 4.

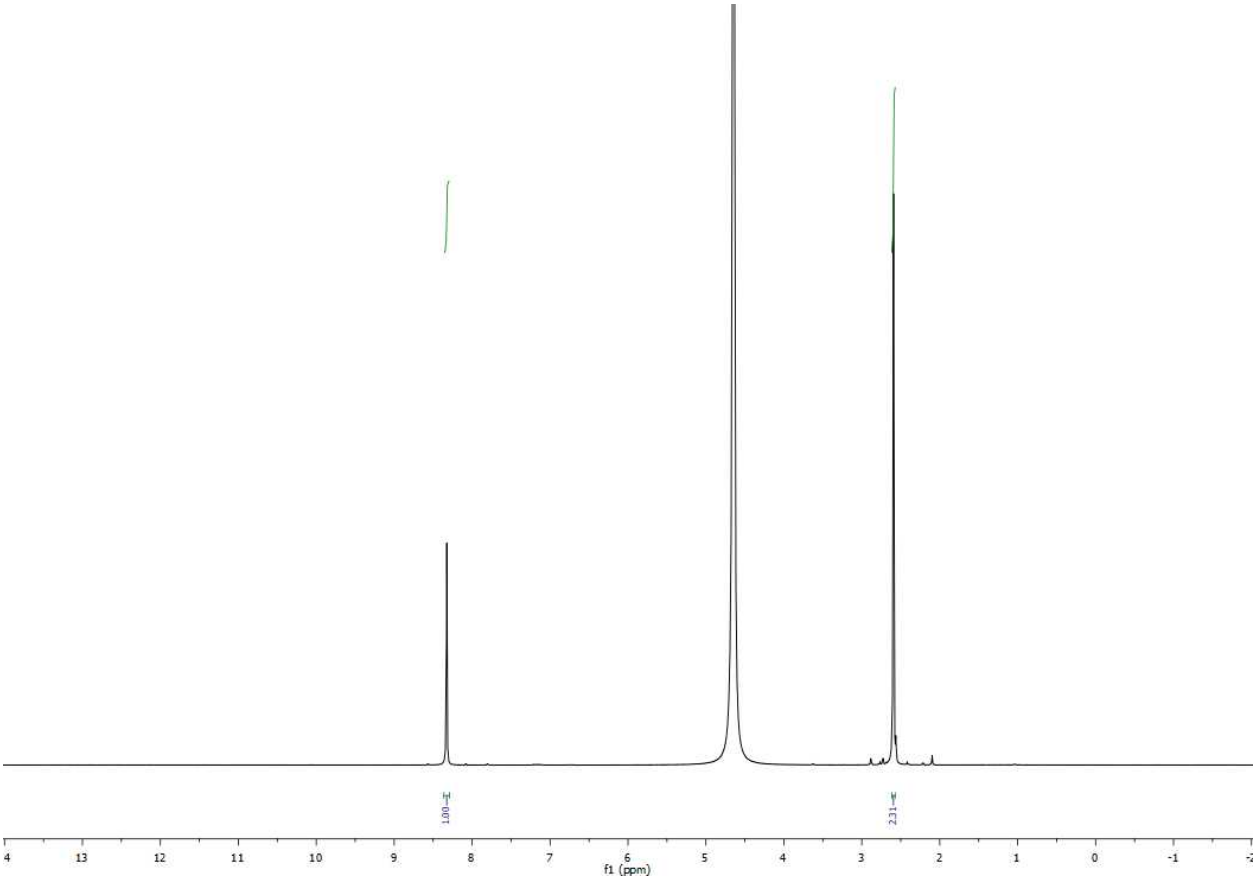

Figure S60. NMR Data belonging to Table S9, Entry 5.

Table S10. Data accompanying Figure 4 of the main for T = 120 °.

Entry	Pressure (bar)	Ratio of DMSO to formate integral	Yield (%)	TON
1	5	53.48	3.2	1135
2	10	25.85	6.6	2348
3	20	14.34	11.7	4233
4	40	6.76	24.7	8979
5	60	3.58	47.4	16954

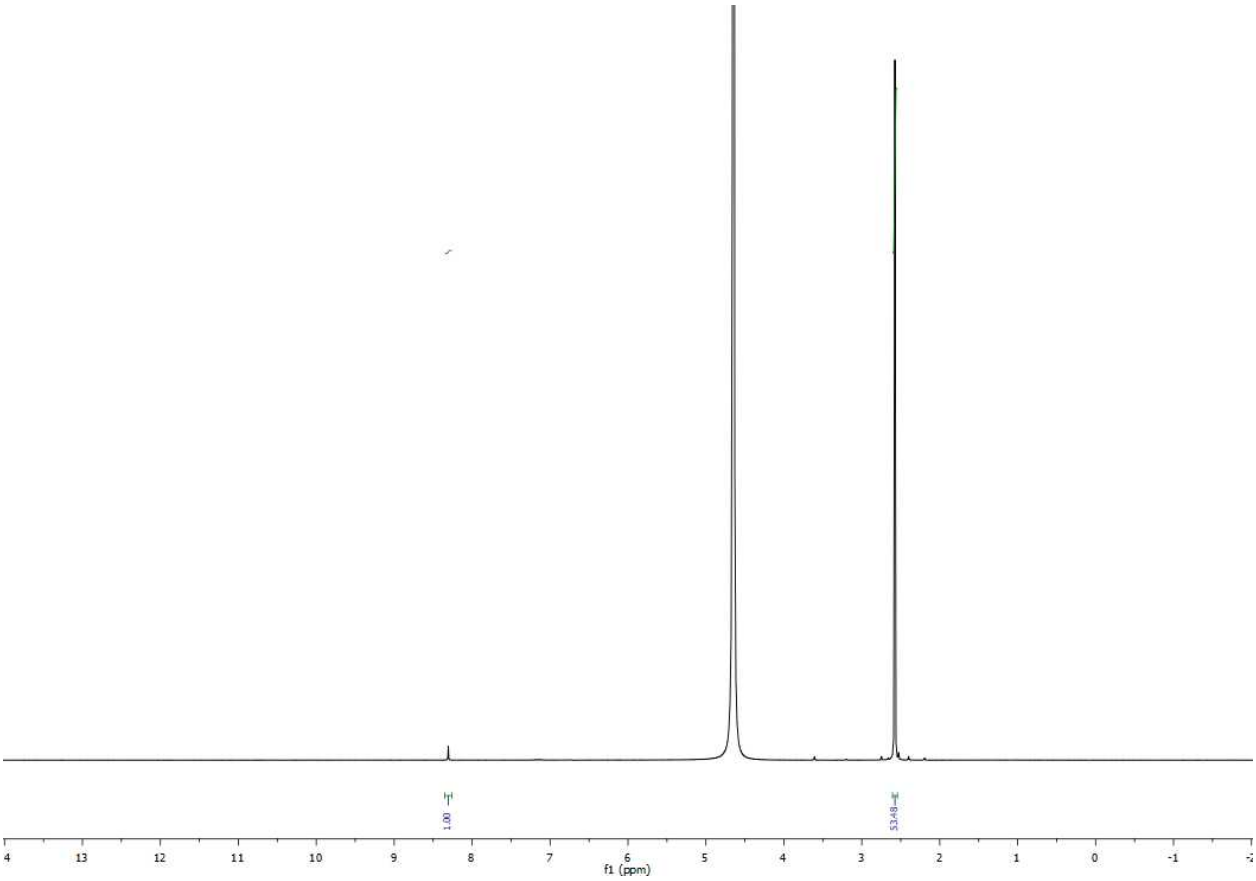

Figure S61. NMR Data belonging to Table S10, Entry 1.

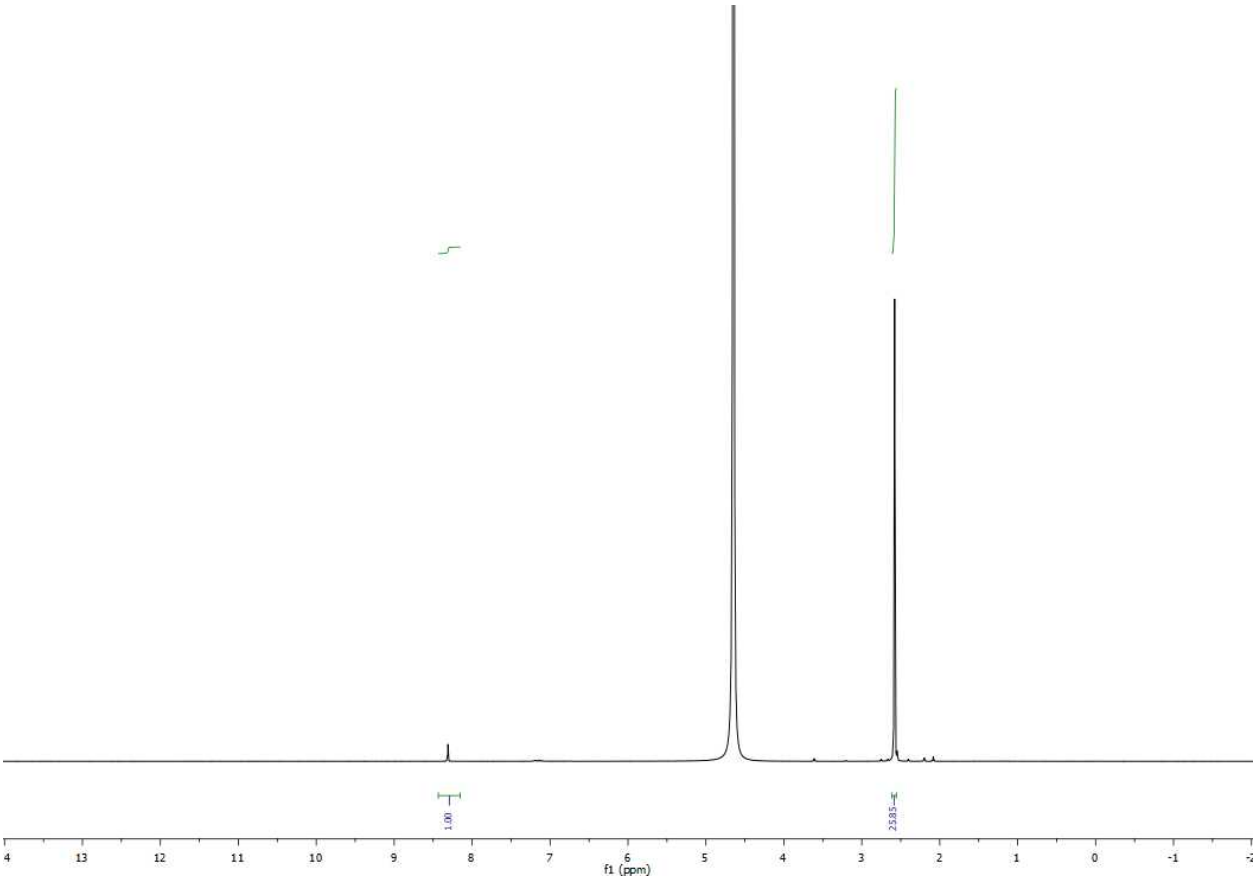

Figure S62. NMR Data belonging to Table S10, Entry 2.

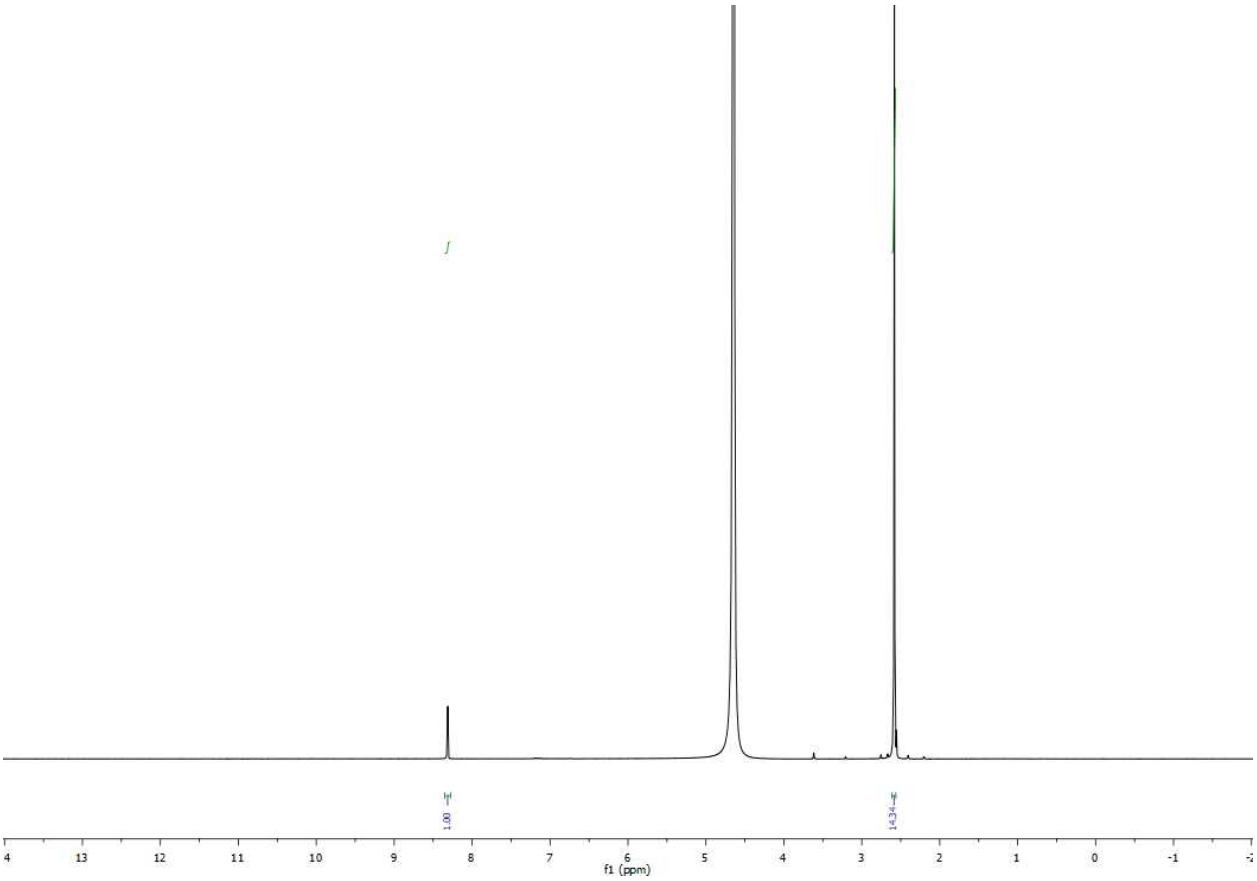

Figure S63. NMR Data belonging to Table S10, Entry 3.

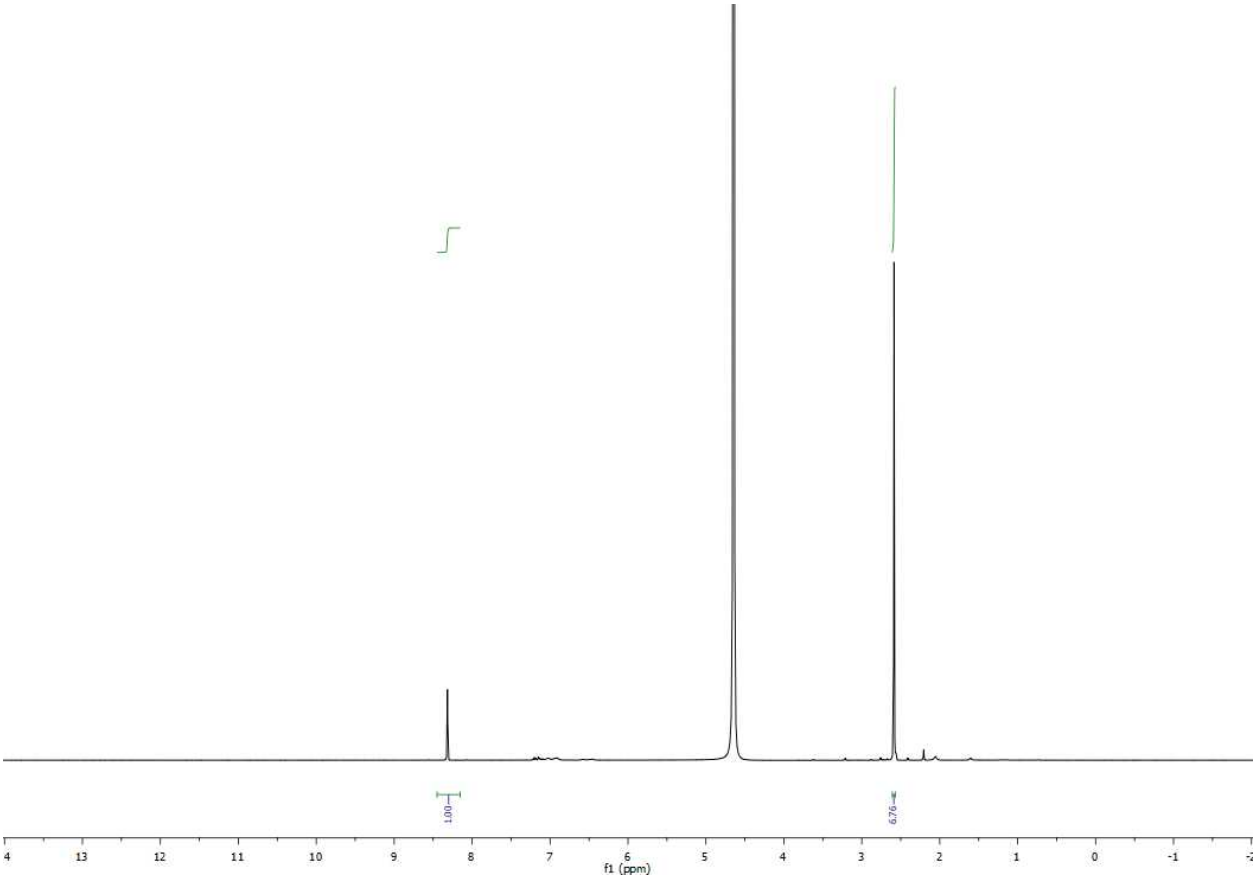

Figure S64. NMR Data belonging to Table S10, Entry 4.

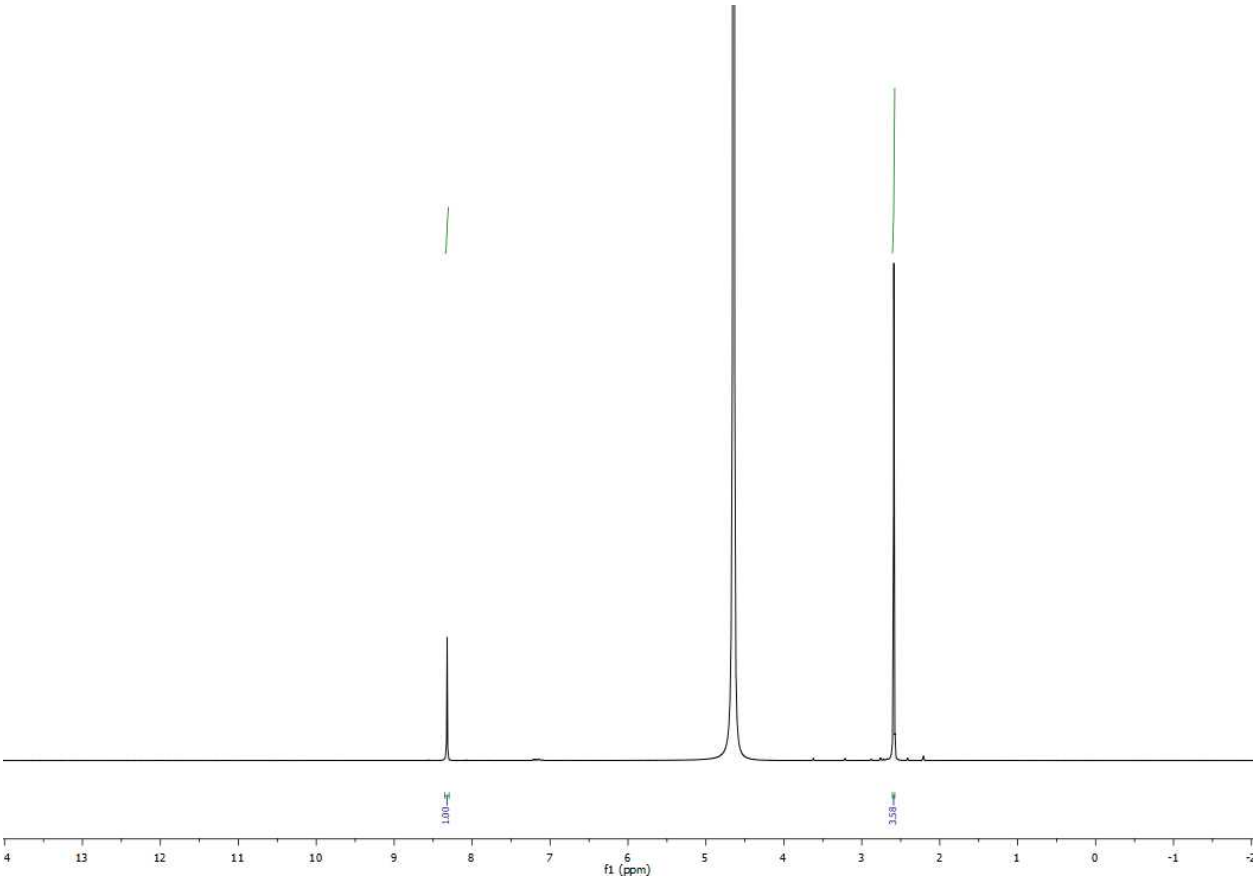

Figure S65. NMR Data belonging to Table S10, Entry 5.

Catalyst concentration dependence analysis

Table S11. Catalyst concentration versus TON and yield. *Reactions conditions*: various µm cat, 55 mM PTC, 1 mL H_2O, 1 mL toluene, 5 M $KHCO_3$, T = 90 °C, p = 45 bar, t = 16h, catalyst complex **1** used in amounts indicated below.

Entry	Catalyst 1 (µmol)	TON	Conversion
1	0.014	12953	4 %
2	0.035	22501	16 %
3	0.070	42297	59 %
4	0.139	25828	70.6 %
5	0.278	14383	80 %

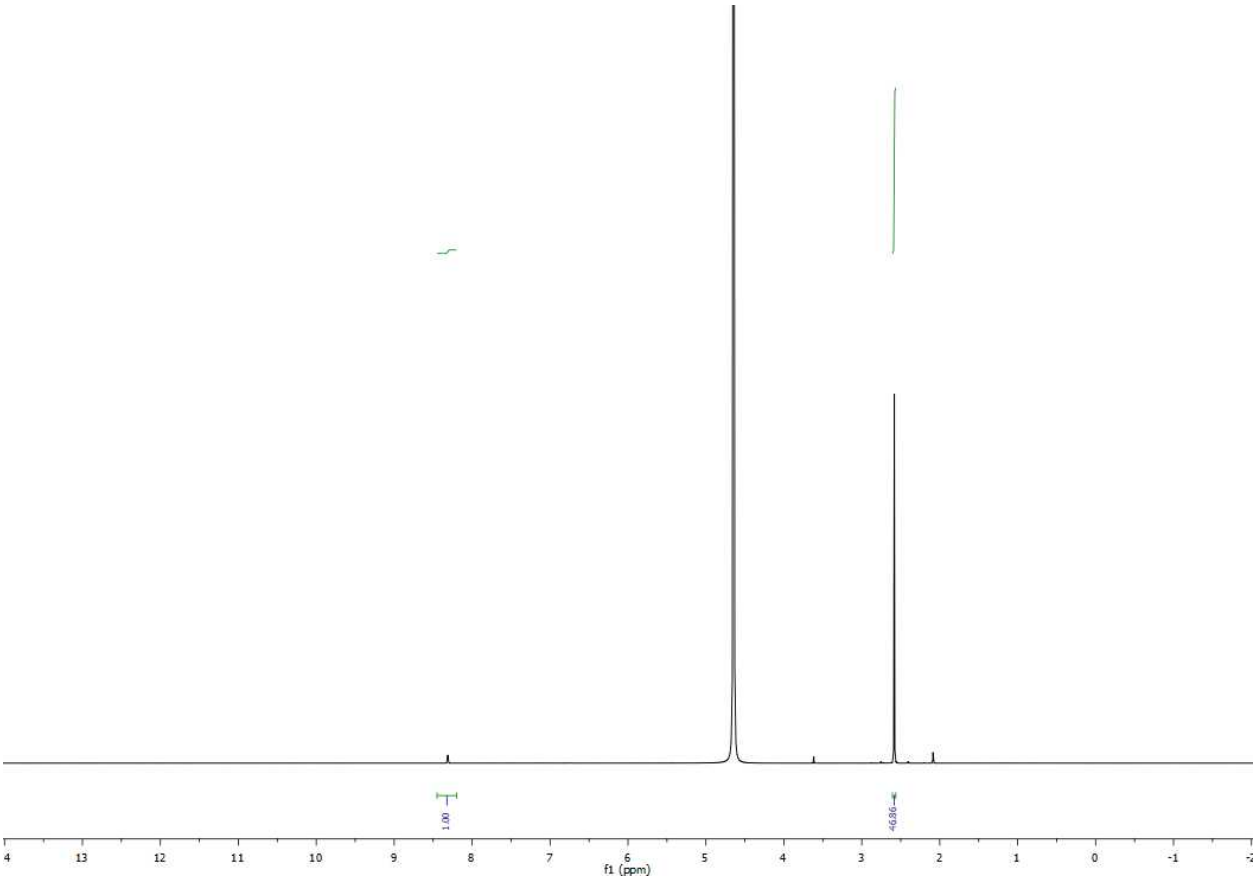

Figure S66. NMR Data belonging to Table S11, Entry 1.

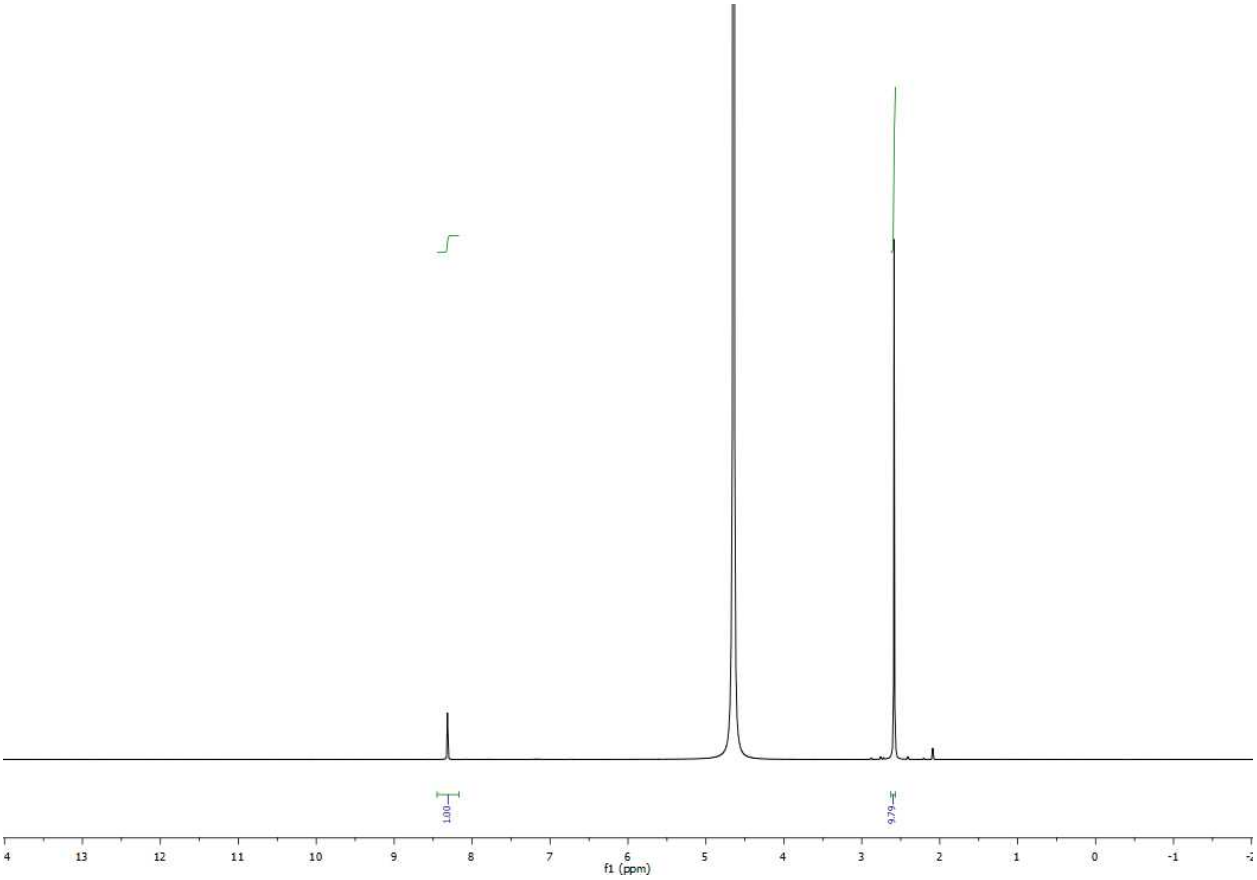

Figure S67. NMR Data belonging to Table S11, Entry 2.

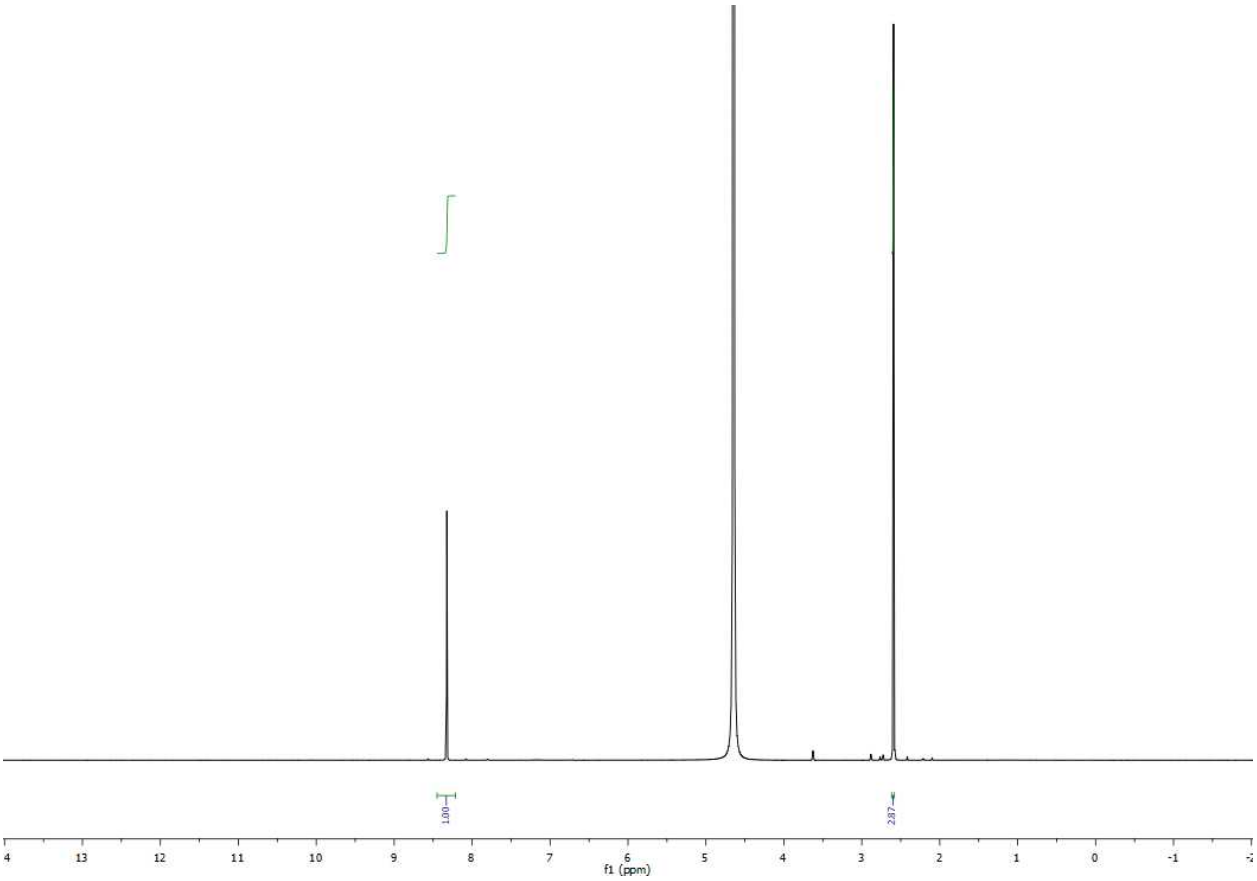

Figure S68. NMR Data belonging to Table S11, Entry 3.

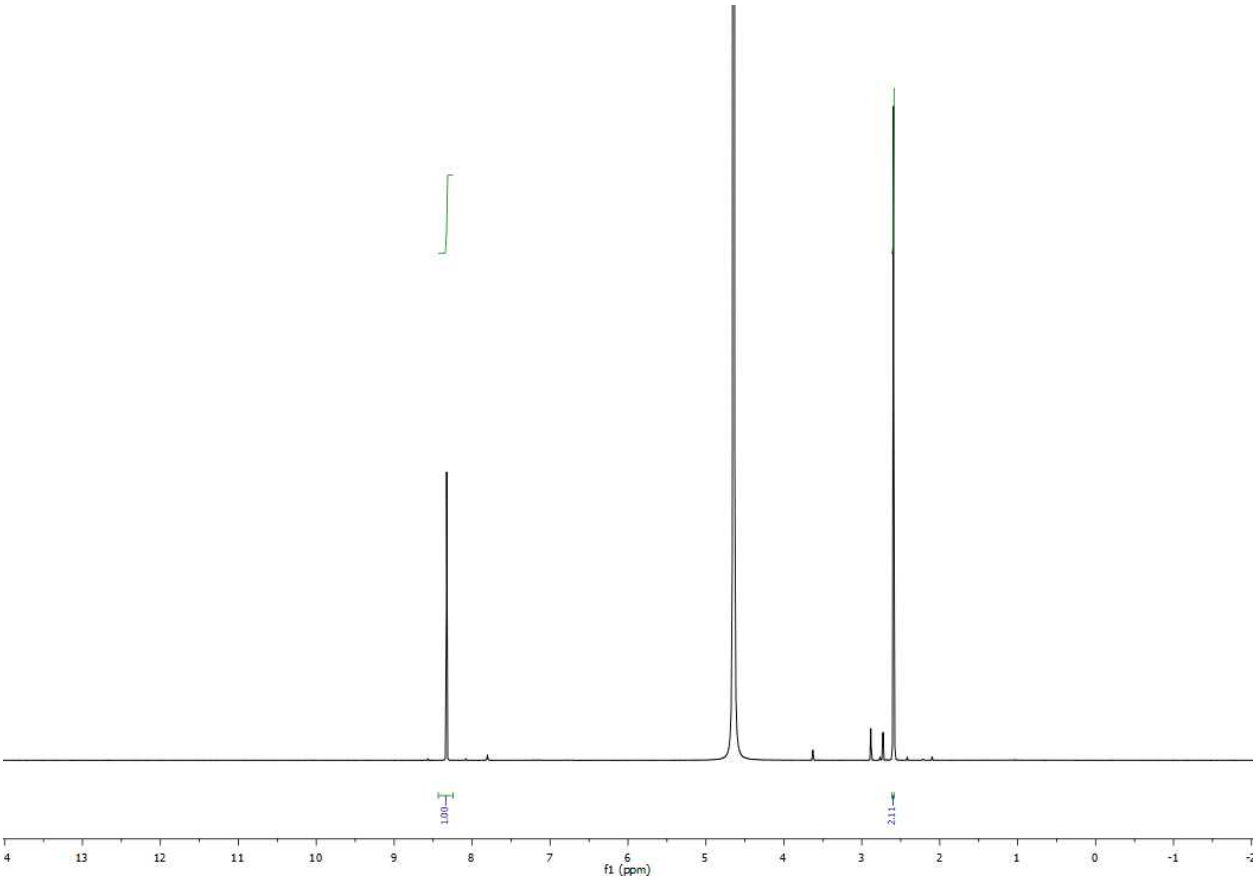

Figure S69. NMR Data belonging to Table S11, Entry 5.

Table S12. ^{1}H NMR peak data belonging to Table S11 and Figures S66-S69.

Entry	**Ratio of DMSO to formate integral**
1	48.86
2	9.79
3	2.87
4	2.35
5	2.11

Hydrogenation in the presence of varied bicarbonate concentration

Table S13. Catalyst concentration versus TON and yield. *Reactions conditions*: 55 mM PTC, 1 mL H_2O, 1 mL toluene, varying amounts of $KHCO_3$, T = 90 °C, p = 45 bar, t = 16h, catalyst **1** (0.14 µmol**)**.

Entry	$KHCO_3$ (mmol)	TON	Conversion
1	1.15	5927	71.8
2	2.5	11878	66.2
3	5	25828	70.6
4	10	37699	52.5

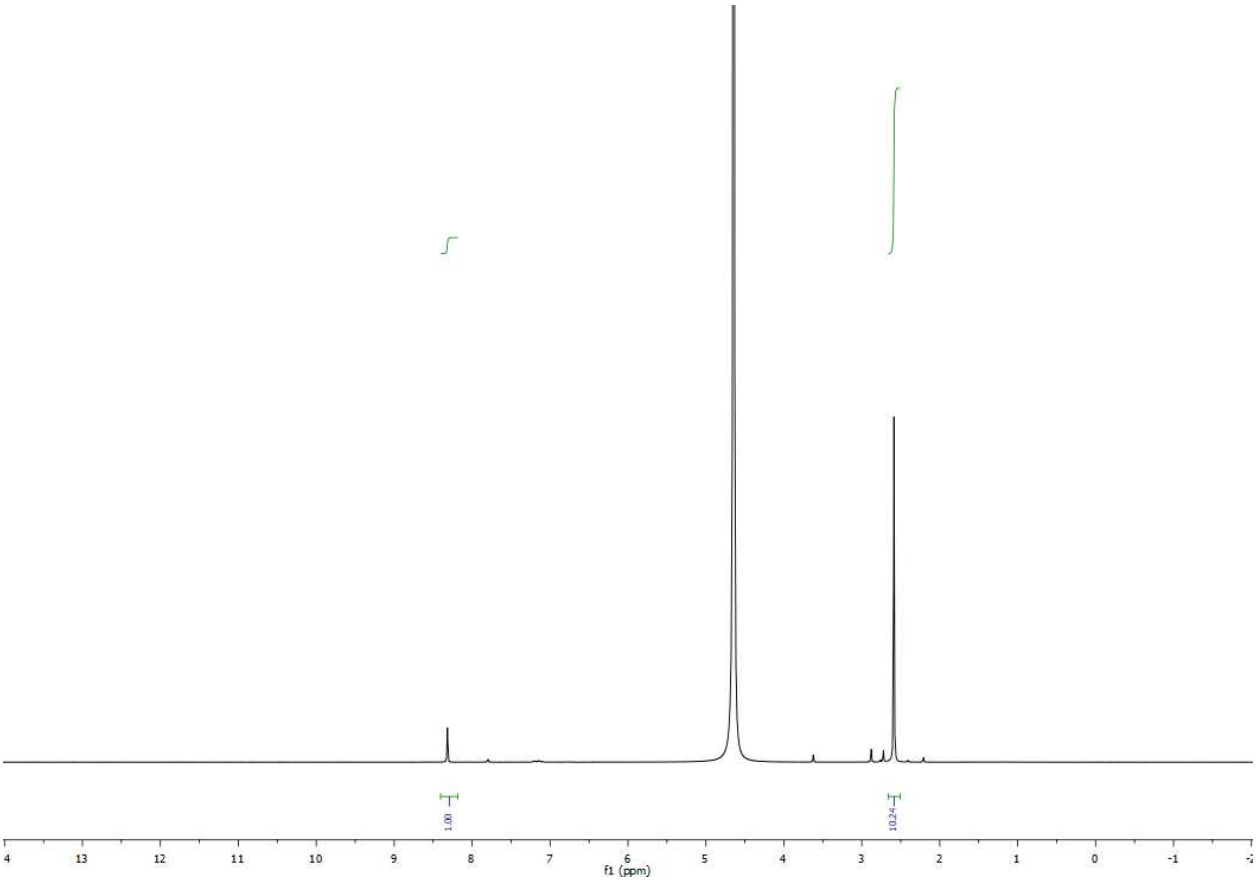

Figure S70. NMR Data belonging to Table S13, Entry 1.

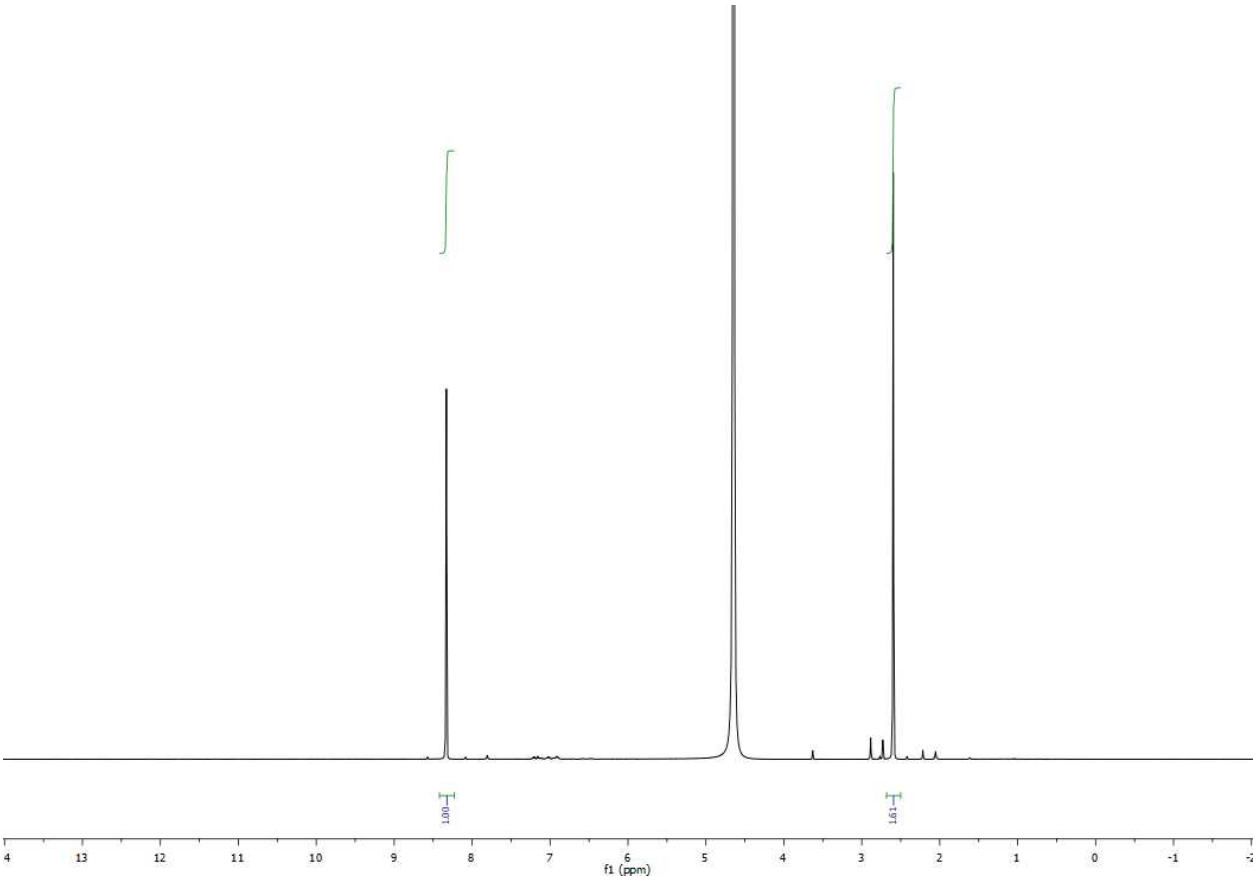

Figure S71. NMR Data belonging to Table S13, Entry 2.

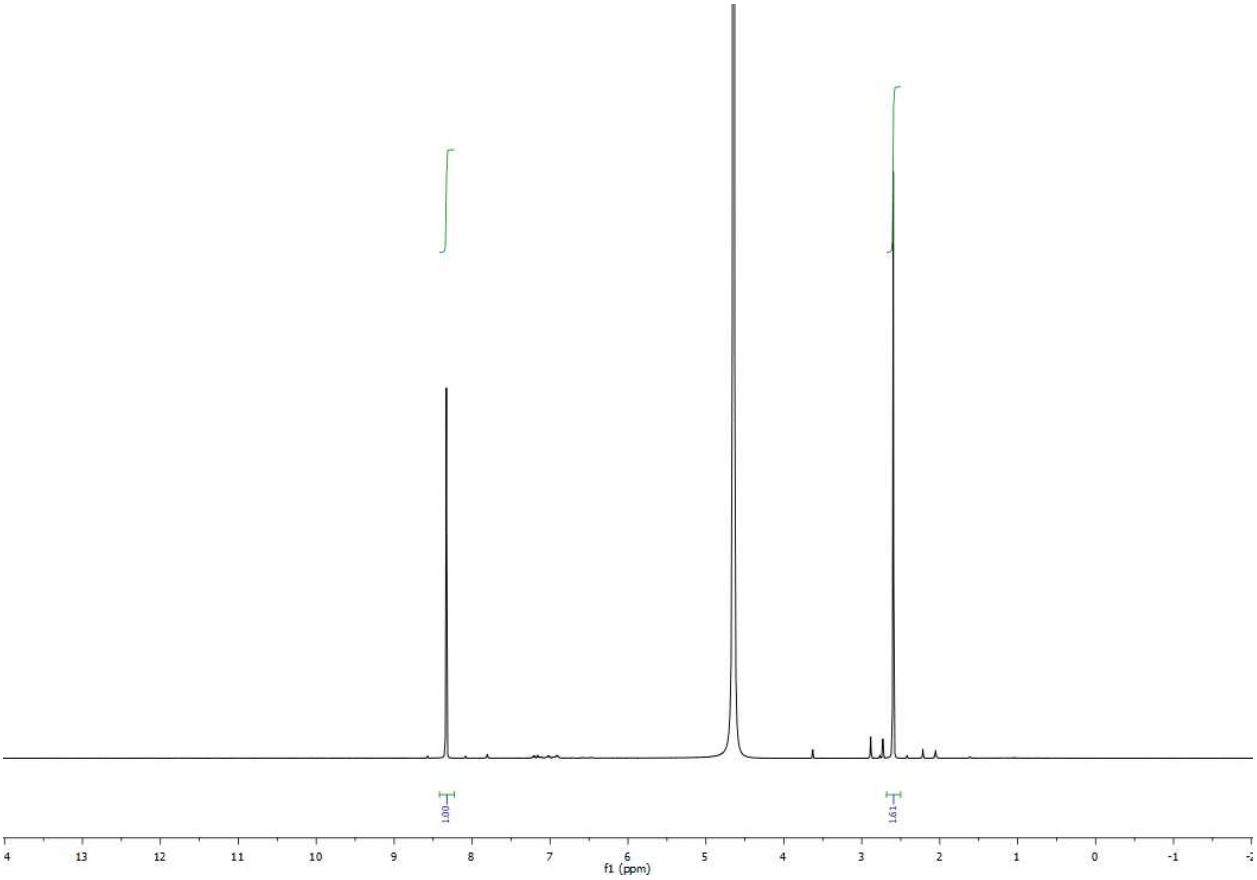

Figure S72. NMR Data belonging to Table S13, Entry 4.

Table S14. ^{1}H NMR peak data belonging to Table S13 and Figures S70-S72.

Entry	**Ratio of DMSO to formate integral**
1	10.24
2	5.11
3	2.35
4	1.61

Scale-up kinetic experiment

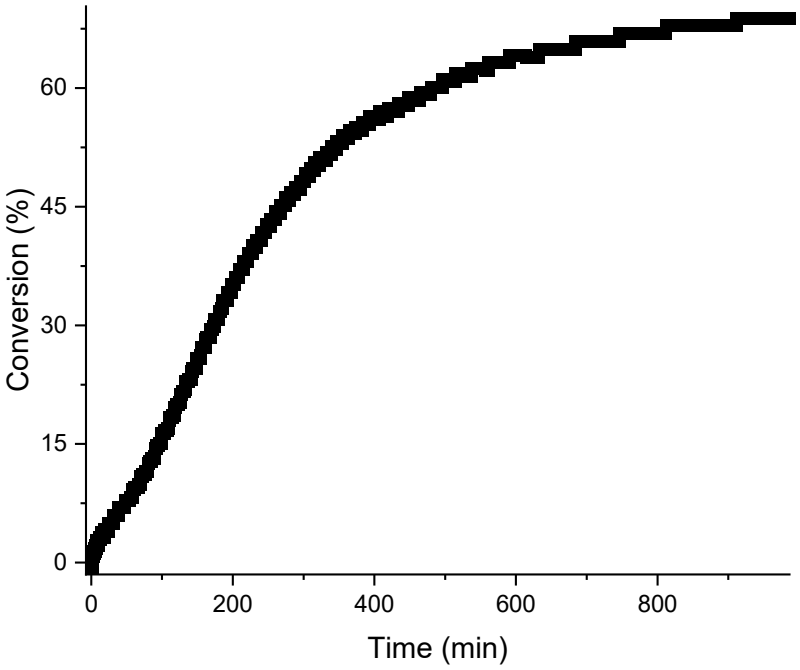

Figure S73. Conversion versus time in the hydrogenation of $KHCO_3$ calculated via hydrogen uptake monitoring corrected by NMR analysis. Reaction conditions: 10 mL solvent (H_2O/ toluene = 1/1), 0.696 µmol of catalyst **1**, methyltrioctylammonium chloride, T = 90 °C, p = 50 bar (p_{H2}=50 bar), $KHCO_3$ = 50 mmol (10M in H_2O).

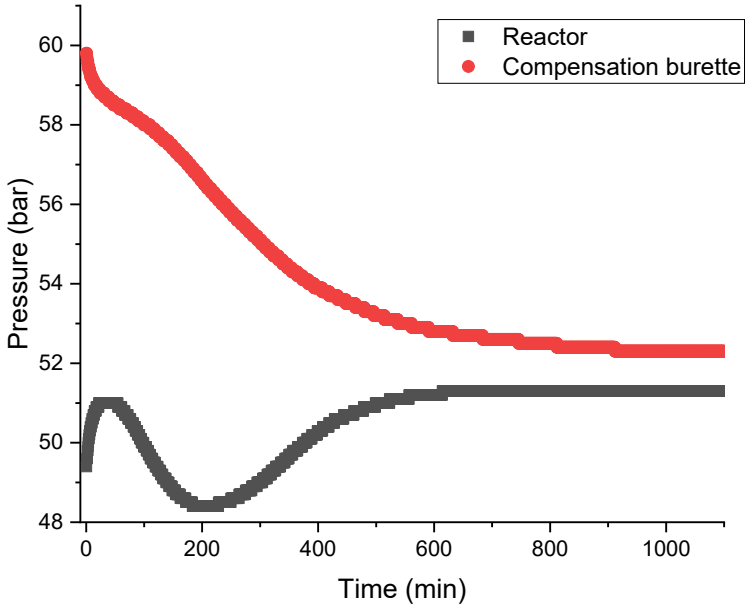

Figure S74. H_2 uptake data accompanying the experiment described in Figure S73. The volume of the compensation burette is 142 mL. The volume of the headspace in the reactor is 45 mL.

The compensation burette is used to maintain constant pressure during the course of the reaction.

S3. pKa analysis and DFT calculations

pKa analysis:

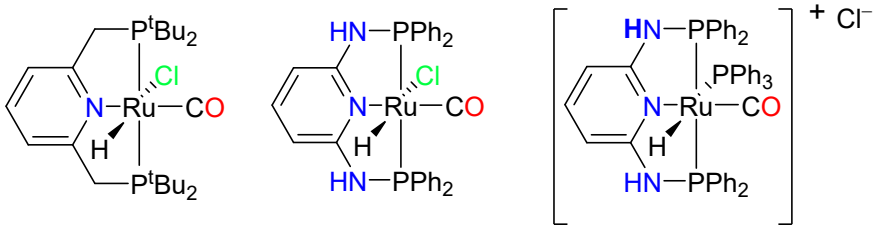

	[RuHCl(PNP)]	[RuHCl(PN^{3}P)]	[RuHPPh3(PN^{3}P)]$^+$Cl$^-$
Computed pK_a	33.9	23.6	pK_{a1} = 22.1, pK_{a2} = 26.6

Figure S75. Computed pKa data for several Ru-PN^{3}P complexes

Density functional theory calculations were used to compute the pKa of [RuHCl(PNP], [RuHCl(PN^{3}P)], and [RuHPPh$_3$(PN^{3}P)] complexes. We used an acid base titration scheme to compute the pK_a assuming that an acid (AH) is titated with an equivalent amount of base B to produce the conjugate base A, and BH. pKa of AH is related to the pKa of BH via the $^{\Delta G^0}$ of the acid base titration reaction.

$$AH + B \rightarrow A + BH$$

$$pK_a(AH) = pK_a(BH) + \frac{\Delta G^0}{2.303RT}$$

In our calculations we used DBU as the base. The pKa of DBUH$^+$ in acetonitrile is 24.34.[4] DFT calculations were carried out using the Gaussian 16 C.01 program package. Geometry optimizations were carried out using the PBE0 (also denoted as the PBE1PBE)[5] exchange–correlation. functional, def2-SVP basis set[6] and the Grimme's dispersion corrections (D3 version).[7] The choice of the PBE0 functional is motivated by our previous experience for prediction of reliable results for TM complexes in good agreement with experimental data.[8] Furthermore our computed pKa of 33.9 for the [RuHCl(PNP)] complex is in agreement with the experimentally reported value of ~ 34.[9] Hessian matrix calculations were performed to characterize all minima (no imaginary frequencies). Thermochemical parameters such as the zero-point energy, enthalpy, and Gibbs free energy (G_{gas}) were calculated using the gas phase Hessian calculations. The DFT computed-energies in the gas phase (E_{gas}) were additionally refined by single point (SP) calculations in acetonitrile solvent using the PBE0-D3 method together with the SMD variation of the IEFPCM implicit solvent model of Truhlar and co-workers[10] and the combination of the def2-TZVP basis set.[6] The Gibbs free energy corrections obtained via the gas phase hhessian calculations were added to the SP energies (E_{sol}) to obtain solvated Gibbs free energies (G_{sol}).

Table S15. DFT computed thermochemical parameters used to compute the pK_a. Subscript "$_{gas}$" and "$_{sol}$" respectively refer to calculations performed in vacuum and solvent (acetonitrile).

Species	E_{gas} (Eh)	G_{gas} (Eh)	E_{sol} (Eh)	G_{sol} (Eh)	ΔG^{0}_{298K}(kcal mol^{-1})	pK_a
DBU	-461.2413991	-461.029522	-461.7422025	-461.5303254		
$DBUH^+$	-461.6615646	-461.435062	-462.2322323	-462.0057296		24.33
[RuHCl(PNP)]	-2306.327323	-2305.748368	-2307.901921	-2307.322966		
$[RuHCl(PNP)]^-$	-2305.763412	-2305.19955	-2307.390656	-2306.826794	13.03	33.9
[RuHCl(PN^3P)]	-2633.068607	-2632.643401	-2635.019663	-2634.594457		
$[RuHCl(PN^3P)]^-$	-2632.521983	-2632.112222	-2634.530515	-2634.120755	-1.07	22.1
$[RuHPPh_3(PN^3P)]^+$	-3207.804195	-3207.116309	-3210.476929	-3209.789043		
$[RuHPPh_3(PN^3P)]$	-3207.360448	-3206.685711	-3209.99315	-3209.318413	3.01	26.6

Small molecule activation over complexes 2 and 3:

Calculations are done using Gaussian 16 C.01 program as described above using the PBE0/PBE1PBE[5] exchange–correlation. functional, def2-TZVP basis set[6] and the Grimme's D3(BJ) dispersion corrections.[7]

The ultrafine grid was uniformly used. The nature of stationary point was confirmed by frequency analysis, in which zero imaginary frequencies for minima and one for transition states. Gibbs free energies (ΔG) were computed using the results based on the results of the normal mode analysis within the ideal gas approximation at a temperature of 298.15K and 1 bar.

Results are summarized below with ΔE and ΔG being ZPE-corrected electronic and Gibbs free energies of transformation and respective barriers denoted with hash sign "#". Optimized structures of the intermediates and transition states are provided within an xyz file with all computed energetics collected in the machine-readable csv file. The columns are denoted as

`Code = structure code,ImFreqs = nr. of imaginary frequencies,E_SCF = total electronic energy,E_ZPE = ZPE-corrected electronic energy,E_T = ZPE- and thermal energy corrected electronic energy, H = enthalpy, G = Gibbs Free Energy,,DE,Dezpe,DH,DG – the respective energy difference with respect to the starting state of the given elementary reaction.`

Direct H_2 activation was analysed for both **2** and **3** to reveal high activation barriers in extent of 100 kJ/mol.

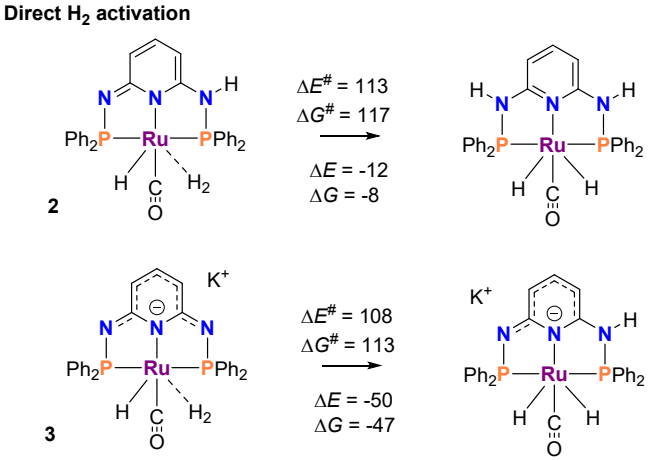

Figure S76. DFT-computed reaction parameters for direct hydrogen dissociation with complexes **2** and **3**

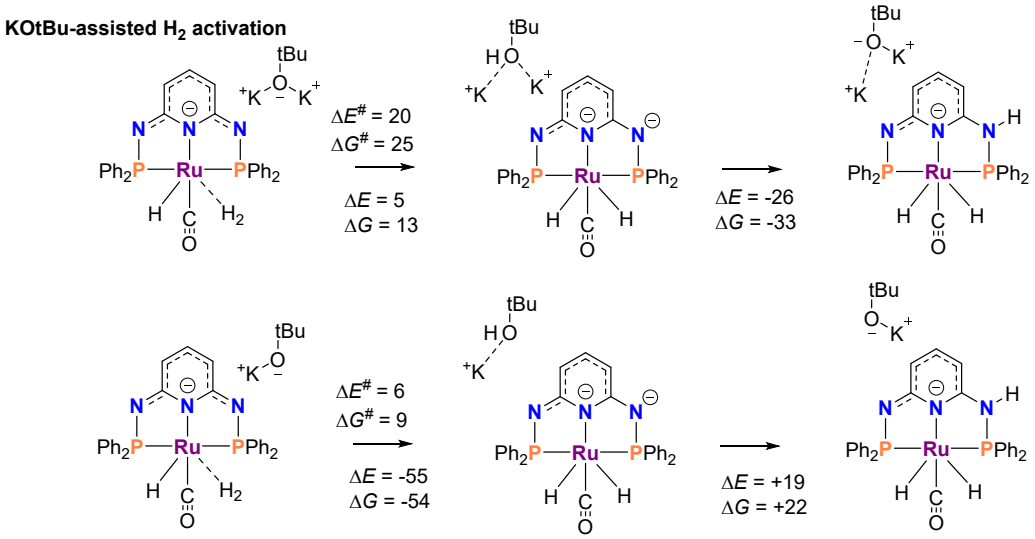

Figure S77. DFT-computed reaction parameters for KO^{t}Bu and ^{t}BuO$^-$ assisted hydrogen dissociation with complex **3**.

S4. X-ray crystallography

General:

All reflections were measured by a Bruker D8-Venture Photon area detector (MoKα radiation for complexes **1** and **2**) and Bruker APEX2 area detector (CuKα radiation for complex 3) at a temperature of 100 K.

Reflections were corrected for adsorption and scaled on the basis of multiple measured reflections using the SADABS program.[11] Using ShelXle[12], the structures were solved with SHELXS-14[13] by using direct methods and refined with SHELXL-2018[13] on *F*2 for all reflections. Non-hydrogen atoms were refined by using anisotropic displacement parameters. Positions of hydrogen atoms were calculated for idealized positions. Geometry calculations and checks for higher symmetry were performed with the PLATON program.[14]

Complex 1: CCDC 2133067

Crystals suitable for X-ray diffraction were obtained by slow ether vapour diffusion into DMF of **1**. Crystallographic data: *Fw* =978.36 g mol^{-1}, colourless block, orthorhombic, *Pbcn*, a = 25.849(5) Å, b = 19.5041(3) Å, c = 21.0152(4) Å, $\alpha = \beta = \gamma$ =90 °

Complex 2: CCDC 2133066

Crystals suitable for X-ray diffraction were obtained by slow pentane vapour diffusion into THF solution of **2**. Crystallographic data: *Fw* = 1804.68 g mol^{-1}, colourless block, monoclinic, $P2_1/c$, a = 14.8971(3) Å, b = 22.7530(4) Å, c = 28.6172(4) Å, α = 90 °, β = 100.3319(6) °, γ = 90 °

Complex 3DMSO: CCDC 2125682

Crystals suitable for X-ray diffraction were obtained by slow ether vapour diffusion into tetrahydrofuran solution of **3DMSO**. Crystallographic data: *Fw* = 793.85 g mol^{-1}, colourless platelet, orthorhombic, *Pca21*, a = 12.6529(5) Å, b = 18.7504(6) Å, c = 15.5836(5) Å, $\alpha = \beta = \gamma$ =90 °

CCDC-2133067: complex **1**, CCDC-2133066: complex **2**, CCDC-2125682: complex **3DMSO** contain the supplementary crystallographic data for this paper. These data can be obtained free of charge from The Cambridge Crystallographic Data Centre *via* www.ccdc.cam.ac.uk/data_request/cif.

References:

1. Guan, C.; Pan, Y.; Ang, E. P. L.; Hu, J.; Yao, C.; Huang, M.-H.; Li, H.; Lai, Z.; Huang, K.-W., Conversion of CO2 from air into formate using amines and phosphorus-nitrogen PN3P-Ru(ii) pincer complexes. *Green Chemistry* **2018,** *20* (18), 4201-4205.
2. Gnanaprakasam, B.; Zhang, J.; Milstein, D., Direct Synthesis of Imines from Alcohols and Amines with Liberation of H2. *Angewandte Chemie International Edition* **2010,** *49* (8), 1468-1471.
3. Rebreyend, C.; Pidko, E. A.; Filonenko, G. A., Homogeneous hydrogenation of saturated bicarbonate slurry to formates using multiphase catalysis. *Green Chemistry* **2021,** *23* (22), 8848-8852.
4. Schwesinger, R.; Willaredt, J.; Schlemper, H.; Keller, M.; Schmitt, D.; Fritz, H., Novel, Very Strong, Uncharged Auxiliary Bases; Design and Synthesis of Monomeric and Polymer-Bound Triaminoiminophosphorane Bases of Broadly Varied Steric Demand. *Chemische Berichte* **1994,** *127* (12), 2435-2454.
5. Adamo, C.; Barone, V., Toward reliable density functional methods without adjustable parameters: The PBE0 model. *The Journal of Chemical Physics* **1999,** *110* (13), 6158-6170.
6. Weigend, F.; Ahlrichs, R., Balanced basis sets of split valence, triple zeta valence and quadruple zeta valence quality for H to Rn: Design and assessment of accuracy. *Physical Chemistry Chemical Physics* **2005,** *7* (18), 3297-3305.
7. Caldeweyher, E.; Bannwarth, C.; Grimme, S., Extension of the D3 dispersion coefficient model. *The Journal of Chemical Physics* **2017,** *147* (3), 034112.
8. Sinha, V.; Laan, J. J.; Pidko, E. A., Accurate and rapid prediction of pKa of transition metal complexes: semiempirical quantum chemistry with a data-augmented approach. *Physical Chemistry Chemical Physics* **2021,** *23* (4), 2557-2567.
9. Mathis, C. L.; Geary, J.; Ardon, Y.; Reese, M. S.; Philliber, M. A.; VanderLinden, R. T.; Saouma, C. T., Thermodynamic Analysis of Metal–Ligand Cooperativity of PNP Ru Complexes: Implications for CO2 Hydrogenation to Methanol and Catalyst Inhibition. *Journal of the American Chemical Society* **2019,** *141* (36), 14317-14328.
10. Marenich, A. V.; Cramer, C. J.; Truhlar, D. G., Universal Solvation Model Based on Solute Electron Density and on a Continuum Model of the Solvent Defined by the Bulk Dielectric Constant and Atomic Surface Tensions. *The Journal of Physical Chemistry B* **2009,** *113* (18), 6378-6396.
11. Bruker **(2013)**. *APEX2*, *SAINT, XPREP* and *SADABS*. Bruker AXS Inc., Madison, Wisconsin USA.
12. B. Hübschle, G. M. Sheldrick, D Dittrich, ShelXle: a Qt graphical user interface for SHELXL. *J. Appl. Cryst.* **2011**, *44*, 1281 – 1284.
13. G. M. Sheldrick, SHELXT - Integrated space-group and crystal-structure determination. *Acta Cryst.* **2015**, *C71*, 3-8.
14. *PLATON*. A. L. Spek, Structure validation in chemical crystallography. *Acta Cryst.* **2009**, *D65*, 148–155.